THE PROPAGATION OF FRACTURE IN MILD STEEL

A thesis presented in supplication for the degree of DOCTOR OF PHILOSOPHY (Engineering)

by

THOMAS ADRIAN CHEETHAM STOCK B.A.

Department of Metallurgy,
Royal School of Mines,
Imperial College,
London.

December 1964

ABSTRACT

The isochromatic strain patterns on the surfaces of mild steel plates containing moving brittle fractures have been determined by using strain birefringent coating and high speed photographic techniques. The major part of these isochromatic patterns may be described by a formula for the isochromatic pattern near a stationary crack in an elastic medium. The variations from this formula are caused by, shock waves in the specimen, inertia effects due to the high velocity of the crack, and yielding near the crack tip. The inertia effects cause a region of biaxial tension ahead of the crack on the plate surface. A crack model which predicts the extent of the plastic zone near the crack tip has been proposed. The predictions from this model and other theories are compared with experimental estimates of the plastic zone depth. The results of a microstructural examination of fracture surfaces supported Tipper's (1957) explanation of the mechanism for crack propagation.

ACKNOWLEDGEMENTS

The work described in this thesis was carried out in the Department of Physical Metallurgy of Imperial College, London under the direction of Professor J. G. Ball, to whom I am grateful for the facilities provided. I wish to thank Professor P. L. Pratt who supervised the work and provided much encouragement, help and valuable discussion.

I am indebted to Mr. P. R. Christopher and his colleagues of Naval Construction Research Establishment, Rosyth for practical help in the construction of apparatus, help during the experimental work performed at Rosyth, and for continuous encouragement and discussion during the whole of this research.

Most of the welding and flame cutting of the specimens was done by Mr. A. W. West, the flash light source was constructed by Mr. H. V. Haddow, and most of the metallographic polishing was done by Mr. K. Camichel; I am very grateful to them and the rest of the college employees for their assistance.

In conclusion I wish to thank the Admiralty for financing this research.

CONTENTS

1 Introduction

The problem of brittle fracture is of great importance in many aspects of constructional engineering for the stress required to propagate a brittle fracture through mild steel may be only one tenth of the measured ultimate strength, and well below the designed working stress. In this thesis the term brittle fracture, as applied to steel, is used to denote fractures which absorb only small amounts of energy as they propagate; in such fractures there are small but quite definite regions of plastic yielding adjacent to the fracture surface, which is composed of regions of both cleavage and shear failure. Catastrophic service failures have occurred in ships, storage tanks, bridges, etc., and in most large steel structures the potential danger of brittle failure must be considered. Low temperatures and impact loading increase the likelihood of brittle fracture but service failures have occurred at ambient temperatures under static loading. Brittle fractures have been reported in both welded and riveted structures, but in a welded

structure there is a higher probability of fracture initiation because of residual stresses induced during welding, the introduction of stress raising defects, and the change of material properties in the heat affected zone. In addition there is a greater danger of completely catastrophic cracks forming because welded structures are continuous. However because of the saving in materials, labour, and time, welding is the more desirable means of fabrication.

As Cottrell (1961) has pointed out, there are two quite distinct conditions which must be fulfilled before a material breaks. The first condition is that there must be an atomistic mechanism available for pulling the atoms apart in the crack path. The other condition, a thermodynamical one, is that the energy available for crack propagation must be either equal to or greater than the energy absorbed in crack propagation. A material subjected to an increasing load will fracture when both the above conditions are satisfied. In a perfect material fracture would occur by the parting of two planes of atoms, at the ideal strength of the material (approximately a tenth of the

elastic constant, $E/10$,); in real materials fracture commences as soon as the stress is sufficiently high to operate one of the available atomistic mechanisms. In normal practice the chances of operating atomistic fracture mechanisms are minimised by trying to eliminate stress raising defects. The same effect could be accomplished by raising the yield stress of the material. However this method is not used in practice because it would reduce the energy absorbed in fracture.

The thermodynamical condition for fracture in steel depends upon two effects; these are the elastic-plastic and mechanical instabilities. The former controls the major part of the energy absorbed during crack formation, while the latter controls the transport of this energy to the crack front. Since both of these effects are governed by the state of stress near the crack tip, there have been many attempts to determine this stress state both theoretically and experimentally. For brittle cracks moving through mild steel the problem is complicated by the strain rate sensitivity of steel, and by inertia effects which change the stress field at high crack velocities.

If a steel specimen is loaded to fracture, a graph of fracture load, energy absorbed, contraction at fracture surface, etc., plotted versus temperature of testing, strain rate, etc., will show a step. This step marks the transition from ductile to brittle failure, and depends upon the steel, upon the specimen size and shape, and upon the method of loading the specimen.

The object of tests for brittle fracture is to provide the engineer with a temperature above which a structure made from a particular steel will not fail by brittle fracture. Of the tests for brittle fracture the one which most nearly represents a running crack crossing a structure is the Robertson test; it is not often used because of the expense involved. Thus it would be useful to have a test which, while measuring the same material properties as the Robertson test, could be carried out economically upon a small specimen. In order to design such a test, the state of stress around a crack moving through a plate must be known.

The object of this research was to determine experimentally the stress field near a moving brittle fracture in mild steel and to compare the results with theoretical predictions. For the reasons discussed in chapter 4, strain birefringent coatings used in conjunction with single frame high speed photography were the techniques chosen for the experimental programme.

2 Theoretical Solutions for the Stress Fields near Cracks

2.1 Introduction

A brittle fracture propagating through mild steel is accompanied by a field of elastic-plastic deformation. This field (in particular the extent of the plastic deformation) determines the energy absorbed in crack propagation, an important variable in the thermodynamical criterion for fracture. In this chapter theoretical solutions for this stress field are reported. Calculations of the stress field for a stationary crack in an elastic medium are dealt with first. This is followed by the consideration of refinements to the crack model which allow for moving cracks and yielding about the crack tip.

2.2 Stationary Cracks in Elastic Media

A solution of the stress field about a crack in an infinite elastic medium under biaxial tension was given by Inglis (1913). Working in curvilinear co-ordinates he found the stress distribution about an ellipse, then took a crack to be an ellipse of zero eccentricity. Neuber (1958) gave the stress field about an ellipse in a material under uniaxial tension. Westergaard (1939) provided a semi-inverse method for the solution of the stress field about a crack in an infinite thin sheet. He put the Airy stress function as:- $F = \mathrm{Re}(\bar{Z}) + y\ \mathrm{Im}(\bar{Z})$; and by choosing suitable expressions for the complex variable stress function Z, he obtained in Cartesian co-ordinates the same result as Inglis (1913) but in a more easily treated form. Westergaard's method also covers cases of cracks subjected to splitting forces, internal pressure, and several other loading conditions. Using the methods of complex variable Rothman and Ross (1955) gave solutions for the stress fields around cracks for various forms of loading. They also plotted the isochromatic stress field (lines of constant principal shear stress) around a crack subject to

uniaxial tension, fig. 2.1. Following the method of Rothman and Ross, Dixon (1961) using a DEUCE computer, gave tables and graphs showing the distributions around a crack of certain stresses and stress combinations. Sneddon (1946) solved the expressions for the components of stress given by Westergaard (1939) to obtain an expression for the maximum shearing stress, and plotted the isochromatic pattern, about a crack under internal pressure, fig. 2.2. His results were identical with those otherwise obtained by Rothman and Ross (1955). Sneddon also determined the distribution of stress in the immediate vicinity of the crack, by making the simplifying approximation that r is small compared with the crack length, where r and θ are polar co-ordinates used to describe the material containing the crack, $r = 0$ describes the crack tip, $\theta = \pi$ the crack. He then gave a solution for the three dimensional case of a "penny-shaped" crack in a solid body.

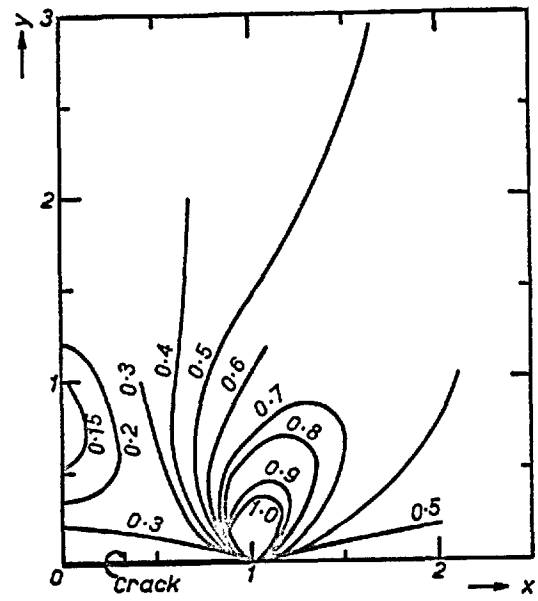

Fig. 2.1 The isochromatic stress field near a stationary crack in an elastic medium under a uniaxial stress. The numerals give values of the ratio of shear stress to applied stress along the lines of constant shear stress. (After Rothman and Ross (1955))

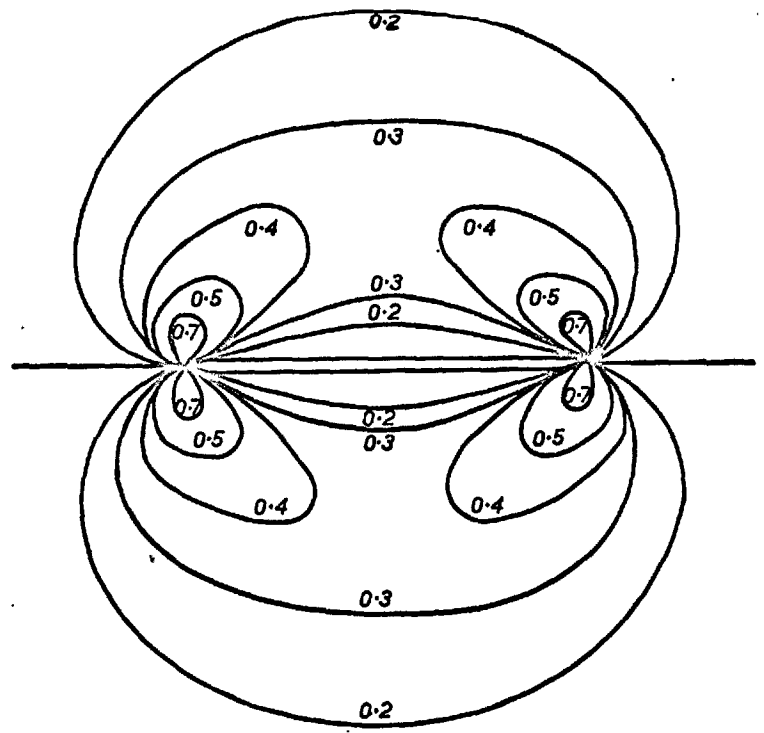

Fig. 2.2 The isochromatic stress field near a stationary crack in an elastic medium under a biaxial stress. The numerals give values of the ratio of shear stress to applied stress along lines of constant shear stress. (After Sneddon (1946))

Using an approximation similar to Sneddon's, Irwin (1957) showed that the stress fields at the crack tip, for five different ways of loading the crack, were identical. He also suggested a method to take account of finite plate width, by using Westergaard's (1939) formula for a series of co-linear cracks, and noting the symmetry of the repeating stress field. Coker and Filon (1931) made an approximate theoretical treatment of the problem of a central elliptical hole in a plate of finite width loaded in tension. Using a similar approach Dixon (1960) gave the stress concentration factor due to a central crack in a finite plate.

2.3 Moving Cracks in Elastic Media

Yoffé (1951) considered a crack of constant length moving with constant speed through a fixed elastic material, fig. 2.3, and obtained a solution for the stresses in the vicinity of the crack from Westergaard's (1939) static solution and the superposition of elastic surface waves. Her analysis showed that for higher speeds of propagation the greatest tensile stress was not in line ahead of the

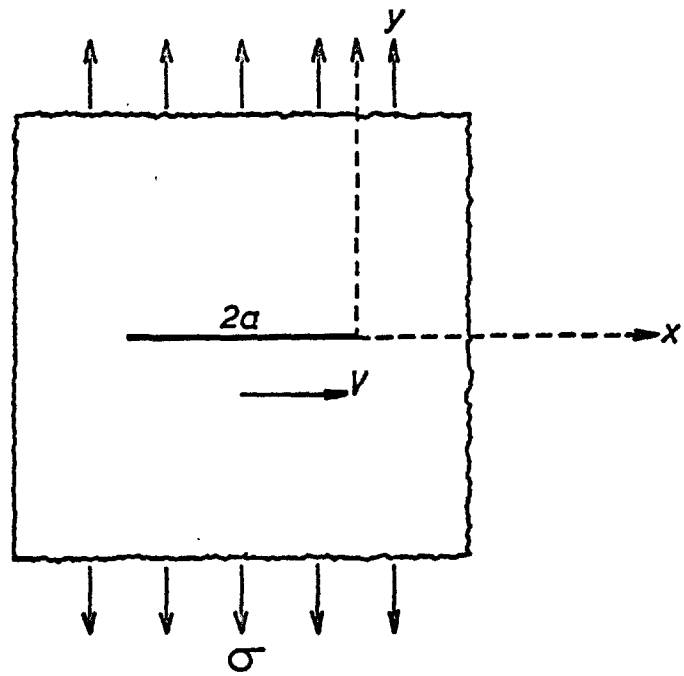

Fig. 2.3 Crack model used by Yoffé (1951).

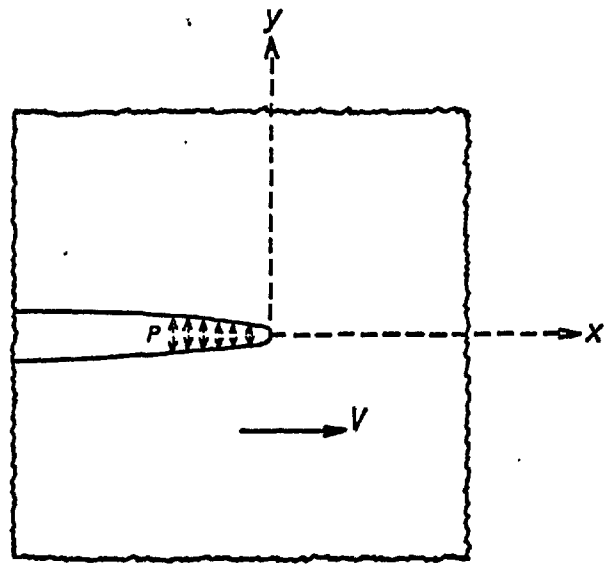

Fig. 2.4 Crack model used by Craggs (1960).

crack, but at an angle to it; thus offering an explanation for the curved or branching fractures often observed in glass. The solution for the stress about a moving semi-infinite crack in an infinite medium, loaded by a region of internal forces following the crack tip, fig. 2.4, was provided by Craggs (1960). He obtained a limiting velocity for the crack which was controlled by the branching velocity. Cotterell (1964) used a similar analysis to explain the relative roughness of fracture surfaces from fast and slow fractures in mild steel. The stress ahead of a slit, growing under a uniaxial stress, was obtained by Akita and Ikeda (1959)(a). Using expanding elliptical co-ordinates they showed that the stress normal to the crack in the material contiguous with the crack tip decreased with increased crack speed. The equation of motion of a slit propagating at constant velocity through a uniform tensile stress field was solved approximately by Yoshiki, Kanazawa, and Itagaki (1961); assuming the form to which the slit opens up, they gave the stress in line ahead of the crack. By using a lattice model Gaus (1961) simulated the transient strain distribution in a plate containing a propagating crack.

2.4 Stationary Cracks in Elastic-Plastic Media

The purely elastic solution for the stress field about a crack gives an infinite stress at the crack tip. In practice; either finite strains, which violate the assumption of infinitesimal deformations, occur, or plastic flow takes place so that the crack tip stress becomes finite. Liu (1961), using Irwin's (1957) approximate formulae for the stress about a crack and neglecting the stress re-distribution caused by plastic deformation, calculated "elastic yield zones". He used the Von Mises yield criterion to show that the plastic enclave for plane strain is smaller than for plane stress, hence accounting for the transition from tensile to single or double shear failure observed in thin sheets. Rooke (1963) pointed out that neither the A.S.T.M. criterion, that yield occurs when the stress normal to the crack equals the yield stress in pure tension, nor the Tresca yield criterion satisfy Liu's model. Rooke also computed values of the "elastic yield zones" using the Tresca, Von Mises, and A.S.T.M. yield criteria, and found the size and shape of the areas about the crack tip where the

stresses exceeded the yield criteria, both for plane stress and strain. He also compared the size of the "elastic yield zones" calculated from Westergaard's (1939) exact formulae with the size obtained from Irwin's (1957) approximation, and found that at large stresses the approximate formulae considerably underestimate the size of the plastic zones, fig. 2.5. Dixon (1962) assumed that the strains in the plastic region were proportional to the applied stress and similar to those predicted by elastic theory. Then, using the Von Mises yield criterion, he was able to calculate the stress distribution near a crack, and forecast plastic zone size for any given applied stress.

Allen and Southwell (1949) using a relaxation technique found the size and shape of the plastic enclaves in a V-notched tensile bar under conditions of both plane stress and plane strain. In this method, firstly the elastic stress distribution is found. Secondly a yield criterion is assumed, Allen and Southwell chose the Von Mises criterion, and the region where the stresses exceed this criterion is determined.

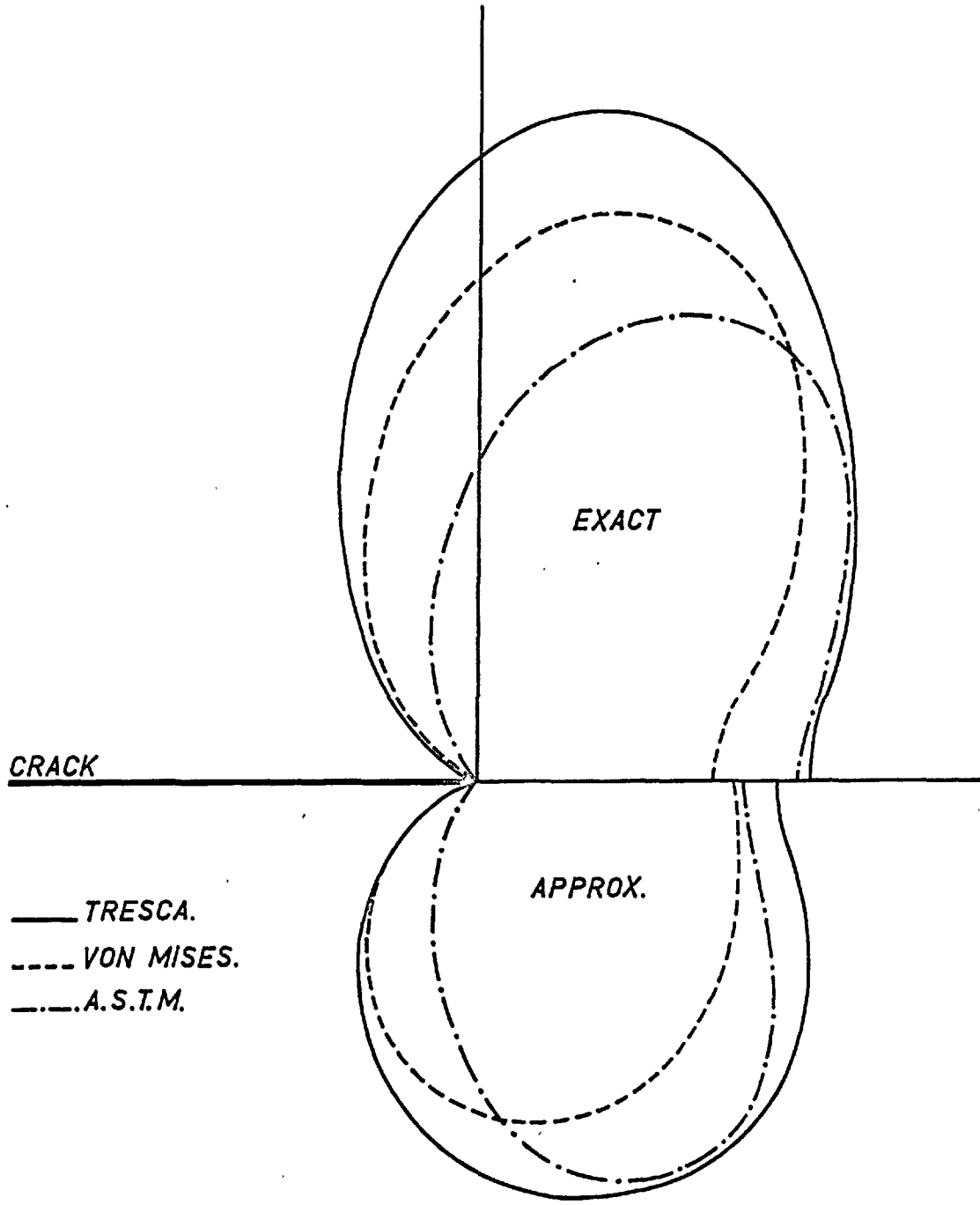

Fig. 2.5 Comparison of exact and approximate yield zones in plane stress for three yield criteria. The applied stress is half the uniaxial yield stress. (After Rooke (1963))

Thirdly the stress within this region is required to be constant and equal to the critical value, which means that the higher stresses already computed there must be decreased. As this step is carried out the excess plastic stress overflows into the originally exclusively elastic region. Then the cycle is repeated until the required accuracy is obtained. Jacobs (1950) applied this technique for plane strain conditions to an externally cracked plate under tension. A similar analysis for plane stress was carried out by Stimpson and Eaton (1961).

Dugdale (1960) obtained an expression for the length of the plastic zone ahead of a crack. His model consisted of an infinite plate under tension containing a crack with internal stresses, which acted to close the crack, at the crack tips; these stresses were equal in magnitude to the yield stress of the plate material, fig. 2.6. Using the stress functions given by Muskhelishvili (1953), and the fact that the proposed yield zones cause the crack tip stress to be finite, he obtained an expression linking plastic zone length, crack length, yield stress, and the applied

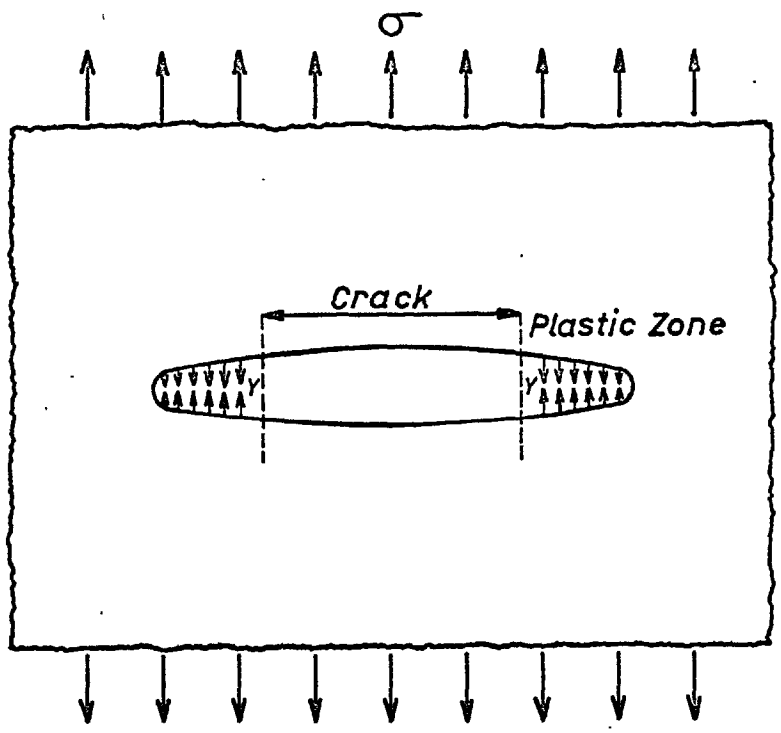

Fig. 2.6 Crack model used by Dugdale (1960).

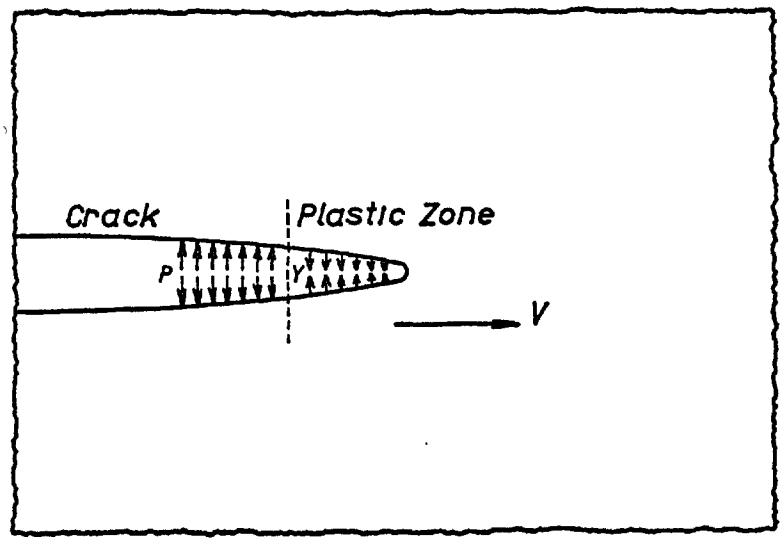

Fig. 2.7 Crack model used by Goodier and Field (1962).

stress acting on the plate. He pointed out that this expression could also be derived from Westergaard's (1939) formulae.

An electrical analogue system representing a stressed plate containing a crack was set up by Redshaw and Rushton (1960). They found that the infinite stress which should arise at the end of a crack could not be represented because of the finite mesh of the network. They also found that for long cracks compared to plate width, the electrical analogue could not be set up, because the stress at the end of the crack was very large, and could not be represented by an equivalent electrical potential. They suggested that the network might have been acting analogously to a metal plate yielding at the end of the crack.

2.5 Moving Cracks in Elastic-Plastic Media

Hahn, Gilbert and Reid (1963) formulated the yielding of low carbon steel in terms of dislocation dynamics. Their formulae described the stress-strain behaviour of steel, and predicted strain-rate sensitivity and yield delay times. Then using the stress concentration formulae given by Inglis (1913) for biaxial loading, and by Neuber (1958) for uniaxial loading; they calculated the maximum stress and plastic-zone size in front of a crack as a function of the applied stress and the crack speed. They assumed that yielding in advance of the crack is analogous to yielding in uniaxial tension and is not retarded by plastic constraint; thus their treatment probably overestimates the size of the plastic zone. Goodier and Field (1962) combined the elastic dynamic solution of Craggs (1960) with the stationary plastic solution of Dugdale (1960), to obtain an estimate of the length of yield zone ahead of a moving crack, fig. 2.7. They removed the stress singularity energy sink in Cragg's analysis by using Dugdale's finiteness condition, thus the available energy was used for plastic work, and not to create new surfaces.

2.6 Cracks Loaded in Shear

The complete solution of the elastic-plastic stress field about a moving crack under tensile loading would be prohibitively difficult, however the case of a crack under shear is simpler. The distributions of stress and strain have been found around a sharp notch in the face of a semi-infinite body subjected to pure shear, by Hult and McClintock (1957). Bilby, Cottrell, and Swinden (1963) used a dislocation model to represent a sheared slit. Their predictions for the length of the plastic zone as a function of stress and crack length from this model, agreed with those of Hult and McClintock (1957) from classical field plasticity, and were similar to the relationships obtained by Dugdale (1960) for a crack under tensile loading.

The stress field around the tip of a crack, subject to longitudinal shear, travelling at a constant velocity in an elastic medium was given by Bilby and Bullough (1954). Their results were extended by McClintock and Sukhatme (1960) to show that in shear there will be a critical branching velocity, in a configuration analogous to the tensile case studied by Craggs (1960).

The elastic-plastic torsion of a cylindrical bar with a circumferential notch was investigated by Walsh and Mackenzie (1959); they gave theoretical predictions of angle of twist, notch root strain and plastic zone length. Rushton (1963) used an electrical analogue to investigate the elastic-plastic torsion of bars containing cracks and other structural discontinuities.

2.7 Further Development of Westergaard's Analysis

The work of Westergaard (1939) and Sneddon (1946) on stationary cracks in elastic material is now given in more detail and their theories used to obtain expressions which are more useful in the analysis of the results presented later in this thesis.
Westergaard gave the following analysis for the stress field around a crack of length 2a lying on the x axis in an infinite plate with a biaxial tensile field σ at large distances from the crack.

Let $\bar{Z}$, Z, and Z' represent successive derivatives with respect to z of a function $\bar{Z}$ (z), where z is x + iy, and let the Airy stress function be:-

$$F = Re\bar{Z} + yIm\bar{Z} \qquad \ldots (1)$$

Then,

$$\sigma x = \frac{\partial^2 F}{\partial y^2} = ReZ - yImZ' \qquad \ldots (2)$$

$$\sigma y = \frac{\partial^2 F}{\partial x^2} = ReZ + yImZ' \qquad \ldots (3)$$

$$\text{and } \tau xy = \frac{-\partial^2 F}{\partial x \partial y} = - yReZ' \qquad \ldots (4)$$

This notation may only be used if τ_{xy} is zero along the x axis. The function Z (z) which solves the problem for the case of biaxial tension is:-

$$Z(z) = \frac{\sigma}{\left[1 - \left(\frac{a}{z}\right)^2\right]^{\frac{1}{2}}} \qquad \ldots (5)$$

Sneddon (1946) investigated the case of a crack opened up by internal pressure, and so added a uniform liquid pressure σ to the entire system, using as his Z (z) function:-

$$Z(z) = \sigma\left[\frac{z}{(z^2 - a^2)^{\frac{1}{2}}} - 1\right] \qquad \ldots (6)$$

Then using a notation similar to that in fig. 2.8, and choosing three related complex variables, he was able to separate real and imaginary parts of Z' to obtain τ_{xy}, and $\frac{1}{2}(\sigma_y - \sigma_x)$, and hence he obtained an expression for the maximum shearing stress at any point as:-

$$\tau = \sigma\frac{r_1 \sin\theta_1}{a}\left(\frac{a^2}{r_2 r}\right)^{3/2} \qquad \ldots (7)$$

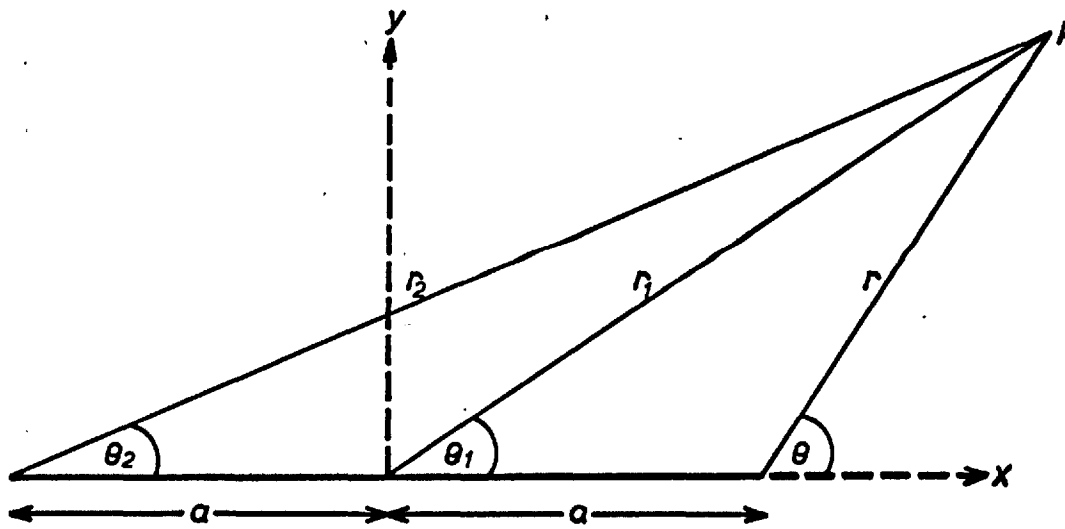

Fig. 2.8 Notation to describe point P in a plate containing a crack of length 2a.

The isochromatic pattern about a crack opened by internal pressure is the same as the pattern about a crack under biaxial tension, as the superposition of liquid pressure will not affect the shear stress.

r_1, r_2 and θ_1 are easily eliminated from equation (7) to give the stress field in terms of r and θ polar co-ordinates with origin at the crack tip as:-

$$\tau = \sigma a^2 \sin\theta \sqrt{\frac{1}{r(4a^2 + 4ar\cos\theta + r^2)^{3/2}}} \quad \ldots (8)$$

This expression may be obtained directly from Westergaard's results:-

By definition $\tau = \sqrt{\left[\frac{\sigma x - \sigma y}{2}\right]^2 + (\tau xy)^2}$ (9)

Thus from (1), (2), (3) and (9),

$$\tau = y\sqrt{(\mathrm{Im}Z')^2 + (\mathrm{Re}Z')^2} \quad \ldots (10)$$

Also differentiation of (5) gives,

$$Z' = \frac{-a^2 \sigma}{(z^2 - a^2)^{3/2}} \qquad \ldots (11)$$

Now $z = x + iy$

or in polar co-ordinates,

$$z = a + re^{i\theta} \qquad \ldots (12)$$

From (11) and (12),

$$(\mathrm{Im}Z')^2 + (\mathrm{Re}Z')^2 = \frac{\sigma^2 a^4}{(r^3)(4a^2 + 4ar\cos\theta + r^2)^{3/2}} \qquad \ldots (13)$$

and as $y = r \sin\theta$ from (10) and (13),

$$\tau = \sigma a^2 \sin\theta \sqrt{\frac{1}{r\,(4a^2 + 4ar\cos\theta + r^2)^{3/2}}}$$

Fig. 2.9 shows the isochromatic pattern near the crack tip, plotted from equation (8), showing values of $\tau/\sigma = 1,\ 1\frac{1}{2},\ 2,\ 3$ and 4. Sneddon plotted the isochromatic pattern further from the crack for values of τ/σ less than 0.7, fig. 2.2.

Using Westergaard's (1939) suggestion a uniform horizontal compressive stress σ may be superposed upon the biaxial stress field to give uniaxial loading. This problem is easily solved using Sneddon's (1946) notation:-

$$\tfrac{1}{2}(\sigma y - \sigma x) = \frac{\sigma r_1 \sin \theta_1}{a} \left(\frac{a^2}{r_2 r}\right)^{3/2} \sin 3/2(\theta + \theta_2) + \frac{\sigma}{2} \qquad \ldots (14)$$

$$\tau xy = \frac{\sigma r_1 \sin \theta_1}{a} \left(\frac{a^2}{r_2 r}\right)^{3/2} \cos 3/2(\theta + \theta_2) \qquad \ldots (15)$$

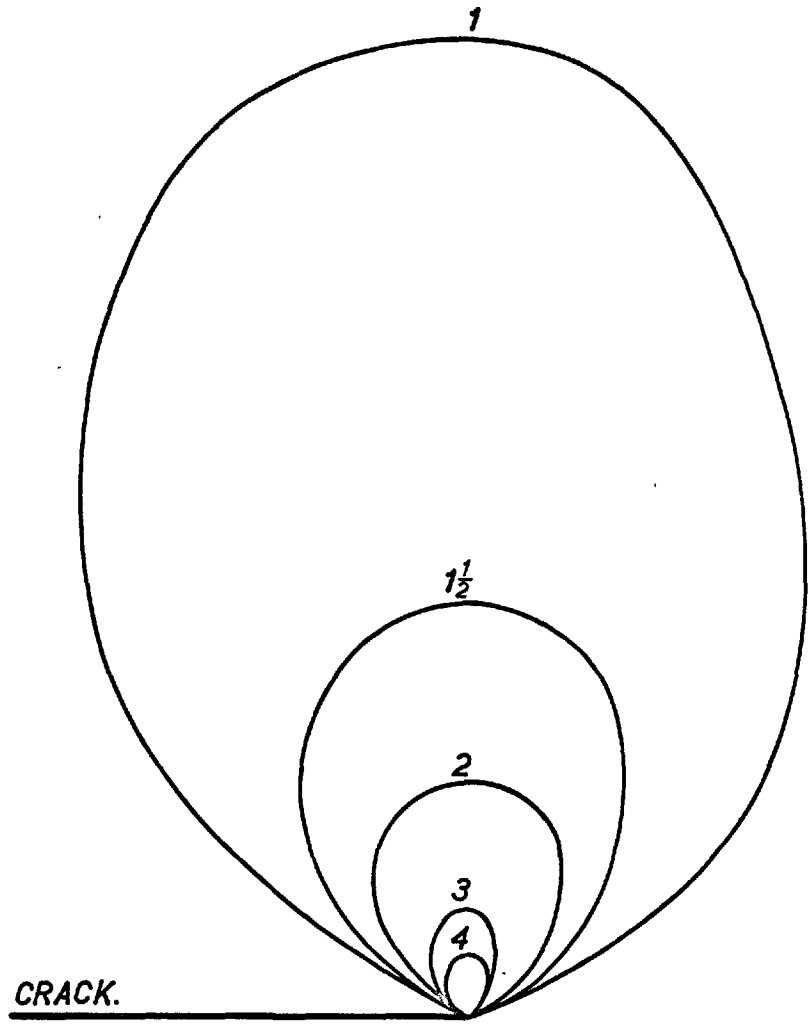

Fig. 2.9 The isochromatic stress field near a stationary crack in an elastic medium under a biaxial stress. The numerals give values of the ratio of shear stress to applied stress along the lines of constant shear stress.

From (9), (14) and (15)

$$\tau^2 = \sigma^2\left[\left(\frac{r_1}{a}\sin\theta_1\left(\frac{a^2}{r_2 r}\right)^{3/2}\right)^2 + \frac{r_1}{a}\sin\theta_1\left(\frac{a^2}{r_2 r}\right)^{3/2}\sin 3/2(\theta+\theta_2) + \tfrac{1}{2}\right] \quad \ldots (16)$$

or in terms of r and θ

$$\tau^2 = \sigma^2\left[\left(\sin\theta\, a^2\sqrt{\frac{1}{r(4a^2+4ar\cos\theta+r^2)^{3/2}}}\right)^2 + \sin\theta\, a^2\sqrt{\frac{1}{r(4a^2+4ar\cos\theta+r^2)^{3/2}}}\right.$$

$$\left. x\sin 3/2\left(\theta+\tan^{-1}\frac{r\sin\theta}{2a+r\cos\theta}\right) + \tfrac{1}{2}\right] \quad \ldots (17)$$

Equation (16) has been obtained by a different method by Rothman and Ross (1955). The isochromatic stress field plotted from equation (17) is shown in fig. 2.10. This shows lines of τ/σ greater than 1. Rothman and Ross (1955) gave the isochromatic pattern for τ/σ less than 1, fig. 2.1.

2.8 Strain Rate Effects for Moving Cracks in Mild Steel

The analysis of the stress field near a crack moving through mild steel is complicated by the strain-rate dependence of the physical properties of mild steel. The only work, known to the author, which makes allowance for this strain-rate sensitivity in steel, is by Hahn, Gilbert, and Reid (1963); this work is now described in more detail, and another solution propounded with a more realistic crack model and yielding criterion.

Hahn et alia formulated the yielding of steel in terms of dislocation dynamics, to describe the stress-strain behaviour of a low carbon steel, predict strain-rate sensitivity and yield delay times, and in particular to calculate the onset of yielding for any

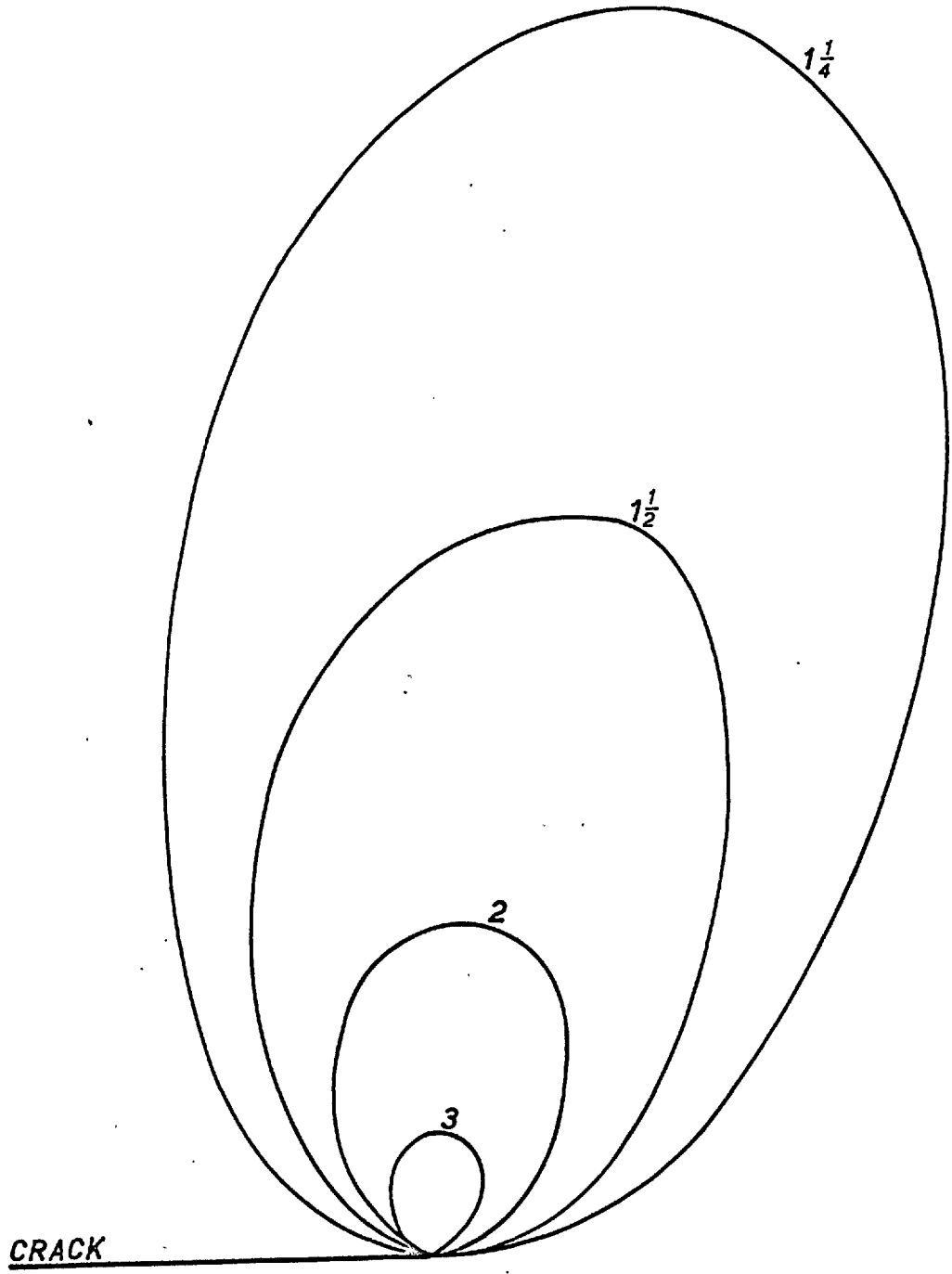

Fig. 2.10 The isochromatic stress field near a stationary crack in an elastic medium under uniaxial stress. The numerals give values of the ratio of shear stress to applied stress along the lines of constant shear stress.

arbitrary loading rate for which the variation of stress with time was known. Their calculated delay times compared well with the experimental results of Krafft and Sullivan (1962). They used the crack model shown in fig. 2.11 which consisted of a sharp crack with circular plastic-zones at its tips. These zones were assumed to support no load; the crack/plastic-zone complex may thus be treated as an elliptical hole in an entirely elastic medium. The stress fields about elliptical holes in elastic media have been solved by Inglis (1913) for biaxial loading and Neuber (1958) for uniaxial loading. By applying these solutions to their model Hahn et alia were able to obtain the stress history of a small element of material δv in line ahead of the crack, as the crack approached it, assuming that the stress field was unaffected by crack velocity. Then combining their equation for yielding with this stress history, they predicted the variations of plastic-zone size and stress at the elastic-plastic boundary with crack velocity and nominal stress upon the plate. Implicit in their treatment was the assumption that yielding in advance of the crack was

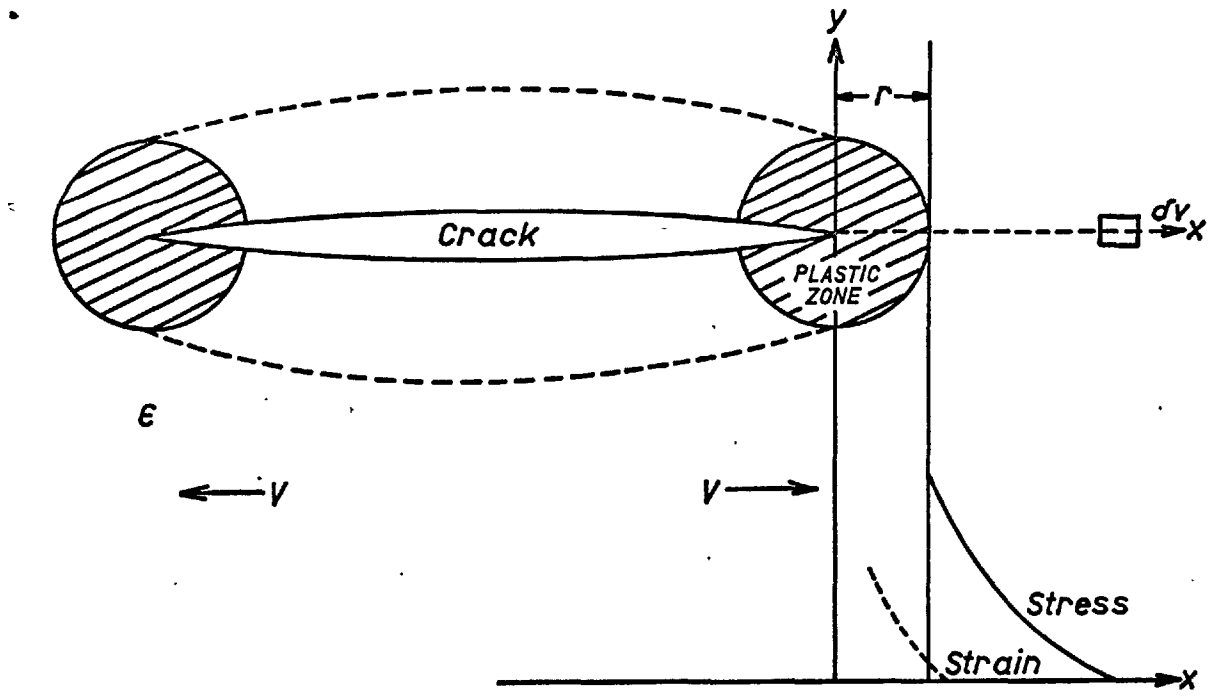

Fig. 2.11 Crack model used by Hahn, Gilbert and Reid (1963).

analogous to yielding in uniaxial tension and was not retarded by plastic constraint.

Now consider a crack with "elastic yield zones" at its tips, where stress redistribution due to yielding is neglected, moving through a steel plate. Assume that the dynamic stress field is similar to the static case; this will be true unless the crack velocity is very high. The shear stress changes for a series of small elements, δ v, ahead of the crack, as the crack passes them, fig. 2.12, may be calculated from equation (17). This has been done and is shown in fig. 2.13; these curves give the variation of τ/σ with x/a along lines of constant y/a, and are sections through the isochromatic pattern of fig. 2.10. Rothman and Ross (1955) gave results, fig. 2.14, similar to fig. 2.13, but for values of y/a from 0.2 to 3, regions relatively far from the crack tip. If the crack is travelling at constant velocity v, the x/a axis may be given in terms of time t as x/a multiplied by a/v, and the curves in fig. 2.13 become the stress histories of

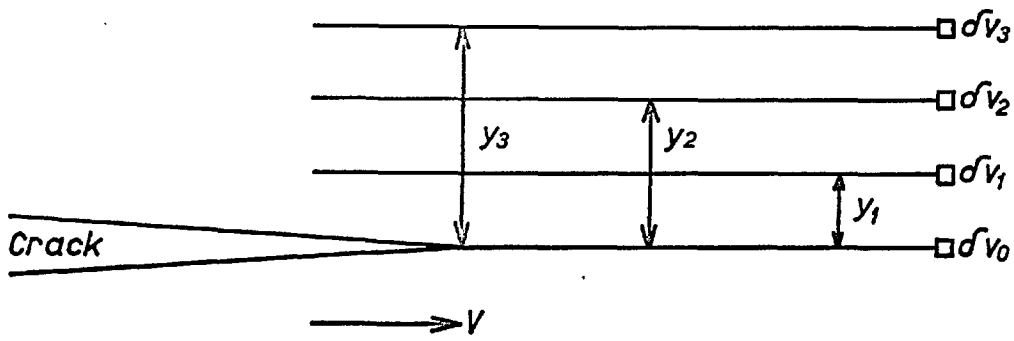

Fig. 2.12 Series of small elements ahead of a moving crack.

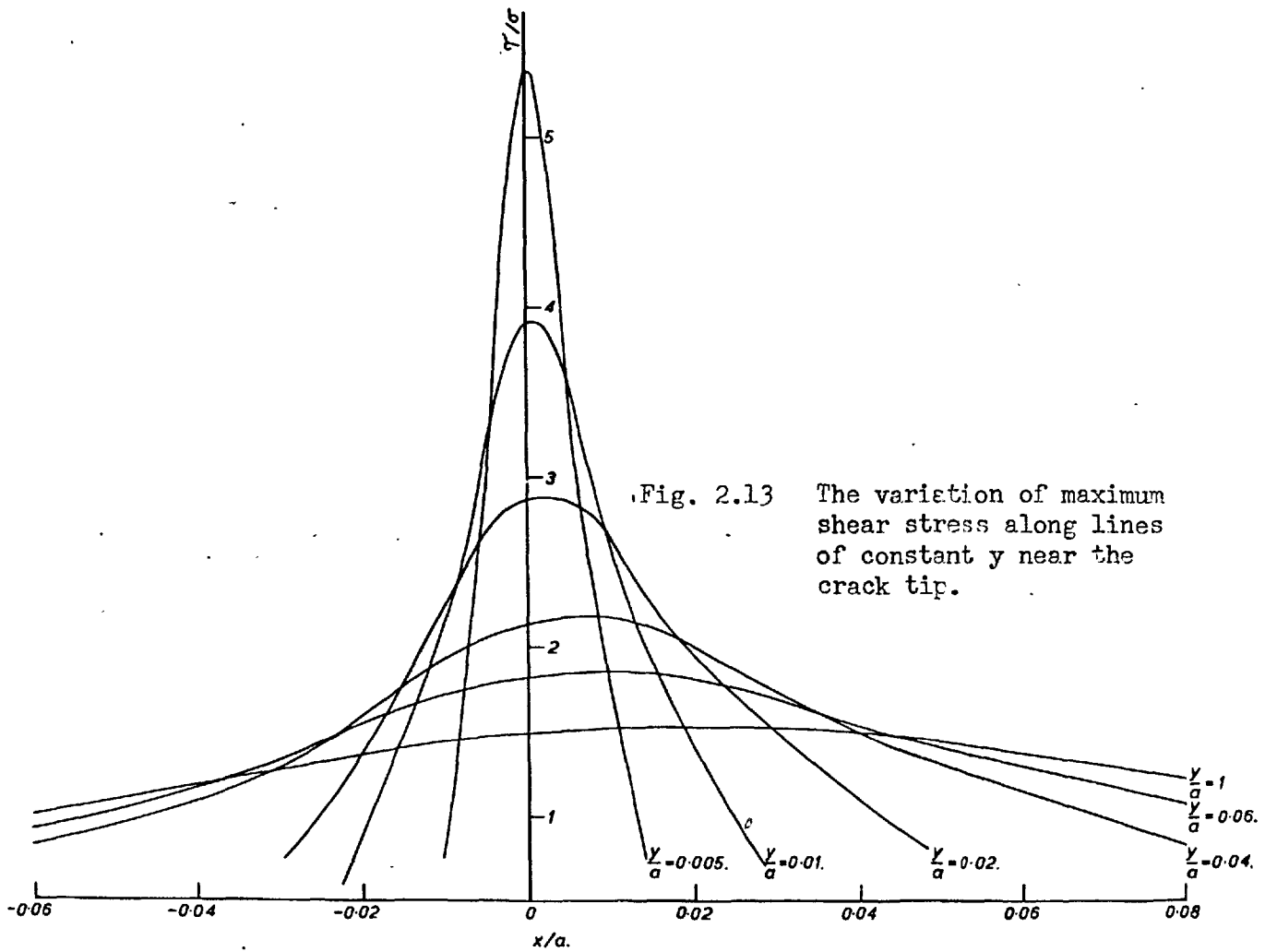

Fig. 2.13 The variation of maximum shear stress along lines of constant y near the crack tip.

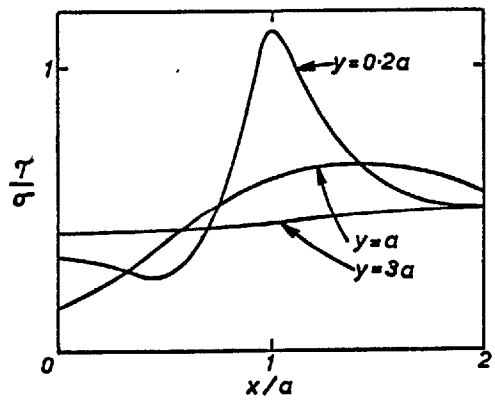

Fig. 2.14 The variation of the maximum shear stress along lines of constant y near the crack tip. (After Rothman and Ross (1955))

the elements of material, assuming that half crack length a is large compared to x and y, so that as the crack grows from 2a to 2a + 2x the stress field is unaltered. These stress histories show that as the crack passes the elements of material they are subjected to a stress pulse; the closer the elements are to the crack the greater the pulse is in magnitude and the shorter it is in time. It would now be possible, using these stress histories, to conduct an analysis similar to that completed by Hahn et alia (1963). Such an analysis would be of doubtful value because of the approximations involved and would also be extremely tedious; this tedium may be circumvented by comparing the stress histories with the results, relating delay time and yield stress, obtained by Krafft and Sullivan (1962) for mild steel.

For the curves of fig. 2.13 the duration of the pulse is taken as the period of time that the stress is greater than $\frac{3}{4}$ of its maximum value and the stress is assumed to remain at the maximum value for this time. Belsheim (1957) used a similar approximation to compare his experimental results with those obtained by other

workers and found good agreement. Now graphs of stress versus time of loading may be drawn, using the above approximation, one point being obtained from each curve of fig. 2.13; figs. 2.15 and 2.16 show the effects of varying crack velocity v, and varying applied stress σ, respectively. On these graphs the lower values of time correspond to smaller values of y; thus as is expected the closer the crack passes to an element of material, the larger is the stress upon it, and the shorter the duration of this stress. The results of Krafft and Sullivan (1962), for a mild steel similar to that used in the experimental work reported later, may be superposed upon fig. 2.16 to predict whether or not the delay time of the steel for a particular stress will be exceeded. Fig. 2.17 shows Krafft and Sullivan's results for supported stress versus delay time plotted upon fig. 2.16; the vertical lines of fig. 2.17 show values of constant y; each of these lines is obtained from one of the curves of fig. 2.13. A 10 inch crack and a crack speed of 5×10^4 inches per second are chosen to illustrate the technique.

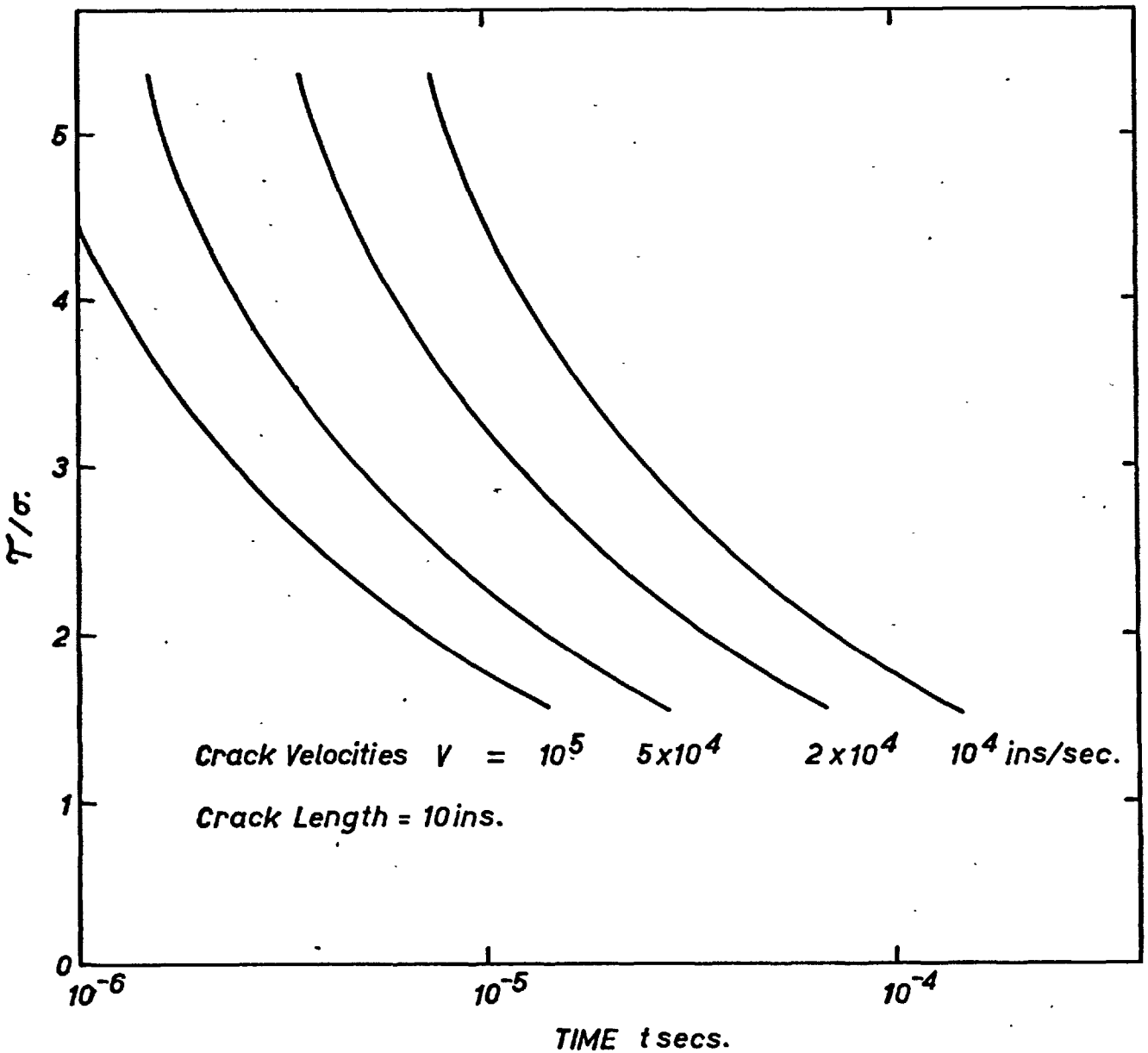

Fig. 2.15
The variation of the magnitude of the shear stress pulse on elements of material near a crack with the duration of the pulse for various crack velocities.

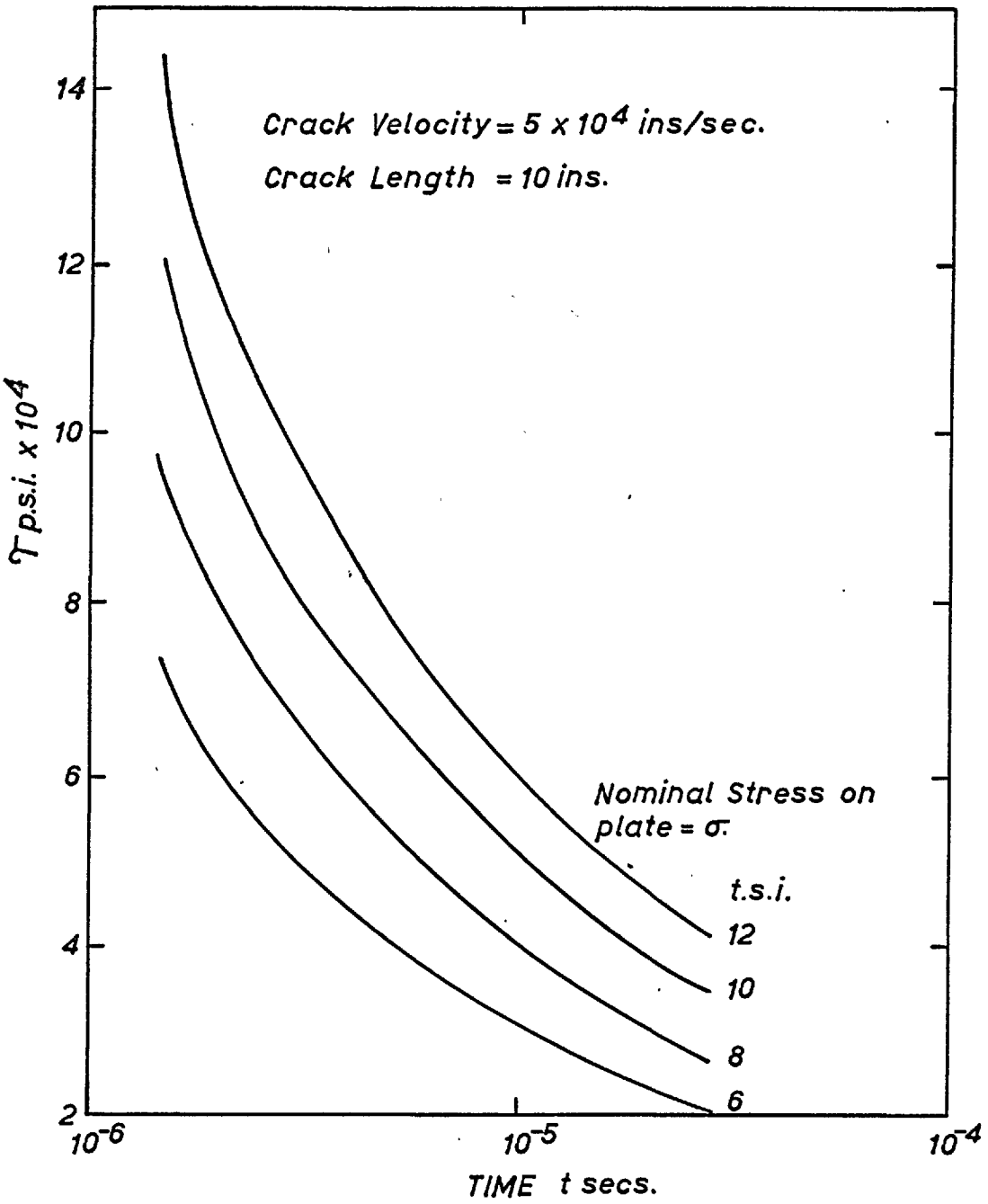

Fig. 2.16 The variation of the magnitude of the shear stress pulse on elements of material near the crack with the duration of the pulse, for various values of applied stress.

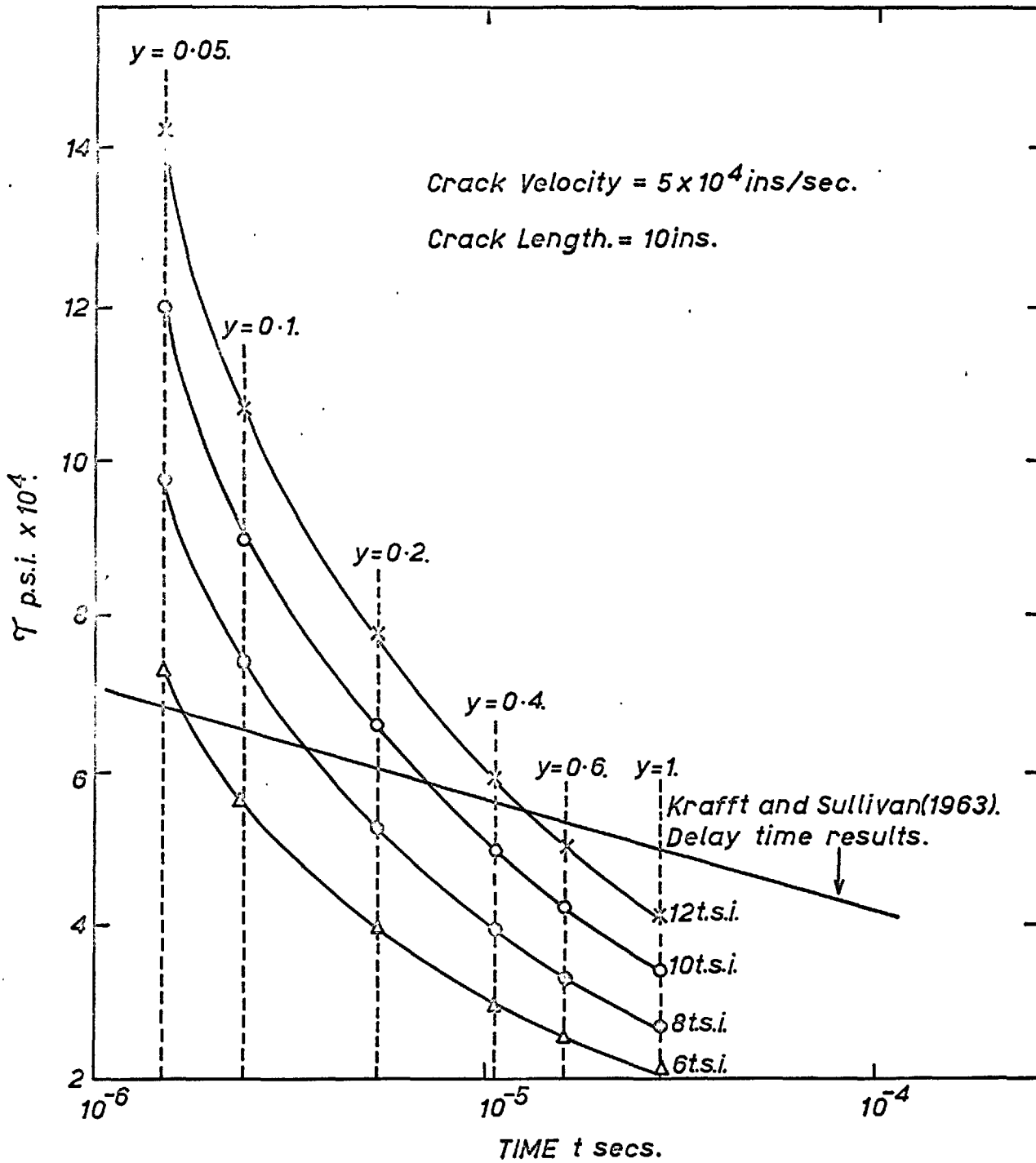

Fig. 2.17 Krafft and Sullivan's (1963) delay time results superposed on fig. 2.16.

Obviously similar curves can be obtained for any desired crack length and velocity. Now only those elements of material which are subjected to a stress pulse which lies above the Krafft and Sullivan (1962) delay time, supported stress line on fig. 2.17 will yield. Thus for example on this model a crack half length 10 inches, with each end extending at 5×10^4 inches per second, under an applied stress of 8 tons per square inch, will have a yield zone extending approximately 0.13 inches above and below it, at its tips. From a series of graphs similar to fig. 2.17, but for varying crack length, fig. 2.18 has been plotted, and shows the variation of y for the elastic-plastic boundary with $\bar{\sigma}$ and a. The effect of varying crack velocity on fig. 2.18 is shown in fig. 2.19.

It is shown later that this crack model gives more reasonable values for plastic zone depth than Hahn, Gilbert, and Reid's (1963) model. In the above model yielding is assumed to occur when the shear stress in the xy plane satisfies certain conditions. This shear stress might not be the largest when stresses in three

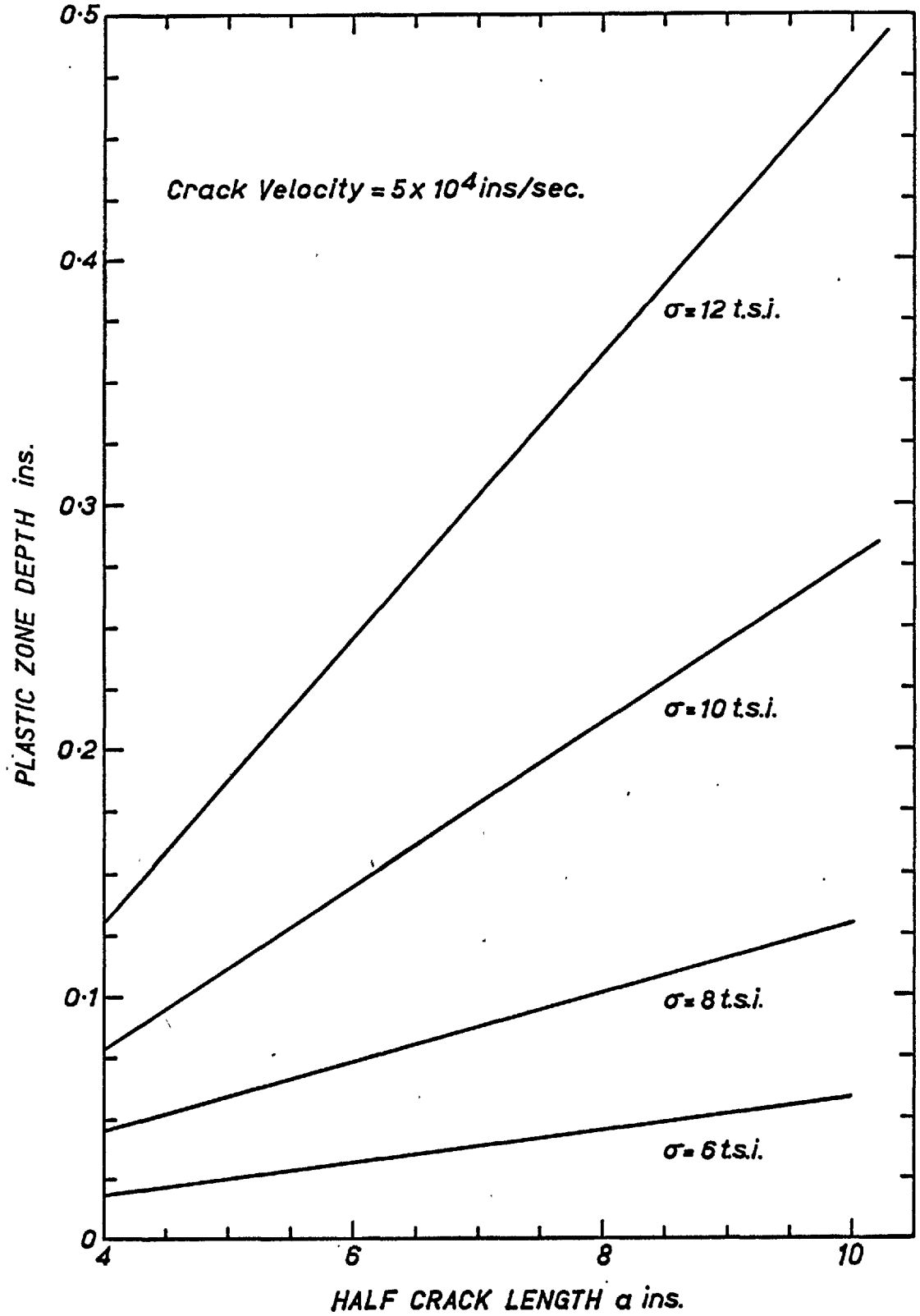

Fig. 2.18 The variation of the plastic zone depth with applied stress and crack length.

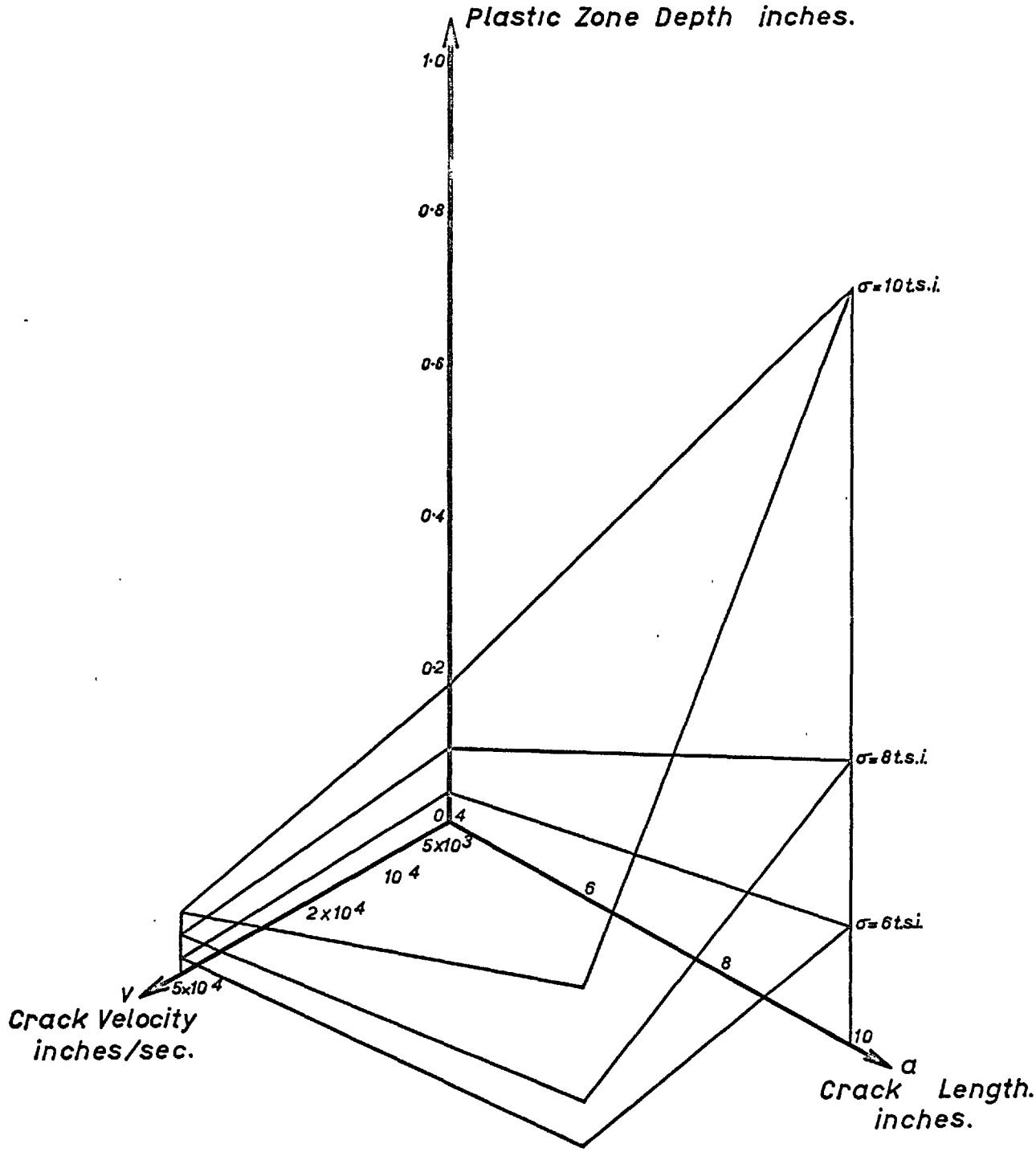

Fig. 2.19 The variation of plastic zone depth with crack velocity, applied stress and crack length.

dimensions are considered. The model will thus represent conditions of plane strain better than plane stress. It should be noted here that the "elastic yield" zone model will be more accurate than may be at first thought, when used for a material which exhibits a delay time, for yielding due to readjustment of stress caused by plastic flow, can only occur after two delay times have elapsed. The assumption that a is large compared to x will for a 4 inch crack moving at 5×10^{4} inches per second cause an error of approximately $\frac{1}{2}$ percent in the estimated plastic zone depth. The assumption that the stress distributions ahead of moving and stationary cracks are similar is not strictly true, as will be shown later; and this effect probably causes errors when quantitative results are obtained from this model.

3 Experimental Measurement of the Stress Field about Stationary Cracks

3.1 Introduction

The strain fields around moving and stationary cracks are similar provided that the crack speed is small compared to the speed of elastic strain waves in the material, and the material is strain rate insensitive. Unfortunately neither of these two criteria are applicable to a brittle fracture propagating through a steel plate. However the stationary stress field is easier to obtain, both theoretically and experimentally, than the dynamic stress field, and is useful as a starting point for the study of the dynamic case.

3.2 Cracks in Elastic Material

Rothman and Ross (1955) found close comparison between their theoretical predictions and experimental results from a photoelastic model with a central slit loaded in tension. Using a photoelastic model of a cleavage crack in a slender rectangular bar, Guernsey and Gilman (1961) found that Irwin's (1957) approximate formula predicted the stress field close to the crack, provided the effects of bending stresses in the cleavage model were not apparent. The theoretical predictions of Westergaard (1939) and Williams (1957) were both found to give the stress concentration factor about edge slits in thick tensile specimens with reasonable accuracy by Fessler and Mansell (1962). They used a stress freezing technique on a photoelastic model, and then cut and analysed slices normal to the plane of the crack. They found no significant differences between the stress concentration factors at the plate surface and in the body of the plate. Using photoelastic coatings on tensile specimens with central cracks, Dixon and Visser (1961) found good agreement between the elastic theoretical predictions of Dixon (1961) and experiment.

3.3 Cracks in Elastic-Plastic Materials

The strain distributions about central fatigue cracks in nine different sheet materials were obtained using a photoelastic coating technique by Dixon and Strannigan (1963). They compared Dixon's (1961) theoretical predictions with their results and showed that the strains in the plastic region near the crack tip were higher than predicted by elastic theory, although the shear strain distributions were similar in form to the elastic solution for all the materials used except mild steel. In the mild steel thin plastic zones grew ahead of the crack; mild steel was the only material used which showed a yield drop. Photostress measurements on the extent of the plastic zones at the tips of axial faults in cylindrical steel pressure vessels under load were made by Bevitt, Cowan and Stott (1964). These measurements showed fair agreement with Dugdale's (1960) formula, relating plastic zone size, gross stress, yield stress and fault length.

Dugdale (1960) measured plastic zone lengths ahead of both central and edge slits in tensile specimens of high nitrogen steel, which responded to strain etching, and found that the results were in good agreement with his theoretical predictions. Yield patterns in Charpy specimens showing the thin yield zones about notches have been obtained using strain etching techniques on steel by Knott and Cottrell (1963) and Wilshaw (1964). By quenching iron-3% silicon from a hydrogen atmosphere, Tetelman and Robertson (1962) formed cracks opened by the internal pressure of hydrogen. This is the problem treated theoretically by Sneddon (1946) and the arrangement of dislocation etch pits near a hydrogen filled crack shows some of the features predicted by the elastic theory.

Lüders line formation in edge notched tensile bars and tensile bars containing circular holes was studied by Durelli, Kobayashi, and Hofer (1961) using a brittle coating on mild steel plate. Their results showed thin yield zones running perpendicular to the largest tensile stress, and disagreed with the predictions of Allen and Southwell (1950) for the edge notched case,

and of Nadai (1950) for the central hole case. Robertson and Christopher (1956) observed the yield zones at the tip of arrested fractures in steel plates, by a brittle resin coating technique, and by measuring the reduction in plate thickness. The contours of the depressions at the ends of central fatigue cracks in mild steel and an aluminium alloy were measured by Bateman, Bradshaw, and Rooke (1964) using a Talysurf and multiple beam interferometry. They found that; for the aluminium alloy, the surface depressions were approximately circular, unlike the plastic zone shapes predicted by relaxation methods, Stimpson and Eaton (1961), but more like the shape predicted for a crack under shear, Hult and McClintock (1957); and, for mild steel the depressions were similar to Dugdale's (1960) results.

4 Experimental Measurement of the Stress Field about Moving Cracks

4.1 Introduction

The stress in a material is always calculated from the measured strain, as there is no method by which stress can be determined directly. None of the methods available for measuring strains in the body of a material is applicable to the problem of a running fracture, because of the high speed of propagation of the fracture, the large strain gradients near the tip of the fracture, and the curved shape of the crack tip. However there are two ways in which information on the state of stress about a crack may be obtained; by measuring the strain upon the surface of the specimen while the fracture is propagating, and by examination of damage in the specimen after fracture. The former method is difficult because of the high speed of propagation of the crack, the large strain gradients in a small area near the tip of the crack, and the variation from small elastic strains away from the crack to large plastic strains near the crack. However this method has been applied to the problem and is discussed in this chapter.

4.2 Wire Resistance Strain Gauge Measurements

There are two main disadvantages of resistance strain gauges when used to determine the strain around a crack. Firstly a strain gauge has a finite gauge length and only records the average strain over this length, thus making the measurement of steep strain gradients difficult. Secondly the gauge only records the strain at one place, so to obtain an overall picture of the strain field many recording channels would be required. The exact fracture path of a brittle crack cannot be anticipated and so the relative positions of the crack and gauge cannot be forecast.

Rolfe and Hall (1961) ran brittle fractures across 6 foot wide plates and measured the strain by eleven strain gauge rosettes mounted near the expected fracture path. Because they had a limited number of recording channels they superimposed their records from five tests to give strain contours around a crack for varying crack lengths. They noted that for cracks longer than 22 inches the strain field did not change with crack length. In a later report on the same

research, Hall and Barton (1963), it was noted that when the strain gauge rosette was mounted within approximately $\frac{1}{2}$ inch of the horizontal crack, both the horizontal and vertical gauges peaked in tension as the crack passed them. This biaxial state of tension was only observed when the gauges were located sufficiently close to the fracture.

Similar work has been reported by Robertson (1957) and Cargill (1963); their results also show a region of biaxial tension close to the crack. One side of their plates were coated with a brittle resin and they observed that the depth of cracking in this coating increased for approximately the first three feet of fracture but remained constant thereafter, indicating that a running crack acquires a steady condition of propagation only after it has travelled for some distance into the plate. Results obtained by Akita and Ikeda (1959)(b) also indicated that there existed a region of biaxial tension associated with the fracture.

4.3 Photoelastic Strain Measurements

By using a photoelastic method to record the strain around a moving crack, the main disadvantages occurring when using wire strain gauges are overcome; the effective gauge length now depends upon the resolution of the optical system, and the strains over a large area may be recorded. However new drawbacks occur, because of the high speed of propagation of the phenomena associated with brittle fracture, a photographic technique with a short effective exposure time must be employed. On account of the short exposure, and light intensity losses in the optical system, an intense light source must be used. One photograph will only yield the strain configuration for one particular crack length, and to gain a fuller picture high speed ciné techniques must be used. Ciné cameras working at these high speeds are expensive and will only yield a limited number of frames. It is only possible to obtain isoclinic or isochromatic recordings from one test, thus rendering separation of individual principal stresses difficult, however the isochromatic pattern is probably the most useful way of

presenting the strains about a crack. There is a limit to the applicability of results from fractures of plastics to the problem of brittle fracture of steel, because of the differing physical properties of the two materials. Thus a photoelastic coating technique should yield more useful results than results obtained from a photoelastic model. The stress-optical coefficient for columbia resin varies with strain rate and this effect must be considered when analysing the results of dynamic investigations on photoelastic models, Wells and Post (1958), and, Goldsmith and Dabaghian (1961). However if a photoelastic coating technique is employed this effect need not be taken into account as the strain-optical coefficients of columbia resin and commercial photostress are strain rate insensitive, Clark (1956) and Cole, Quinlan and Zandman (1960) respectively. However the speed of propagation of elastic waves is higher in metal than in photostress coatings, Cole, Quinlan and Zandman (1960), and, Duffy and Lee (1961); this effect will cause errors if thick photoelastic coatings are used.

The strain-optical coefficient of photostress varies with temperature, but over the range usually of interest in crack propagation tests (-50°C to 25°C) it is reasonably constant, Folister (1961). Errors in the results obtained by the photoelastic coating technique might be caused by the coating not following the deformation of the steel. This effect would be most likely to occur in the vicinity of the crack tip where the large strains and high rates of strain might break the bond between the coating and the steel, or crack the coating before the steel fractures. Dixon and Visser (1961) reported cases for fatigue where the underlying metal cracked but the coating remained whole, and where the adhesive bond between the coating and metal had broken.

The isochromatic patterns about moving cracks in columbia resin were obtained by Wells and Post (1958). They found that the dynamic stress distribution was very similar to the static stress distribution for cracks of comparable length, and that the strain perturbation associated with a running crack grew uniformly in all directions proportionally to the crack

length, provided specimen edge effects were negligible, fig. 4.1. Irwin (1958) showed that Wells and Post's (1958) results compared well with Westergaard's (1939) theoretical predictions.

The strain field about a propagating crack in mild steel has been studied by van Elst (1964)(b) using a photoelastic coating technique. This is the method used in the research reported in this thesis. Both research projects started at the same time, but I learnt of van Elst's work at a late stage in this research. Van Elst used a high speed framing camera to obtain sequences of isochromatic patterns around moving fractures, initiated by impacting the specimens with a bolt gun in the direction of crack propagation. These isochromatic patterns (fig. 4.2 shows a typical example) exhibit a region of low shear strain close to and ahead of the fracture, which corresponds to the biaxial tension revealed by strain gauges. The results also show stress waves ahead of the fracture and a complex pattern of waves behind the fracture front. Van Elst correlated the frequency of the stress waves ahead of the crack with the step-wise

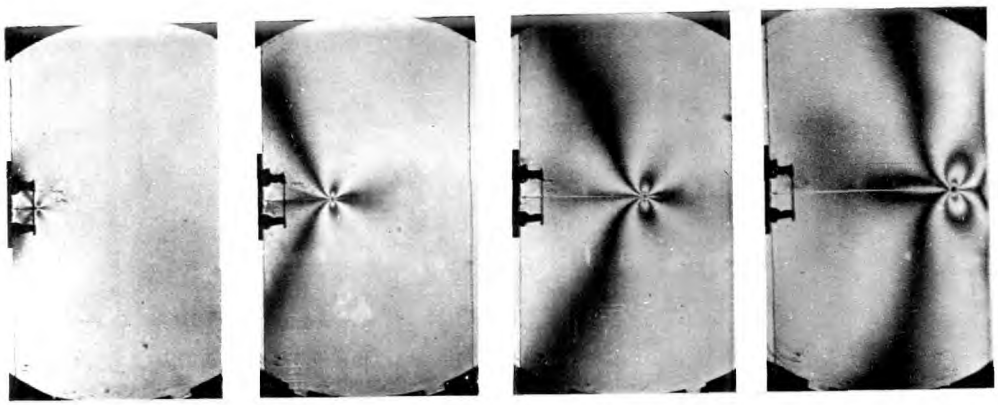

Fig. 4.1 Isochromatic patterns around successive positions of a crack moving from left to right through columbia resin. (after Wells and Post (1958))

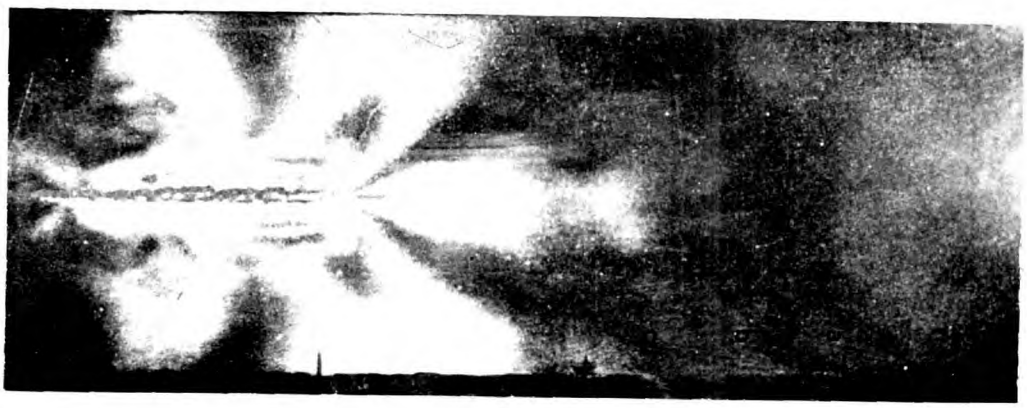

Fig. 4.2 Isochromatic pattern in a birefringent coating on the surface of steel containing a brittle fracture moving from left to right. (after van Elst (1964))

propagation of the crack. Using streak and framing camera recordings of the surface deformation during crack propagation van Elst obtained more evidence for the intermittent propagation of brittle fracture. These fractures often exhibited large shear lips, van Elst (1963).

5 Apparatus

5.1 Introduction

Of the tests for brittle fracture the one which most nearly simulates service failures is the Robertson test. In this test a crack is caused to run into a steel plate at a controlled temperature and stress, and the response of the steel recorded in various ways. The Robertson type test was chosen for this research. To record the strains about the moving crack, the photoelastic coating technique was used, the resultant isochromatic pattern being photographically recorded.

5.2 Tensile Machine

Four loading rigs were used to provide the tensile stress necessary for fracture, in separate tests, a 100 ton Avery machine in the Mechanical Engineering department of Imperial College, a 300 ton machine made for this research, and a C.A T 600 ton machine and a 1200 ton wide plate machine at the Naval Construction Research Establishment, Rosyth.

Some initial tests were performed on an Avery universal testing machine up to loads of 70 tons. The specimen size and shape are shown in fig. 5.1. The loading lugs were tapered to 4 inches wide over the last few inches as this was the maximum size the machine would hold. The specimen was mounted in the machine by means of wedge grips; because of the design and short length of these grips, the specimen sometimes slipped in the grips while a crack was running across the specimen. This slipping caused a reduction in load and the fracture to arrest. A specimen containing an arrested fracture is shown in fig. 5.2.

Because of the unsuitability of the Avery tensile machine's grips, and its limited availability, a tensile rig capable of producing a 300 ton load was made, fig. 5.3. This consisted of a portal frame (F), fabricated from 1 and 2 inch thick plate, on top of which a hydraulic jack (J) was mounted. The load was transferred from the jack to the crosshead (C) by six tie rods (T) with spherical seatings at each of their ends. The crosshead was connected to the upper loading lug by a loading pin (P), again through a spherical

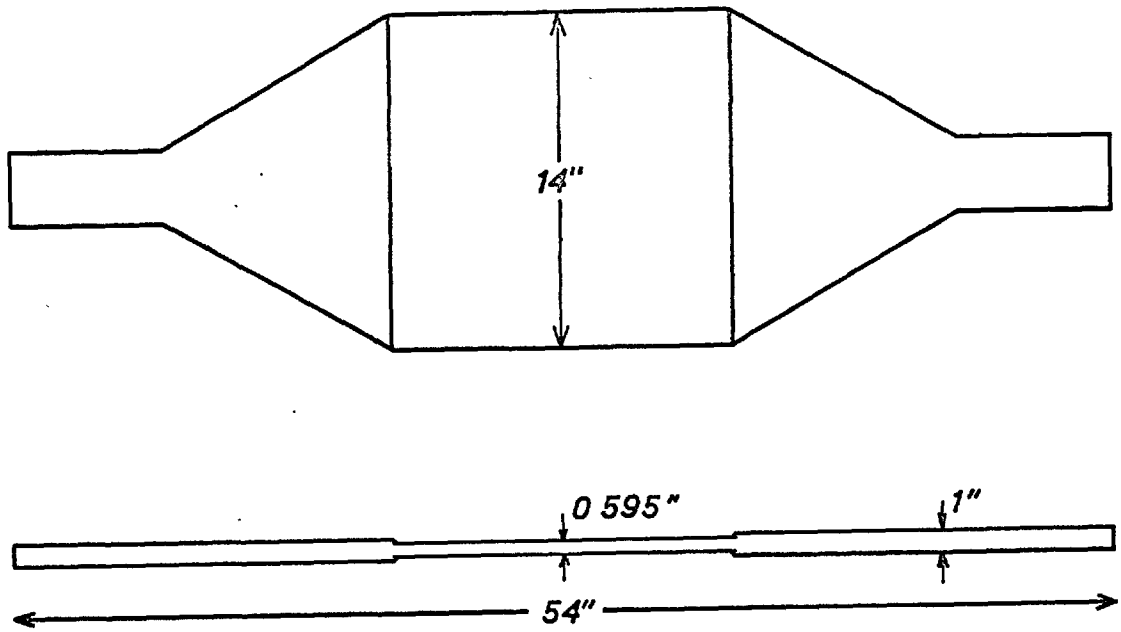

Fig. 5.1 Dimensions of specimens used in the 100 ton Avery machine.

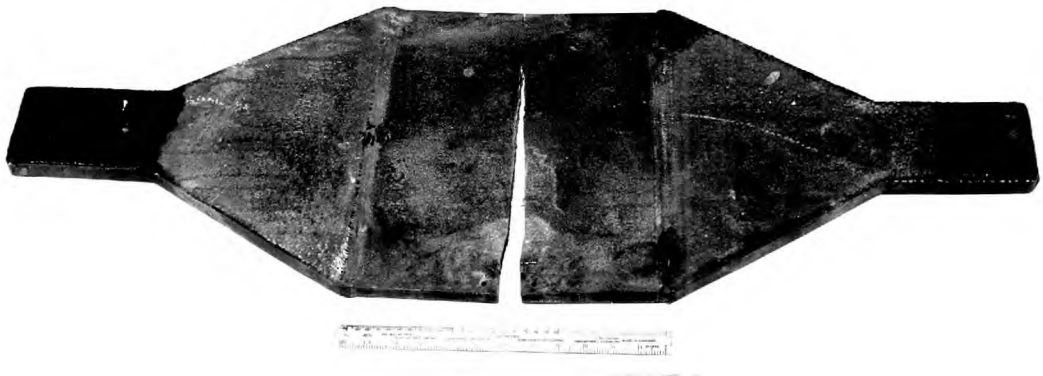

Fig. 5.2 Specimen as used in the 100 ton Avery machine containing an arrested fracture.

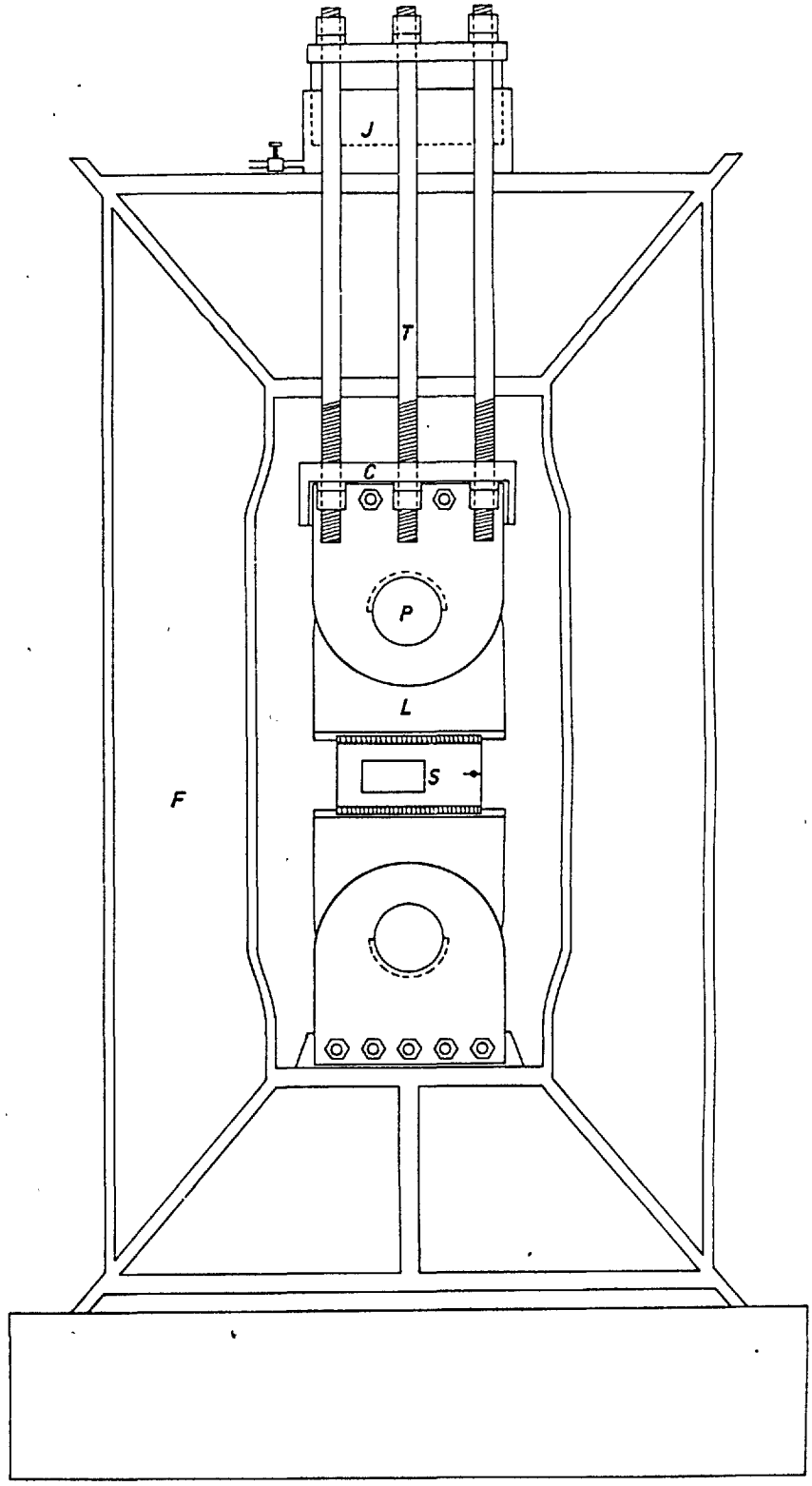

Fig. 5.3 300 ton tensile rig.

seating. The specimen (S), 15" x 6" x $^{27}/_{32}$", was welded between the two loading lugs (L), fig. 5.4. The lower lug was attached to the base of the portal frame through another spherically seated loading pin; these spherical seatings helped ensure uniform loading of the specimen.

The portal frame was one which had been used for compression testing by N.C.R.E., Rosyth. The frame was modified and the rest of the machine fabricated by N.C.R.E. to my design. The crosshead was made up from two 2 inch high tensile plates and proved difficult to fabricate by welding. In transit from N.C.R.E. to Imperial College one of the welds cracked; all the welds were machined out and rewelded, the crosshead being stress relieved after every few weld passes. Forging would have been a better means of fabricating the crosshead.

When in use the rig was mounted on 4 inch timbers on a 2 foot thick block of concrete, on a solid basement floor. The top of the machine protruded 3 feet through a temporary ground floor of the building, giving easy access to the jack and tie rods.

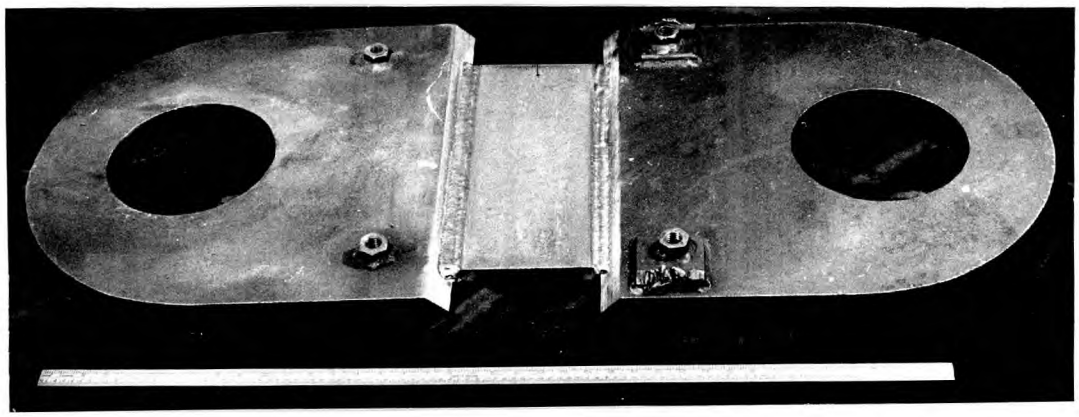

Fig. 5.4 Specimen and loading lugs as used in the 300 ton tensile rig.

During crack propagation tests the machine was steadied by a 5 ton crane, which was also used to load specimens into the machine. During testing the area around the rig was blacked out by rolling a 3 sided hut along the temporary ground floor to cover the top of the machine, the fourth side of the hut and the spaces between the two floors were covered over with blackout material.

Tests at N.C.R.E., Rosyth, were performed on their C.A.T. and 6 foot wide plate machines, which have already been described, Robertson (1953), and Robertson and Christopher (1956) respectively. No special tests were arranged for this research, and so records were taken from specimens broken in the course of the normal research programme at N.C.R.E.

5.3 Specimen Material

Two mild steels, donated by N.C.R.E., Rosyth, were used in the experimental programme.

Steel	Testing Machine	Thickness	Yield Stress	Ultimate Stress	Crack Arrest Temperature
		inches	tons/ sq.in.	tons/ sq.in.	^{o}C
M.S.K.R.	Avery 100 ton	0.595	15.6	27	+ 15^{o}C
F.B. 39	300 ton Rig	0.845	15.3	27.1	+ 17^{o}C

The steels were chosen because of their high crack arrest temperatures, reasonably similar properties, and the large number of tests that had previously been performed on them. The steel F.B. 39 was part of the material from the Fawley tank which failed in 1953, Robertson (1955).

5.4 High Speed Spark Light System

Because of the expense and operational difficulties involved in high speed cine techniques, single shot photography was used to record the isochromatic patterns about moving cracks. High speed photographs may be obtained in two ways: either by means of a fast camera shutter, e.g. a Kerr cell type, or a rotating mirror camera, and a continuous light source; or by means of a continuously open camera and a high speed light flash; both systems have disadvantages. If the former method is employed, the light transmitted by an open Kerr cell is approximately only 1000 times the light transmitted by a closed cell, thus a suitably triggered light source with a low rise time must be used at the beginning of the exposure and a shatter shutter used to end the exposure. The same problems arise when using a rotating mirror camera because after one revolution the mirror will start to rewrite. These two techniques are also difficult to set up and to operate. In the latter method, as the camera is open continuously, the experiment must be performed in darkness, also the light source must be

accurately triggered and have low rise and decay times. This technique was the one used in this research. The flash may be either electrically or explosively generated. The danger to personnel and apparatus of an argon bomb type flash, Cole, Quinlan, and Zandman, (1960), ruled this out as a possible means of illumination. As only about 7% of the light output of the source remains after transmission through the polarizing filters and photoelastic coating, a very intense light source must be used.

A spark light source similar to the one designed by North (1959) was constructed. Only where the source differs from that described by North are details given. A circuit diagram and a photograph of the set up are given in figs. 5.5 and 5.6 respectively. For simplicity a trigger system, fig. 5.7, was used; this varied from North's system in the means of supplying the thyratron grid voltage. The flash may be fired by breaking a contact between B and C, by making a contact between A and B, or manually by closing switch S. When the thyratron fires, the capacitor X discharges through the thyratron and the primary

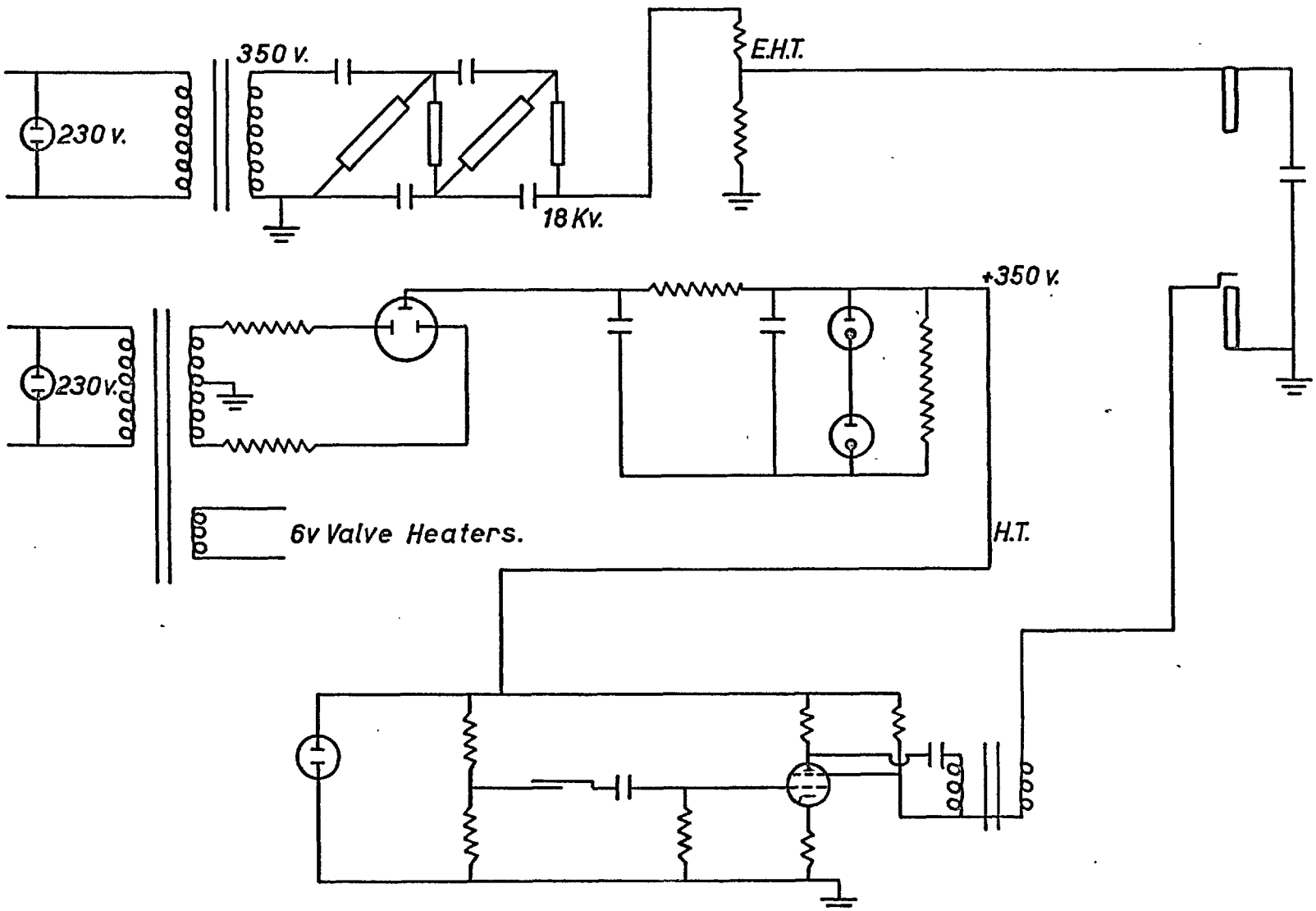

Fig. 5.5 Circuit diagram of high voltage flash light source.

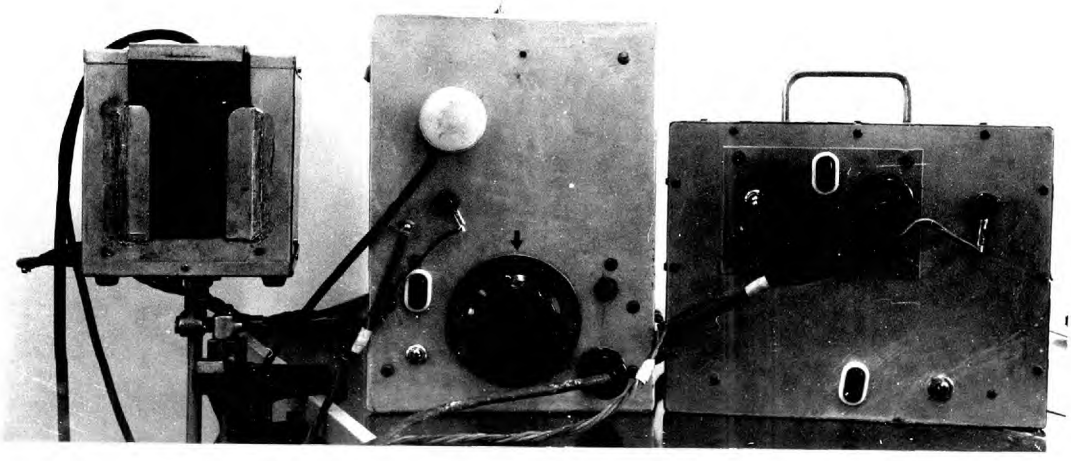

Fig. 5.6 The light source with the extra high tension power supply and the trigger system.

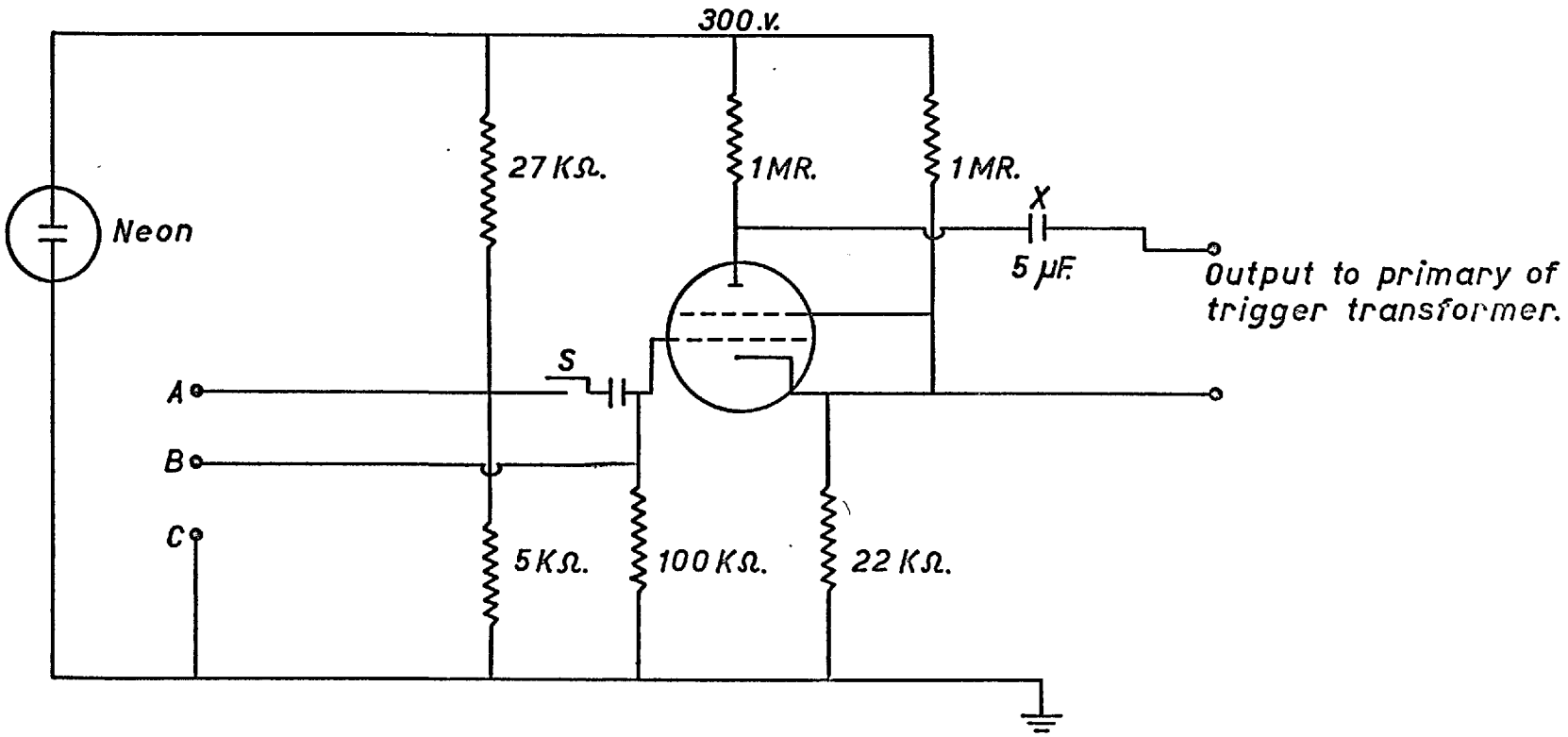

Fig. 5.7 Trigger system used with light source.

windings of the trigger transformer, causing a spark to jump the trigger gap. The main differences between the light source shown in fig. 5.8 and the North unit are: that eight condensers are used instead of one, and a concave mirror is mounted behind the flash, both these features give a greater light output from the source; and the positioning of the trigger gap.
For convenience this gap was in parallel with part of the main flash gap, whereas in North's unit the gaps were mounted in series.

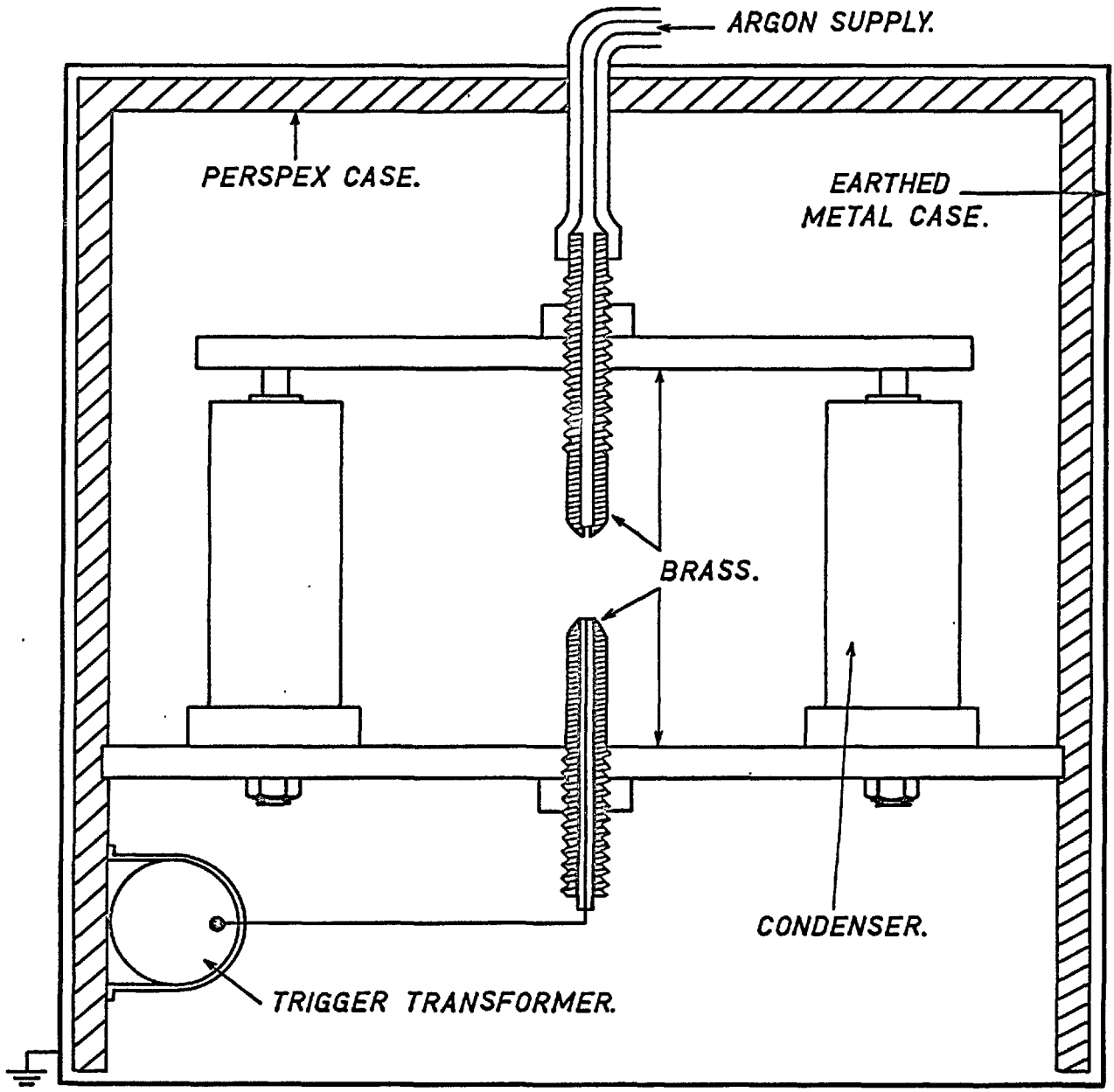

Fig. 5.8 Argon stream light source.

6 Experimental Technique

6.1 Static Tests

The specimens used for static tests were similar to that shown in fig. 5.1, except that plate thickness was 0.13 inches. Cracks were simulated by saw cuts 4 inches long and 0.05 inches wide; if finer cuts were used the photoelastic coating fractured at low loads. Cuts were made from either one edge to simulate a crack advancing across the plate, or from both edges to remove bending stresses. The plates were loaded in the Avery tensile machine, the load being increased in small increments; the residual plastic strain resulting from these loads was recorded by removing the load in between each increment.

6.2 Tensile Loading

Care was taken when welding the specimen into the loading lugs to minimise bending and residual stresses. The specimen and lugs for the 300 ton rig, fig. 5.4, together weighed 3½ hundredweight, and were loaded into the tensile rig by means of a crane. An electrically

driven oil pump was used to raise the hydraulic jack and hence stress the specimen, the oil pressure inside the jack being measured by a gauge, the accuracy of which had been checked to $\pm$ 20 p.s.i. at a load of 1000 p.s.i. The uniformity of loading in the specimen was checked by clamping Huggenberger Tensometers to the specimen and varying the load; because of the careful welding procedure and the spherical seatings on the machine, it was found that the extensions at both ends and on both sides of the specimen were uniform to within 10%, except for one specimen which was not initially straight and showed bending stresses on loading; this specimen was scrapped.

6.3 Temperature Control

The desired testing temperature was attained by cooling the specimen with crushed carbon dioxide held in contact with the specimen and lugs in metal trays; thermal contact between the carbon dioxide and steel was improved by wetting the system with methylated spirit. The temperature was measured by thermocouples spot welded to the plate surface. The metal close to the notch from which the crack was started was cooled

by pouring liquid nitrogen into a container bolted to the specimen. Fig. 6.1 shows the solid carbon dioxide cooling trays and liquid nitrogen container with pouring funnel clamped on to a specimen in the loading rig. The cold junction for the thermocouples, a thermos flask containing melting ice, can be seen with its clamped spring mounting at the right of fig. 6.1.

6.4 Crack Initiation

The fracture was started from a notch, fig. 6.2, consisting of a saw cut, up to a $^{3}/_{16}$ inch diameter hole with a fine jeweller's saw cut continuing $^{1}/_{8}$ inch beyond the hole. To start the fracture a $\frac{1}{2}$ inch diameter bullet, made from hardened silver steel, in the form of a shallow circular wedge, was fired from a "Rapid Hammer" bolt gun into the hole, near the end of the notch. The gun was clamped into position, its barrel being held in place by a jig bolted to the specimen. After passing through the plate the bullet was caught in the lead filled end of the liquid nitrogen container. If a crack was not initiated at the first attempt, a 1 inch diameter hole was drilled in the plate, the hole filled with weld metal, and a new notch cut.

Fig. 6.1 Rear view of specimen mounted in 300 ton tensile rig, showing cooling trays and liquid nitrogen container/bullet catcher.

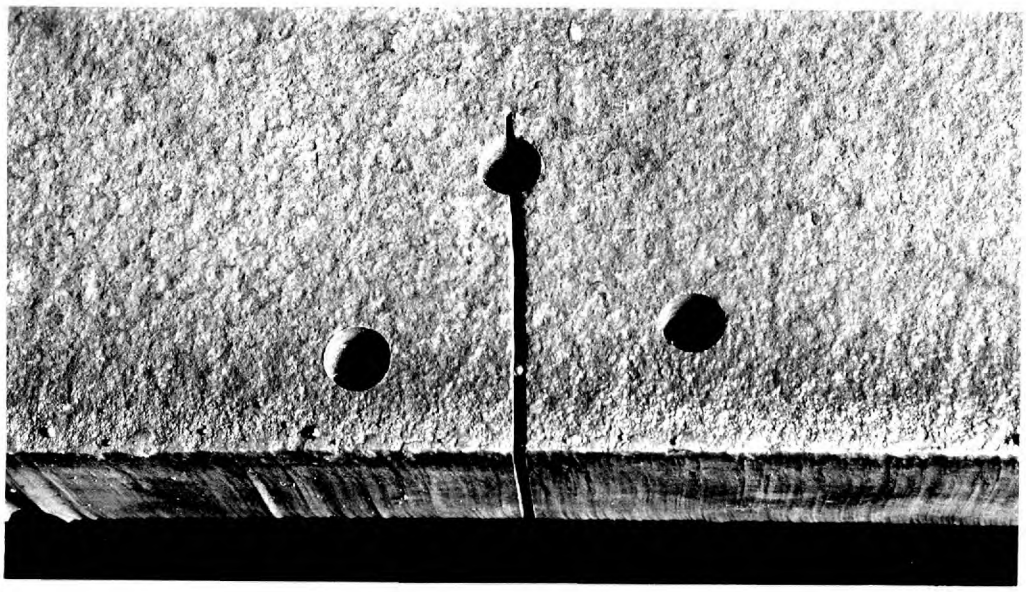

Fig. 6.2 Notch from which the fracture is initiated.

6.5 Strain Measurement

The strains were measured using the photostress technique, where a thin sheet of strain birefringent material is bonded to the surface of the specimen. When a stress is applied to the specimen, the resulting strains on the steel surface are assumed by the layer adhering to the surface, the Young's modulus of the coating being small compared to that of the steel. Coating thicknesses of 1, 2 and 3 millimetres were used, depending on the applied stress and the field of view of the camera. Circularly polarized light passes through the photoelastic sheet twice, being reflected from the bonding material, to give an isochromatic pattern, fig. 6.3. Ideally the polarized light should be normal to the surface coating; this may be accomplished by means of a half silvered mirror. This method was not used, because of the light intensity losses involved, the polarizing effect of the mirror, and because the top surface of the birefringent coating acts as a mirror and would reflect the flash directly back into the camera, masking the isochromatic pattern. However, the flash source and

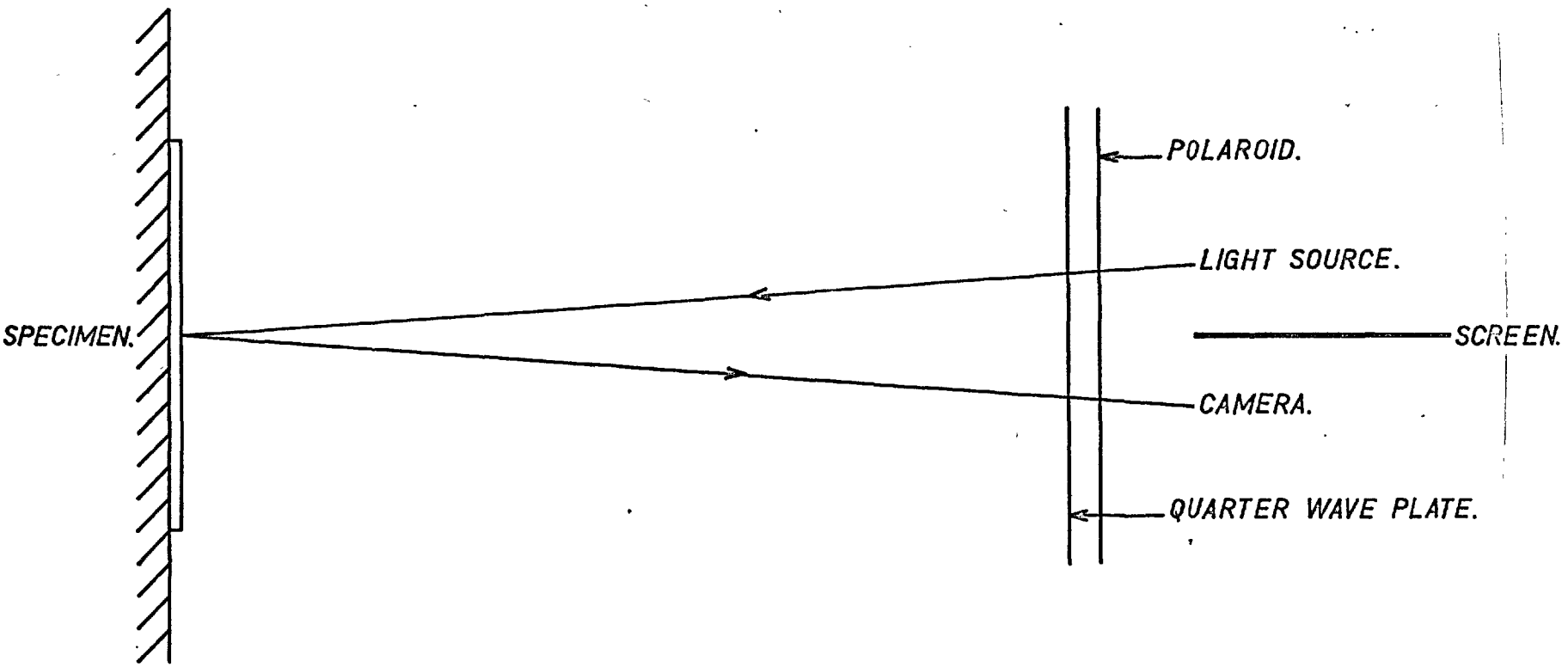

Fig. 6.3 Optical arrangement used to obtain isochromatic recordings.

camera were positioned so that the light rays were nearly perpendicular to the coating, minimising the errors involved. At low temperatures frost formed on the coating but was easily removed with alcohol. At temperatures below - 50°C it was found that the birefringent coating became very brittle, and often cracked; and also that the bonding between the steel and coating weakened.

6.6 Photography

The results from the static tests were recorded on black and white film using a narrow cut filter. This method is used wherever possible, as more fringe orders may be resolved than when colour photography is used, for as the relative retardations of different wavelengths of light increase, extinction overlapping occurs, giving approximately uniform white light. For the dynamic tests a high speed (A.S.A. 140) colour film was used, scarcity of light ruling out the use of a close cut filter and black and white photography. Dark field circularly polarized light was used for all the experiments reported here. A lens from a gunnery

range finder with aperture 1.5 and short focal length was mounted on a reflex camera back, and used to photograph the dynamic patterns, because a large aperture was required to make the best use of the available light. This camera worked well in conjunction with the flash source. A second camera 4 feet from the plate was used to photograph a larger area of plate surface than the first camera. The flash source was triggered by the breaking of a brittle (bismuth) wire bonded to the specimen in the expected fracture path a fixed distance ahead of the area to be photographed. Fig. 6.4 shows the front surface of the specimen with light source and camera with polarizing screens, and bolt gun positioned ready for a test; the brittle wire and birefringent coating can be seen to the left of the gun.

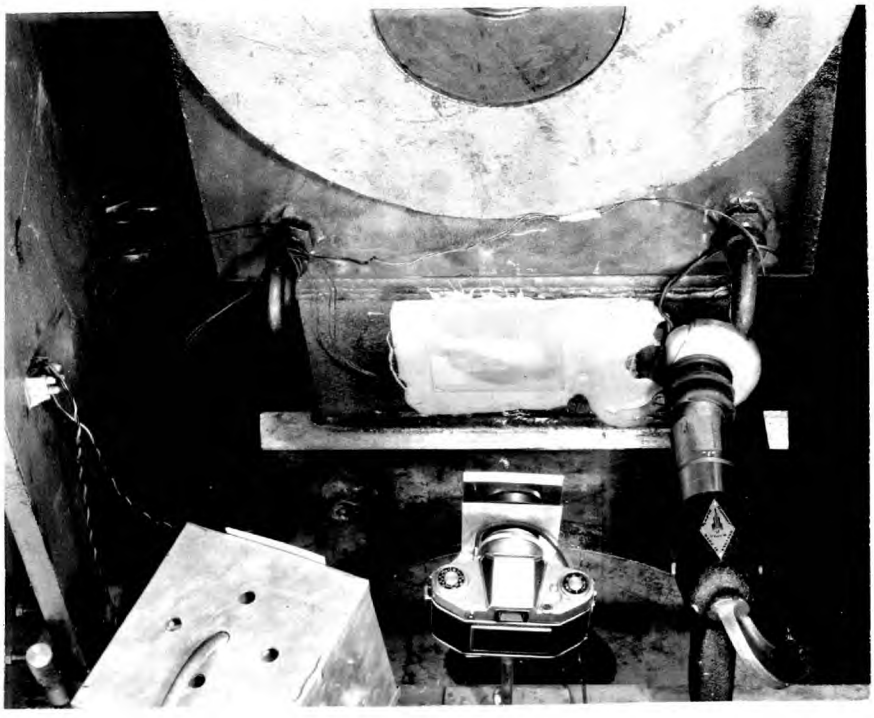

Fig. 6.4 Front surface of specimen in tensile rig showing light source, camera and bolt gun positioned for testing.

6.7 Testing Sequence

The testing procedure in chronological order was as follows:-

1) Load the specimen.
2) Cool specimen to required temperature.
3) Photograph any markings or apparent strain in the coating, that may have formed due to yielding of the steel or temperature effects; the steel and coating have different coefficients of expansion.
4) Connect the brittle wire crack detector to the flash source trigger unit.
5) Check that the flash source is functioning properly.
6) Black out the testing area.
7) Check the load.
8) Check the temperature.
9) Cool the notch with liquid nitrogen.
10) Recheck the temperature.
11) Open cameras.
12) Fire gun to initiate the crack.
13) Close the cameras.

6.8 Drawbacks of the Techniques

The above techniques gave fairly reproducible results but the following difficulties sometimes occurred:-

1) Premature fracture of the brittle wire and cracking of the photoelastic coating.

   This effect occurred at low temperatures and high stresses. If the coating bonding material, an aluminium filled epoxy resin, was used to bond the brittle wire to the steel, this tendency to fracture was lessened.

2) Failure of the light source.

   Initially saturation of the light source with argon caused breakdown of the spark gap under the applied voltage. This was cured by improving the ventilation of the light box.

The condensers in the light box were rated as 5 Kilovolt but were used at about 3 times this value and occasionally had to be replaced. These condensers were used because of their small size and low inductance.

3) Failure to initiate the crack.

Because of the reasonably small size of the specimen, it was difficult to cool the metal near the notch severely while maintaining the rest of the plate at the required temperature. Thus sometimes on firing the gun a crack would not be initiated, presumably because the notch was not sufficiently cold. This could be cured by replacing the metal near the notch with weld metal.

4) Premature crack initiation.

Two specimens fractured while their notches were being cooled; this effect occurred when high stress and low temperature tests were being performed. This effect has been noted by Christopher (1959).

5) Crack failing to follow expected fracture path.

On one specimen the fracture curved away from the centre line of the specimen and did not break the brittle wire. Usually, however, the fracture path did not deviate by more than an inch from the expected path.

Most of the main reasons for the failure of the technique listed above were overcome and towards the end of the experimental programme a successful isochromatic recording of the stress field about a moving crack was obtained in about 80% of the tests performed.

7 Experimental Results for the Strain Fields around Cracks

7.1 Interpretation of the Isochromatic Recordings

For the static tests 3 millimetre thick birefringent coating was used with a strain optical constant, K = 0.08.

where $K = \dfrac{\delta}{(\epsilon p - \epsilon q)(2t)}$

or $\epsilon p - \epsilon q = \delta/(2t)K$

ϵp is the major principal strain

ϵq is the minor principal strain

δ is the relative retardation of the light wave on passing through the coating, the retardation in the direction of the major principal strain minus the retardation in the direction of the minor principal strain

and t is the thickness of the strain birefringent coating. (2t is used in the formula as light passes through the coating twice.)

A Kodak Wratten No. 29 deep red narrow-cut filter and 'Plus X' panchromatic film were used to record the strain patterns. The filter transmits light in the visible range with wavelengths from 6,100 Å to 7,000 Å, while the sensitivity of the film starts to decrease for wavelengths above 6,600 Å; and for measurement purposes the light was taken to be monochromatic with wavelength 6,400 Å. The first black fringe occurs when the relative retardation is one wavelength, or when:-

$$\epsilon_p - \epsilon_q = \frac{(6{,}400 \times 10^{-8})}{(2 \times 3 \times 10^{-1}) \times (.08)}$$

$$= 0.00133$$

Also the principal shear stress is half the principal stress difference or

$$\tau = \frac{\sigma_p - \sigma_q}{2}$$

$$\tau = \frac{(\epsilon p - \epsilon q)}{2} \frac{E}{(1 + \nu)}$$

E is Young's modulus, taken as 30×10^6 p.s.i. for steel, and ν is Poisson's ratio, taken as 0.3 for steel.

Thus the shear stress corresponding to the first black fringe is:-

$$\tau = \frac{0.00133}{2} \times \frac{30 \times 10^6}{1.3} = 15,400 \text{ p.s.i.}$$

The 'n'th black fringe occurs when the relative retardation is n whole wavelengths i.e. when τ is (15,400)n p.s.i.

When white light is used to observe the isochromatic pattern, one particular wavelength of light is extinguished for any given shear strain, and so complementary spectra are seen. Of the colour changes in these complementary spectra the eye is most sensitive to the change from red to blue, or red to green, these changes are called tints of passage and correspond to the extinction of yellow light with wavelength 5,890 Å. Thus, as above, the shear stress

may be found for the first tint of passage as:-

$$\tau = \frac{(5890 \times 10^{-8})}{(2 \times 3 \times 10^{-1}) \times (.08)} \times \frac{1}{2} \times \frac{(30 \times 10^{6})}{1.3}$$

$$= 14,100 \text{ p.s.i.}$$

for 3 millimetre plastic with K factor 0.08.

Subsequent tints of passage occur for values of τ of (14,000) x n p.s.i. where n is a whole number. As the shear stress increases extinction overlapping occurs, thus a relative retardation of one wave length of the extreme red (7,200 Å) is approximately two wave lengths of violet and both of these colours are eliminated together. At larger shear stresses this effect becomes more pronounced, until eventually, at very high retardations, the colour bands become extremely faint and merge into each other giving approximately uniform white light.

7.2 Static Tests

7.2a Specimen Containing a Single Edge Slit

Fig. 7.1 shows the apparent strain field in the specimen under a small load, 0.3 tons giving a stress on the gross section of 0.16 t.s.i. The dark area immediately ahead of the notch occurred during polymerization of the bonding material and must be taken into account when interpreting other results obtained from this specimen. Fig. 7.2 is the same specimen under a gross section stress of 5.93 t.s.i. and shows the isochromatic pattern about the slit plus the superimposed residual apparent strain. Fig. 7.3 gives the pattern caused by the residual plastic strain resulting from a stress of 5.93 t.s.i., on loading the specimen above this stress the birefringent coating fractured.

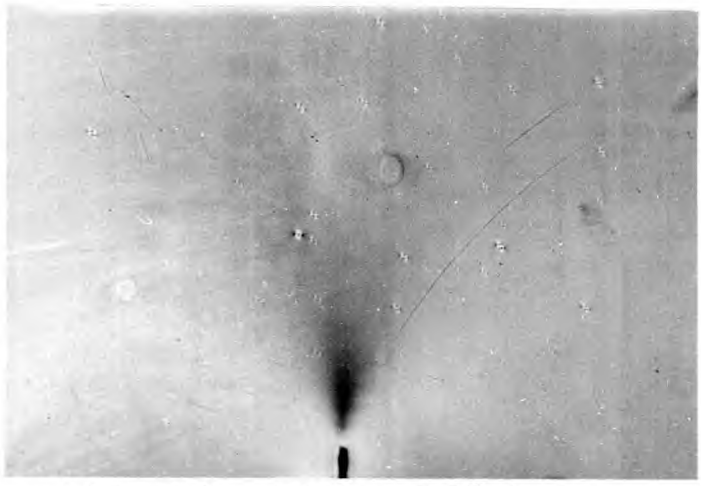

Fig. 7.1 Stress 0.16 t.s.i.

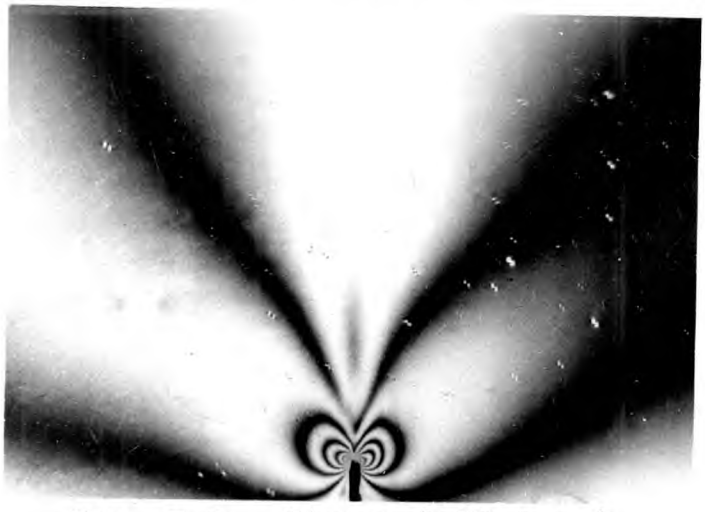

Fig. 7.2 Stress 5.93 t.s.i.

Fig. 7.3 Unloaded from 5.93 t.s.i.

Isochromatic patterns in 3 mm. thick birefringent coating on specimen containing a single edge slit. Scale full size.

7.2b Specimen Containing Two Edge Slits

For zero load there was no residual birefringence in the coating on this specimen. Fig. 7.4 shows the isochromatic pattern for a gross section stress of 5.93 t.s.i., and fig. 7.5 the effects of the plastic strain resulting from this stress. Figs. 7.6 and 7.7 are similar to the above except that a stress of 8.41 t.s.i. was used.

7.3 Dynamic Tests

7.3a Tests on the 100 ton Avery Machine

Fig. 7.8 shows the isochromatic patterns before (left side) and during (right side) brittle fracture propagation. The stress on the steel was 8 t.s.i. and its temperature + 15°C. The photoelastic coating was 3 millimetres thick and 10 inches square. The fracture, which propagated from left to right, arrested 2 inches from the right hand side of the plate; the specimen with the arrested fracture is shown in fig. 5.2. Both the pictures in fig. 7.8 show, the stress pattern due to an edge slit on the right hand side, yield lines at the top left corner emanating from a weld, and a

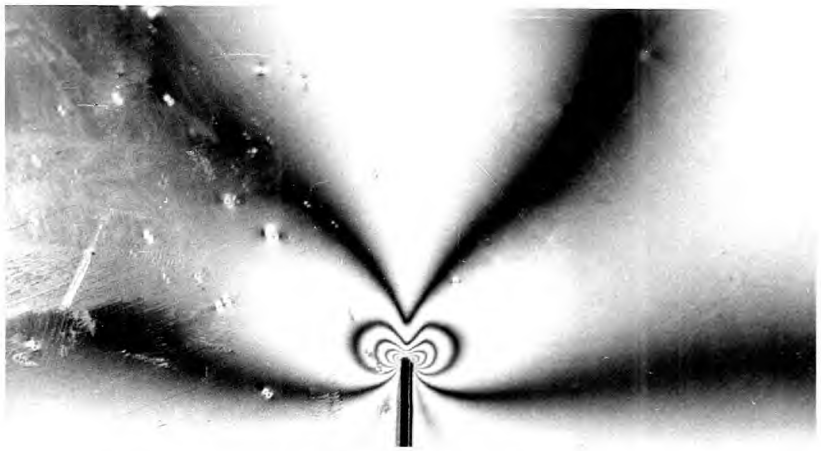

Fig. 7.4 Stress 5.93 t.s.i.

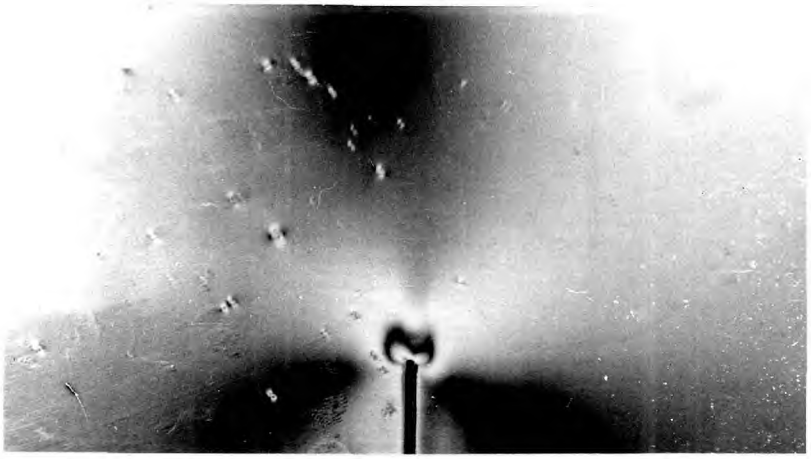

Fig. 7.5 Unloaded from 5.93 t.s.i.

Isochromatic patterns in 3 mm thick birefringent coating on specimens containing two edge slits. Scale full size.

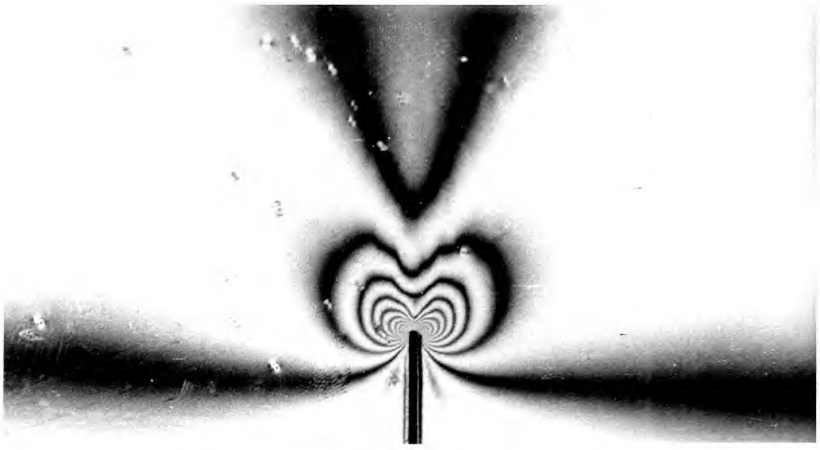

Fig. 7.6 Stress 8.41 t.s.i.

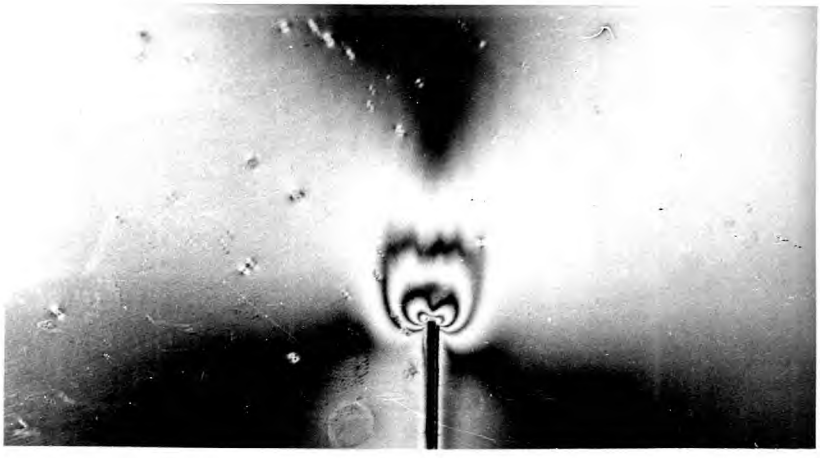

Fig. 7.7 Unloaded from 8.41 t.s.i.

Isochromatic patterns in 3 mm thick birefringent coating on specimens containing two edge slits. Scale full size.

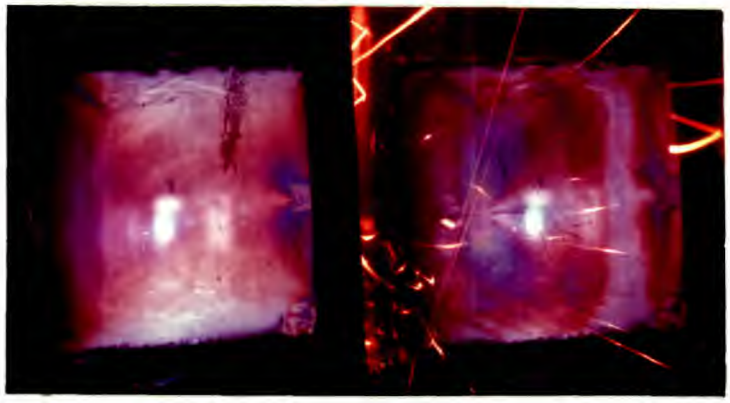

Fig. 7.8 The isochromatic pattern in the photoelastic coating on a specimen at 15°C and under a stress of 8 t.s.i. before (left hand side) and during (right hand side) brittle fracture propagation. The photoelastic coating is 10 inches square. Both photographs show a white spot in the centre of the coating caused by a direct reflection of the flash from the top surface of the coating, and the effects of a saw cut notch at the right hand side of the coating.

white spot near the centre due to the direct reflection of the flash from the top surface of the photoelastic coating. The sparks, orange lines on the picture, are debris from the bolt gun's cartridge; in later experiments a cardboard shield was used to deflect them from the area photographed. The right hand picture shows stress discontinuities ahead of the crack, similar to the shockwaves reported by van Elst (1964). It should be noted that the largest discontinuity lies on the perimeter of a circle centred about the notch; this would indicate that this wave was initiated by the bolt gun. If this wave travels at 16,000 feet per second the crack speed may be calculated as approximately 5,000 feet per second, assuming the wave and crack are initiated simultaneously; this is a reasonable value. This wave represents a tensile pulse in the horizontal direction. The other smaller waves are of opposite sign but also appear to have been initiated by the bolt gun.

Figure 7.9 gives a result similar to the above, though for this test the temperature was + 10°C and the crack propagated through the plate. The bond between the metal and the coating failed over a small area near the crack while the crack was propagating; this caused the disturbance at the left side of the right hand picture. Fig. 7.10 shows the fracture surface with the photoelastic coating; the fracture was half way along this section when fig. 7.9 was obtained.

Figs. 7.11 and 7.12 show the isochromatic pattern before and during fracture propagation in a specimen at 10°C and 10 t.s.i. The coating was 3 millimetres thick and 10 inches square. Stress discontinuities ahead of the moving fracture, of the same sign as the smaller ones in fig. 7.8, are visible. The photographic record of this test was underexposed but is included as it is one of the two records which show shock waves ahead of the fracture. The fracture surface is shown in fig. 7.13.

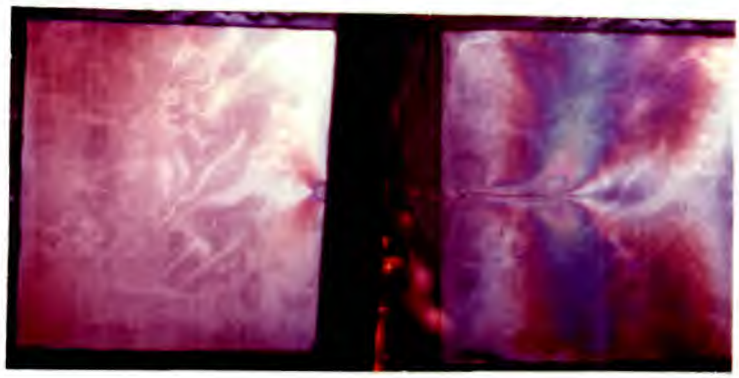

Fig. 7.9 Isochromatic pattern in the photoelastic coating on a specimen at 10°C and under a stress of 8 t.s.i. before (left side) and during (right side) brittle fracture propagation. The photoelastic coating is 10 inches square.

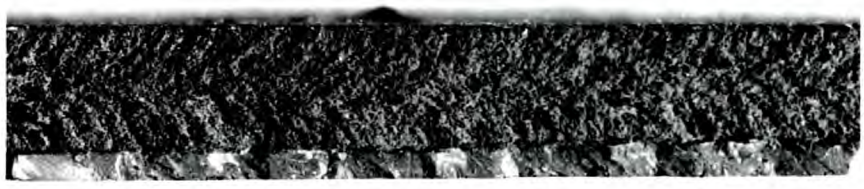

Fig. 7.10 Fracture surface with the photoelastic coating, the fracture was half way along this section when fig. 7.9 was obtained. (Scale full size)

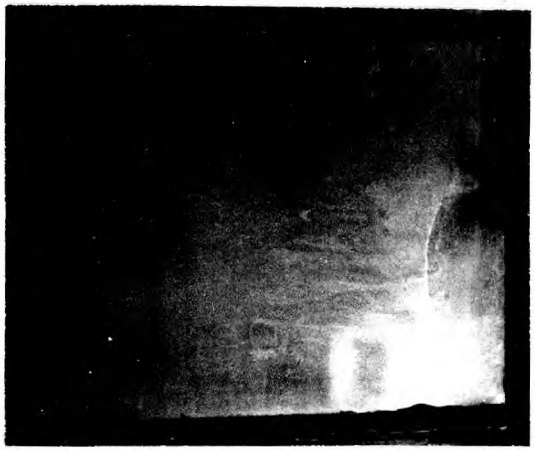

Fig. 7.11 Specimen with 3 mm. thick coating under a load of 10 t.s.i., at 10°C. The area shown is 10" square.

Fig. 7.12 Brittle fracture moving across the area shown in fig. 7.11.

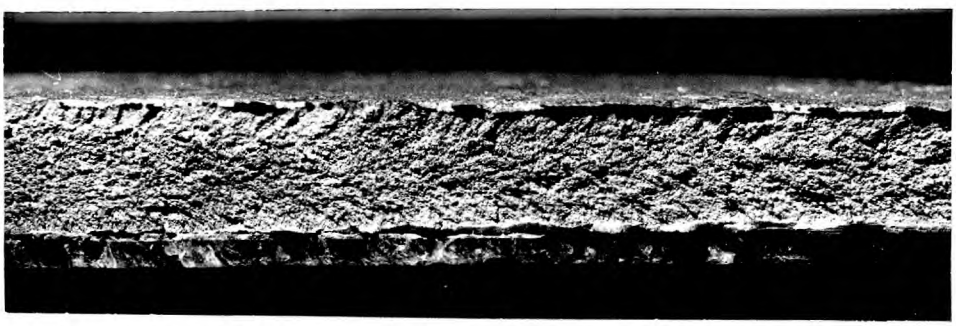

Fig. 7.13 Fracture surface corresponding to fig. 7.12. Scale full size.

An attempt to fracture a specimen at 18°C and 9.5 t.s.i. failed; on replacing the metal adjacent to the notch with weld metal, the birefringence shown in fig. 7.14 was introduced into the photoelastic coating. This specimen was then fractured at 18°C and 10.8 t s.i., the crack arresting after running 11 inches. Fig. 7.15 gives the isochromatic pattern about the propagating fracture; the area photographed was 3.2 inches x 2 inches, and the photoelastic coating 3 millimetres thick. The fracture surface, fig. 7.16, shows pronounced shear lips.

7.3b Tests on the 300 ton Rig

In the tests using this rig no stress discontinuities ahead of the fracture, nor complex stress patterns behind the crack, were recorded by either of the two cameras. All the results presented were obtained with a wide aperture camera 7 inches from the coating, the field of view being 2 inches x 3¼ inches.

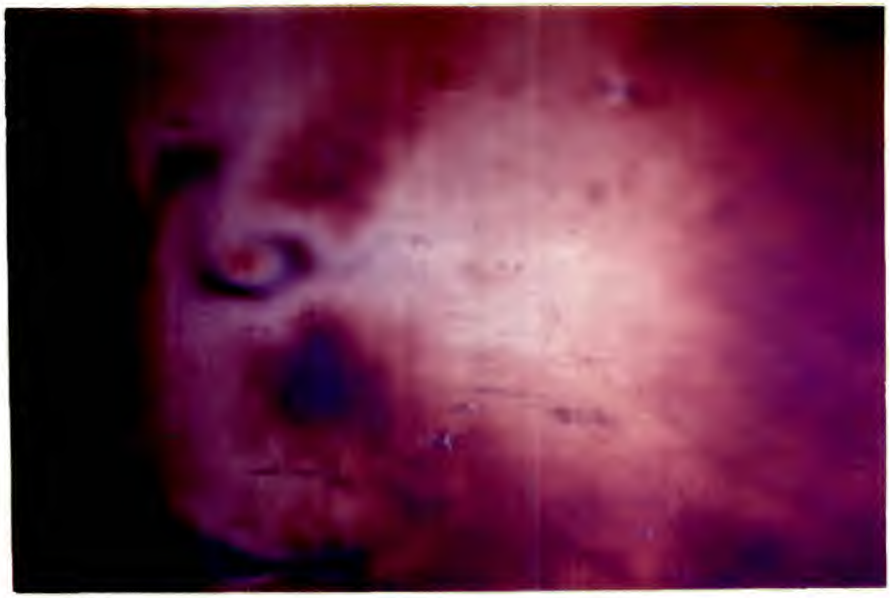

Fig. 7.14 Birefringence caused in 3 mm. thick photoelastic coating while rewelding the specimen notch. The area shown is 2" x 3½".

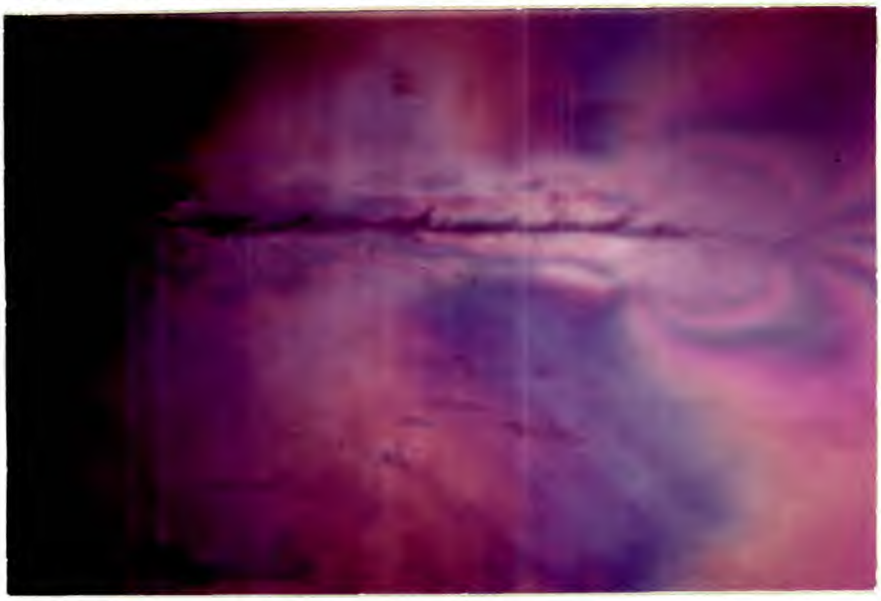

Fig. 7.15 Brittle crack moving under a stress of 10 t.s.i. across the specimen shown in fig. 7.14. The specimen temperature was 18°C.

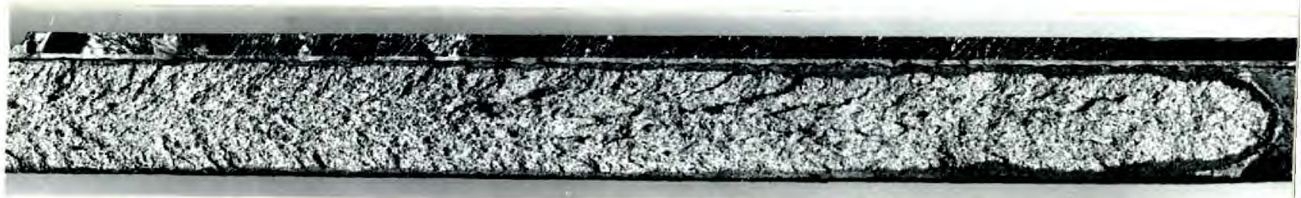

Fig. 7.16 Fracture surface corresponding to fig. 7.15. Scale full size.

Fig. 7.17 shows the isochromatic pattern about a crack moving under a stress of 11.2 t.s.i. in steel at a temperature of - 24°C. The photoelastic coating was 2 millimetres thick. No residual birefringence was visible in the coating before the fracture occurred. The resulting fracture surface is shown in fig. 7.18, the crack being half way along the section shown when fig. 7.17 was obtained.

Fig. 7.19 and 7.20 show the birefringent pattern before and during fracture propagation in steel at + 15°C. and under a stress of 9.9 t.s.i. The photoelastic coating was 1 millimetre thick. Fig. 7.21 is the resulting fracture surface; the crack was halfway along the section shown when fig. 7.20 was obtained.

Figs. 7.22, 7.23 and 7.24 are similar to figs. 7.19, 7.20 and 7.21, except that a stress of 7 t.s.i., a temperature of - 15°C, and coating thickness of 2 millimetres were used. Fig. 7.25 shows the birefringence caused by plastic deformation which occurred while the crack propagated.

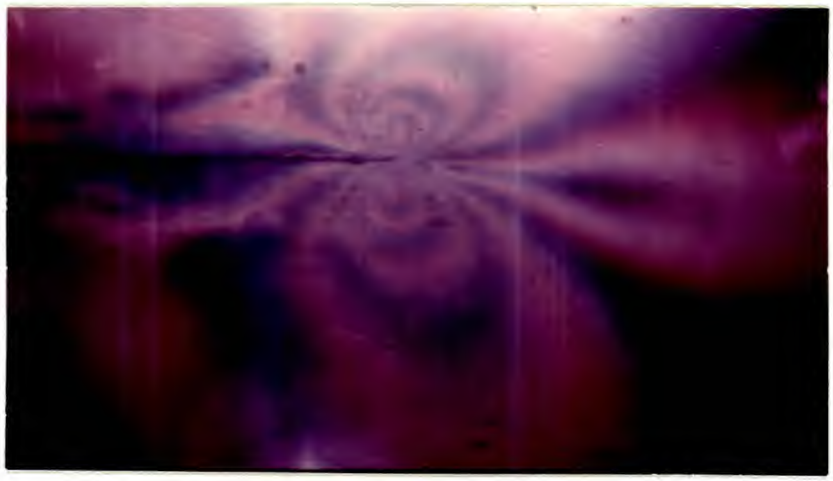

Fig. 7.17 Isochromatic pattern about a crack moving under a stress of 11.2 t.s.i. in steel at a temperature of - 24°C. The photoelastic coating is 2 mm. thick.

Fig. 7.18 Fracture surface corresponding to fig. 7.17. Half actual size.

Fig. 7.19 Isochromatic pattern in a specimen at 15°C under a stress of 9.9 t.s.i.
The photoelastic coating is 1 mm. thick.

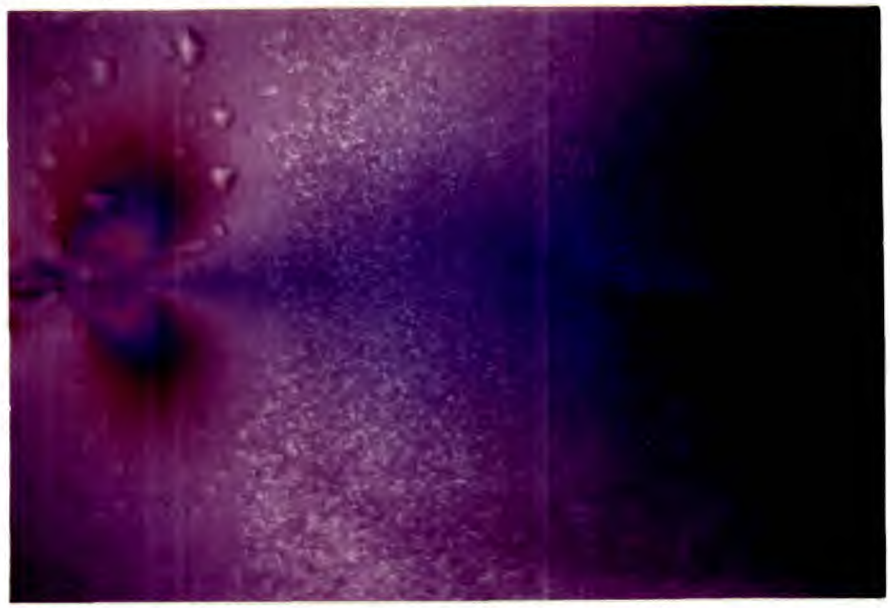

Fig. 7.20 Isochromatic pattern about a crack moving through the area shown in fig. 7.19.

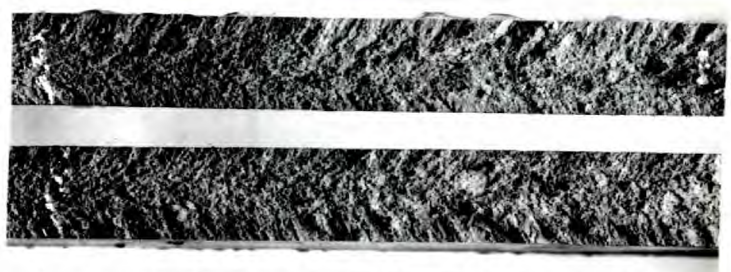

Fig. 7.21 Fracture surface corresponding to fig. 7.20.
Half actual size.

Fig. 7.22 Isochromatic pattern in a specimen at - 15°C under a stress of 7 t.s.i.
The photoelastic coating is 2 mm. thick.

Fig. 7.23 Isochromatic pattern about a crack moving through the area shown in fig. 7.22.

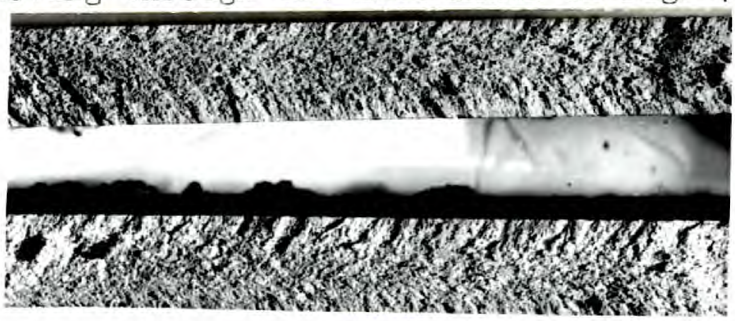

Fig. 7.24 Fracture surface corresponding to fig. 7.23.
Half actual size.

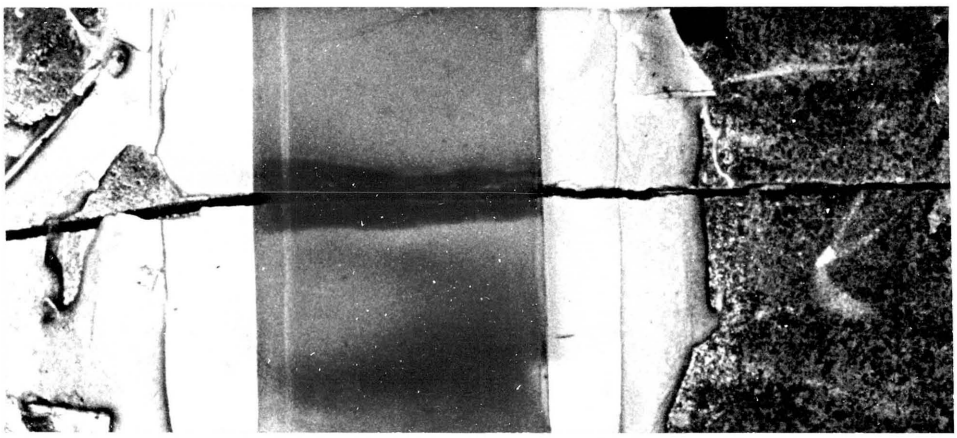

Fig. 7.25 Residual birefringence after fracture in the photoelastic coating on the specimen shown in fig. 7.22.

A photograph of an area approximately 2 inches ahead of a fracture showed no shear stress changes, due to the moving fracture, observable in 2 millimetre thick coating. The temperature was + 14°C and the stress 8.5 t.s.i.; the resulting fracture surface is shown in fig. 7.26.

Two tests were performed to find the stress state immediately behind the crack tip. Fig. 7.27 shows yield lines in the plate before fracture propagation, the stress being 10.5 t.s.i. and the temperature - 3°C. The photoelastic coating was 1 millimetre thick. Fig. 7.28 gives the isochromatic pattern behind the fracture; the crack tip is estimated to be 1 inch beyond the right hand side of the photograph. Fig. 7.29 shows the resulting fracture surfaces; the centre of the section shown corresponds to the length of fracture in fig. 7.28. Figs. 7.30 and 7.31 are similar to those in figs. 7.28 and 7.29 but a stress of 4.9 t.s.i. and a temperature of - 23°C were used. The moving crack was estimated to be $\frac{1}{4}$ inch beyond the area shown in fig. 7.30. For this test no residual birefringence was observed in the photoelastic coating before the fracture occurred.

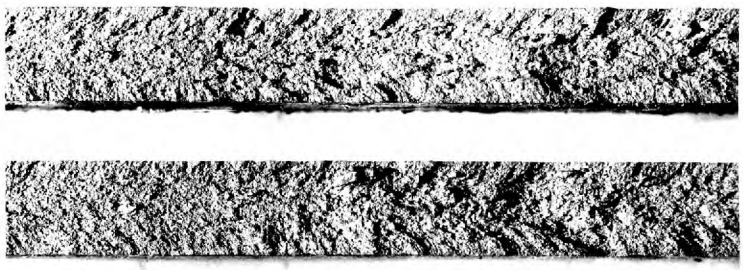

Fig. 7.26 Fracture surface of a specimen broken at 14°C under a stress of 8.5 t.s.i. Half actual size.

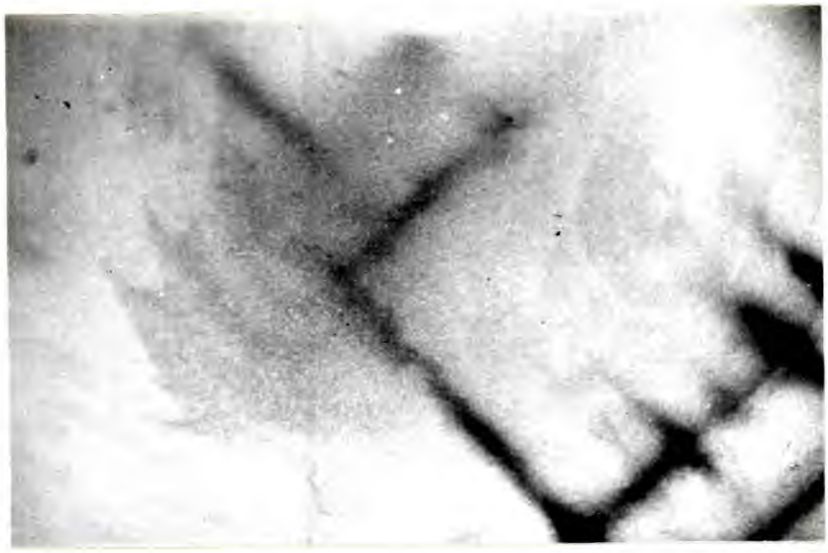

Fig. 7.27 Yield lines in a specimen at a temperature of - 3°C under a stress of 10.5 t.s.i. The photoelastic coating is 1 mm. thick.

Fig. 7.28 The isochromatic pattern immediately behind a brittle crack. The area shown corresponds to fig. 7.27.

Fig. 7.29 Fracture surface corresponding to fig. 7.28.

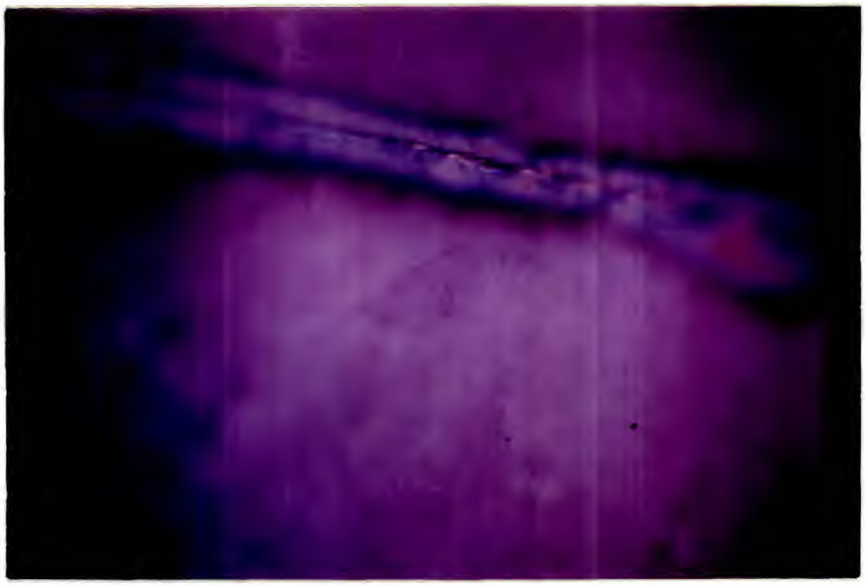

Fig. 7.30 The isochromatic pattern in 1 mm thick photoelastic coating immediately behind a brittle crack moving through steel under a stress of 4.9 t.s.i. at a temperature of -'23°C.

Fig. 7.31 Fracture surface corresponding to fig. 7.30. Half actual size.

7.3c Tests at N.C.R.E., Rosyth

In the C.A.T. rig the fracture is initiated by impacting the specimen with a bolt gun in the direction of crack propagation; this will introduce a large amount of elastic energy into the specimen. Fig. 7.32 shows the isochromatic strain patterns observed in a 3 millimetre thick coating. The steel was 1 inch thick, the stress 10 t.s.i. and the temperature - 20°C. The strain field is more complex than those already reported, but the general shape is similar.

The isochromatic pattern near a crack 15 inches long propagating in a 6 foot wide steel plate under a stress of 12 t.s.i. and at - 48°C is shown in fig. 7.33; the area covered by this photograph is 3 inches by $4\frac{1}{2}$ inches. The crack is just entering the photoelastic coating which was 2 millimetres thick with strain optical constant K = 0.02. This type of birefringent coating was used as it was found to stand up well to low temperatures and high stresses. Fig. 7.34 shows the fractured specimen with the photoelastic coating still adhering to it; on the right of the coating are

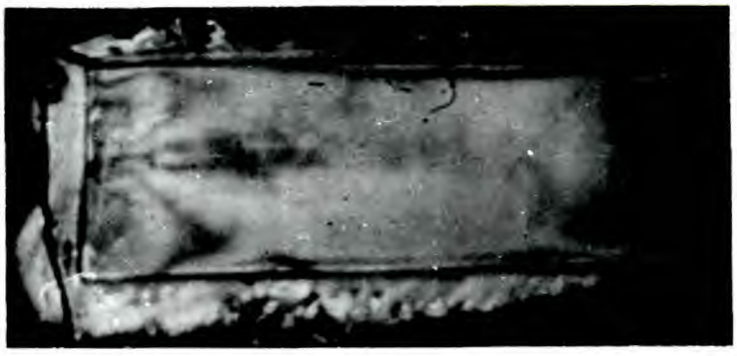

Fig. 7.32 The isochromatic pattern about a moving crack in a C.A.T. specimen at - 20°C under a stress of 10 t.s.i. The photoelastic coating is 10" x 4" and 3 mm. thick.

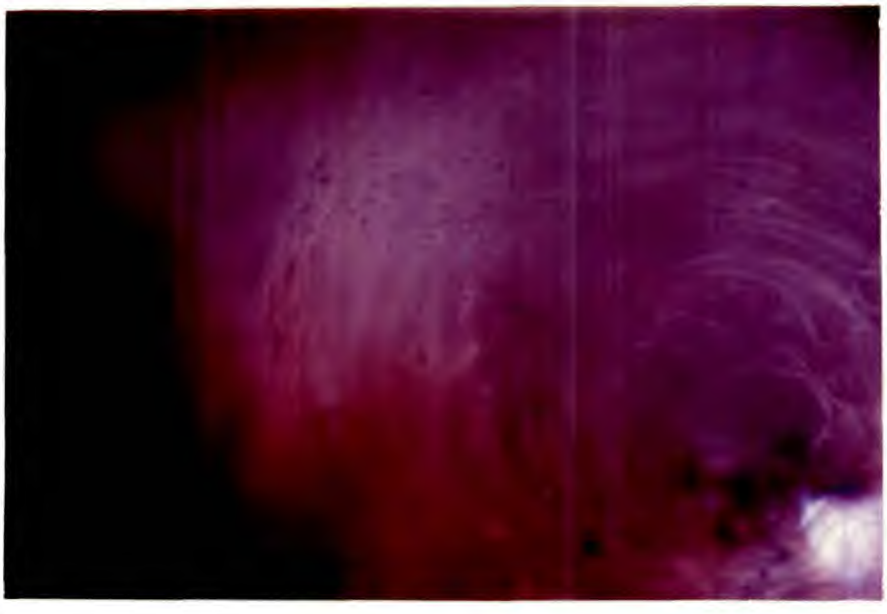

Fig. 7.33 The isochromatic pattern about a moving crack in a 6' wide specimen at - 48°C under a stress of 12 t.s.i. The area shown is 3" x $4\frac{1}{2}$".

Fig. 7.34 Fractured 6 foot wide specimen, crack ran along specimen-loading lug weld for the rest of the specimen length. ($\frac{1}{6}$ actual size)

Fig. 7.35 Fracture surface corresponding to fig. 7.34.

the remains of a sheet of birefringent coating with strain optical constant K = 0.08 which fractured before the crack was initiated. The crack, after crossing the area shown in fig. 7.34, ran along the specimen-lug weld for the rest of the testpiece length. The fracture surface corresponding to fig. 7.34 is shown in fig. 7.35. It was hoped to obtain resistance strain gauge recordings from the rear side of the plate, fig. 7.36, and compare the results with the isochromatic recording, fig. 7.36, but for this test the high speed camera, which records the results from the strain gauges, failed.

In a second instrumented wide plate test two cameras were used; the camera further from the plate and at an oblique angle to it showed the 31 inch long crack just entering the area covered by the 2 millimetre thick birefringent coating; the close up camera photographing an area $1\frac{1}{2}$ inches to $4\frac{1}{2}$ inches ahead of the crack recorded no change in stress. Strain gauges were mounted on the rear of the specimen to measure vertical and horizontal strains, fig. 7.37. From the strain gauge results the crack speed was estimated as

Fig. 7.36 Rear side of specimen shown in fig. 7.34 1/16 actual size.

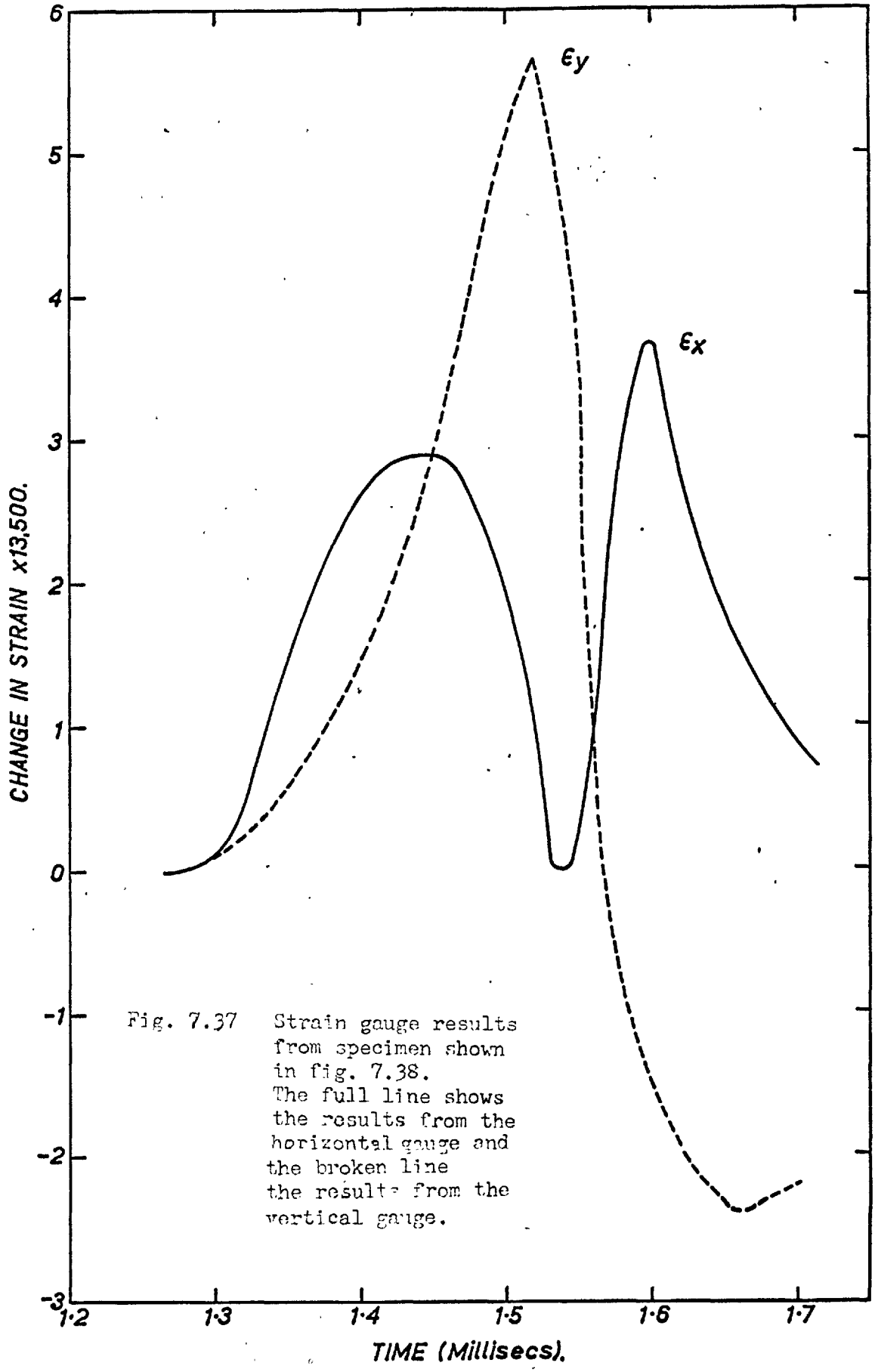

Fig. 7.37 Strain gauge results from specimen shown in fig. 7.38. The full line shows the results from the horizontal gauge and the broken line the results from the vertical gauge.

2,000 feet per second. The stress on the plate was 9 t.s.i. and its temperature - 20°C. The broken specimen and fracture surface are shown, figs. 7.38 and 7.39; large shear lips occurred in the region near the photoelastic coating.

Fig. 7.38 6 foot wide specimen containing straight through fracture, 1/12 actual size.

Fig. 7.39 Fracture surface corresponding to fig. 7.38, note well defined large shear lips.

8 Discussion of Experimental Results

8.1 Static Tests

The static stress patterns are similar to those presented by Dixon and Visser (1961), for an aluminium alloy with central or edge cracks and for mild steel with a central slot; but cover a range of plastic strains which they did not report. The isochromatic stress patterns in a plate with a single slit were reasonably similar to the patterns in a plate with two edge slits.

The predictions of equation (17) in chapter 2 are in good agreement with the isochromatic records obtained, provided plastic flow is small and allowance is made for finite plate width.

For example, for fig. 7.4:-

half crack length, a = 4 inches

half plate width, b = 6.5 inches

Dixon (1959) showed that for a central crack

$$\frac{K}{K_\infty} = \left[1 - \left(\frac{a}{b}\right)^2\right]^{-\frac{1}{2}}$$

where K is the ratio of the maximum stress at the head of the crack to the nominal stress across the gross section, and K_∞ is the ratio of the maximum stress at the head of the crack to the nominal stress across a plate with infinite width.

Assuming that the stresses near the crack increase proportionally with K, and that the results for a central slit may be applied to an edge slit; the values of the stress obtained by infinite plate theory must be multiplied by a correction factor of $\left[1 - \left(\frac{a}{b}\right)^2\right]^{-\frac{1}{2}}$ to obtain the stresses in a finite plate.

For fig. 7.4

$$\left[1 - \left(\frac{a}{b}\right)^2\right]^{-\frac{1}{2}} = 1.27$$

the applied stress σ = 5.92 t.s.i.

For the first and second order fringes:-

τ = 6.9 t.s.i. and 13.8 t.s.i.

whence τ/σ = 1.17 and 2.33

The values predicted by infinite plate theory will then be $\tau/\sigma \times \frac{1}{1.27}$ i.e. 0.92 and 1.83.

The fringes for these values are shown, fig. 8.1, superimposed on the measured isochromatic pattern, fig. 7.4. The first fringe fits well, and the fit is even better if allowance is made for the movement, due to plastic flow, of the effective crack tip. The second fringe fits the pattern in the elastic region. Fig. 7.5 shows the residual isochromatic pattern when the load is removed from the specimen.

It would be difficult to determine the exact shape and size of the plastic zone from the recordings of the birefringence caused by plastic strain, because the regions near the plastic enclave will show some elastic strain due to the misfit of the plastic enclave. However the general shapes of the plastic zones appear to be as predicted by Stimpson and Eaton (1961) using a relaxation procedure, but unlike those observed by

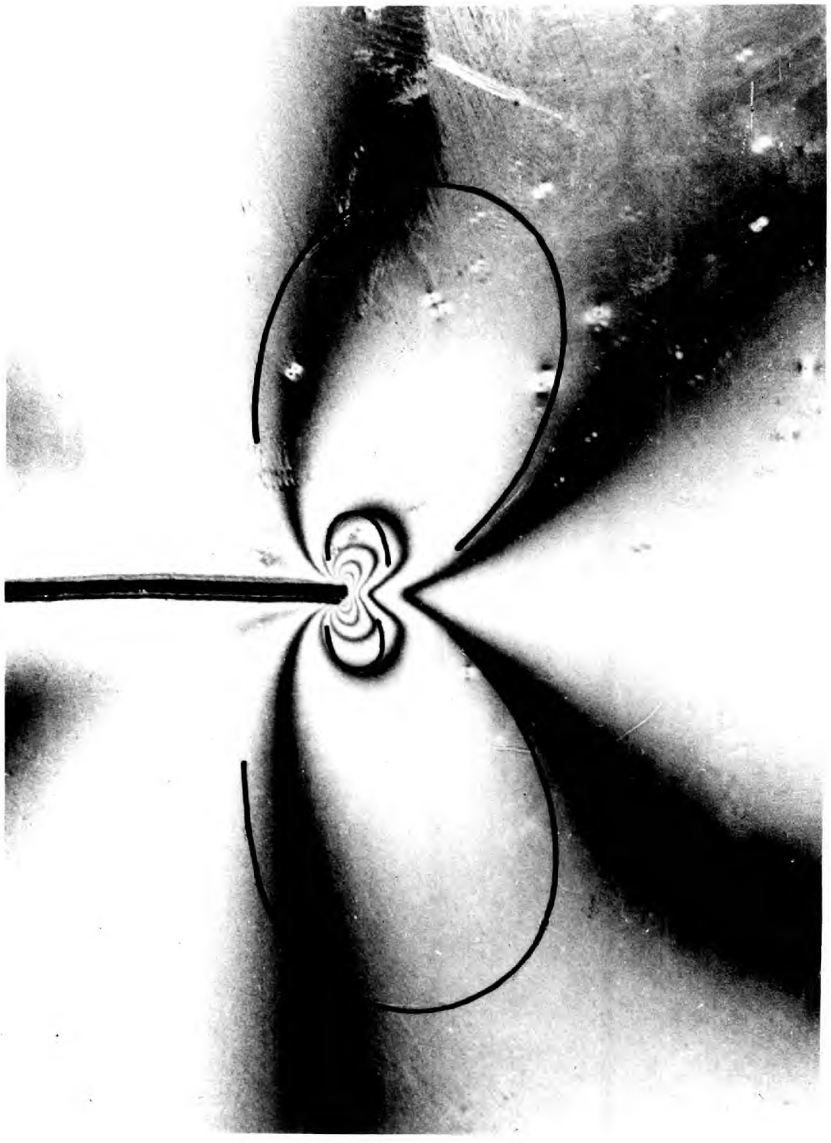

Fig. 8.1. Theoretical isochromatic fringes superposed on Fig.7.4.

Bateman, Bradshaw and Rooke (1964) who used comparatively large stresses, and obtained long yield zones. Approximate estimates may be made of the size of the plastic zones from the isochromatic patterns, by taking the area included within the first order black fringe in the unloaded specimens. The values for plastic zone length ahead of the crack estimated in this manner are in reasonable agreement with the predictions of Dixon's (1962) theory. For example for figs. 7.5 and 7.7:-

Plastic zone lengths, estimated from the isochromatic pattern are s = 0.2 inches and 0.5 inches respectively.

From Dixon (1962) $^{s}/a = 0.053$ and 0.11 for these particular loading conditions, and a = 4 inches

therefore s = 0.21 inches and 0.44 inches

Dugdale (1960) measured plastic zone lengths ahead of slits in a high nitrogen steel, and reported that the plastic zone tapered to a fine point. If the plastic zones as estimated above are smoothed to a fine point by eye, Dugdale's theory predicts the plastic zone length better than does Dixon's.

8.2 Dynamic Tests

8.2a General Form of the Isochromatic Pattern

By superposition of resistance strain gauge measurements, Rolfe and Hall (1961) obtained the full stress pattern about moving cracks of various lengths up to within approximately 1 inch of the crack tip. They presented contours of maximum principal strain, fig. 8.2, but stated, "in spite of the slightly non-uniform nature of the shear strain contours, they are similar in shape to the maximum principal-strain contours, and likewise similar to those observed in the photoelastic studies of Wells and Post (1958)."
The strain gauge results obtained at N.C.R.E. indicate an isochromatic pattern similar in shape to those reported above, Christopher and Cargill (1964).
The general shape of the isochromatic patterns reported in chapter 7, and the magnitudes of the elastic strains, agree with those found by Rolfe and Hall (1961).

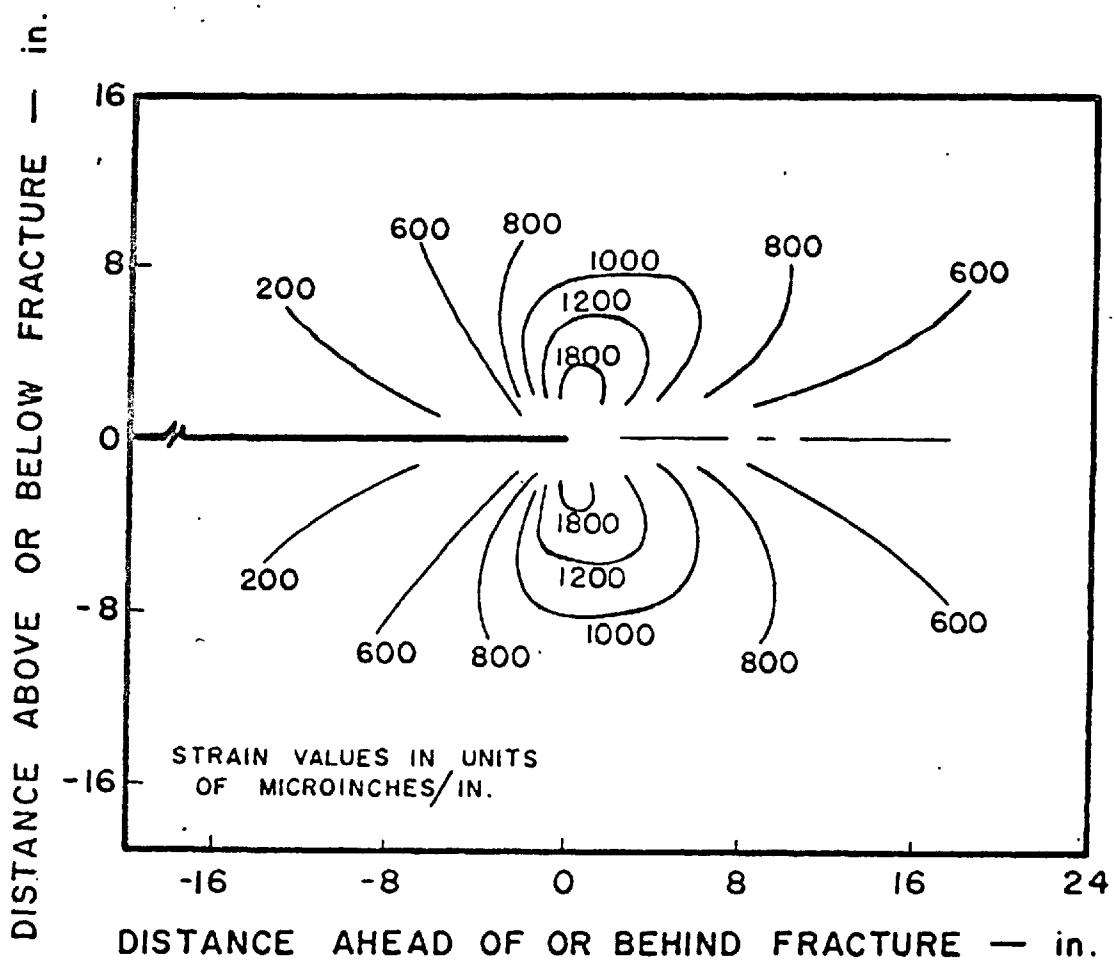

Fig. 8.2 Typical set of principal-strain contours for 22 in. to 50 in. crack length. (After Rolfe and Hall (1961).)

8.2b Shock Waves

A comparison between a typical isochromatic strain pattern near a running brittle fracture obtained by van Elst (1963), fig. 4.2, and those reported in chapter 7 shows that whilst the general shapes of the stress patterns near the crack tips are similar, van Elst finds two additional effects; the stress waves, A, B and C, ahead of the crack, and the complex pattern of shock waves behind the crack front. Van Elst showed that the frequency of the shock waves was consistent with the intermittent nature of shear lip failure. The waves A, B and C, correspond to a lowering of shear stress, and appear to have been reflected from the specimen edges back into the field of view. In a later paper van Elst (1964) (a), large pulses, fig. 8.3, similar to that shown in fig. 7.8, were reported. These waves appear to have travelled directly from the fracture to the field of view, and correspond to a lowering of shear stress. Van Elst (1964) (b) stated, "One can expect the observation of the stress waves only at optimal conditions" due to "blurring effects",

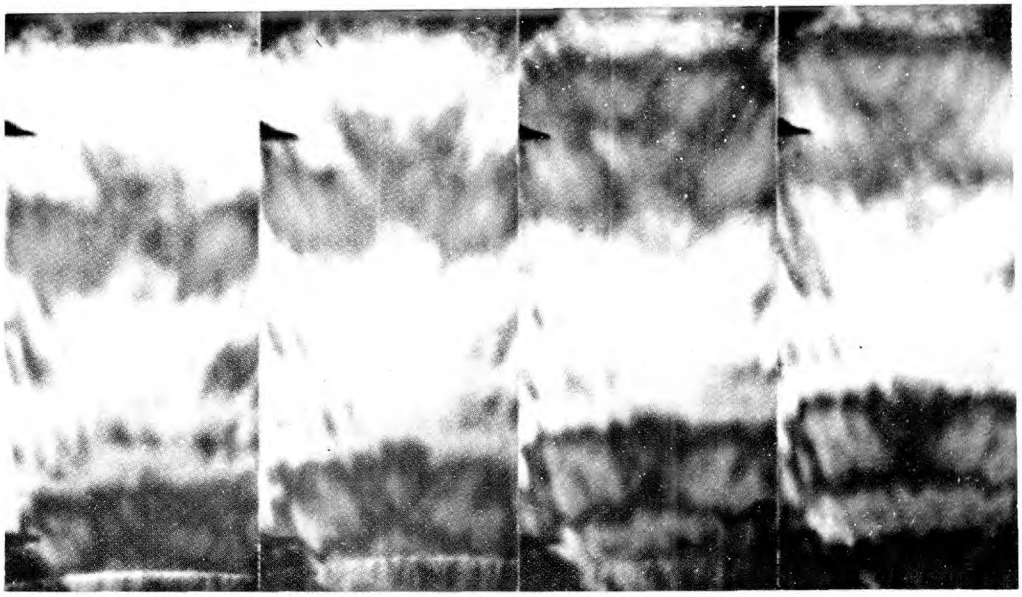

Fig. 8.3 High speed ciné recording of large stress pulses ahead of a moving brittle crack.
(after van Elst (1964) (a))

of the different velocities of shock waves in steel and the photoelastic coating, and dispersion effects caused by the steel.

Of the results obtained in this research, none showed the complex pattern of stress waves behind the fracture, and only two showed waves ahead of the fracture. In one of these two results the waves appear to have been caused by the bolt gun, and only a poor record was obtained of the other. Van Elst's results appear to consist of a steady state stress pattern with superposed stress pulses, which he has correlated with the progression of yielding on the plate surface. Thus it seems likely that the stress pulses are caused by the shear lips and are a surface effect; while the steady state configuration is more likely to represent the condition due to a brittle failure. However the second of the two wide plate tests reported in chapter 7 and the specimen shown in fig. 7.15 had large shear lips but no shock waves were observed; all the other specimens had only very thin shear lips.

8.2c Biaxial Stress Field

All the isochromatic patterns near moving cracks obtained in this research show a region ahead of the crack where the shear stress is lower than predicted by stationary crack theory. It is impossible to separate principal stresses from a single isochromatic pattern, but the stress state may be inferred from theoretical and experimental work reported by other researchers.

A region of low shear stress ahead of a crack is predicted by the theoretical solutions for stationary cracks in elastic media reported in chapter 2, and was seen by Dixon and Visser (1961), Fessler and Mansell (1962), etc. This region of low shear stress may be seen in figs. 7.2, 7.4 and 7.6. The theoretical solutions for stress fields about moving cracks, Yoffé (1951), Akita and Ikeda (1959) (a), etc., all suggest that as the crack speed increases to relativistic values the stress field changes from the static configuration, and the larger the crack speed, the greater is the change. The theoretical work of Yoshiki, Kanazawa and Itagaki (1961) predicts that for

high crack velocities the stress in the vertical direction, σ_y, will have a minimum value a short distance ahead of the crack tip. The lattice model used by Gaus (1961) forecasts that when strain energy is released by crack formation, a tensile stress pulse is generated and propagates away from the crack tip, to create a zone of biaxial tension ahead of the crack.

The wire resistance strain gauge results reported by Rolfe and Hall (1961), fig. 8.2, and Cargill (1963), fig. 8.4, indicate a lowering of shear strain approximately 4 inches ahead of the crack, due mainly to an increase in the horizontal strain, ϵ_x. This effect is similar to that predicted by Gaus (1961). Cargill's results and some of those reported by Videon et alia also show a small decrease in vertical strain in this area, as forecast by Yoshiki, Kanazawa and Itagaki (1961). The results obtained from the strain gauges as the crack approaches and passes them depend upon their positions relative to the crack path:-

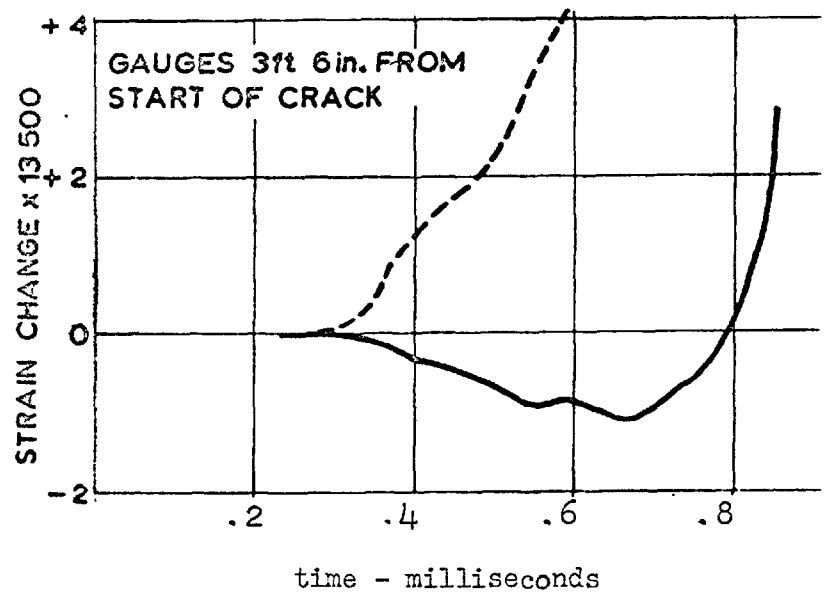

Fig. 8.4 Results from strain gauges positioned ahead of a moving brittle fracture. (After Cargill (1963).)

1) If the gauges are more than approximately 1 inch from the fracture path, a strain history similar to that shown in fig. 7.37 is obtained; the vertical gauge peaks in tension while the horizontal gauge starts to rise but has a compression peak, probably due to the Poisson ratio effect of the vertical gauge's tension peak.

2) If the gauges are within about 1 inch of the fracture path, both vertical and horizontal gauges peak in tension as the crack passes, but there still exists a large shear strain, as well as the large biaxial tension. Videon et alia (1963) noted that as the crack speed increased, the area over which this effect was noticeable also increased.

3) If the gauges are too near the fracture path, their strain readings continue to rise until the gauges break down.

Wells and Post (1958) interpreted their results from strain birefringent models to show that the dynamic stress distributions in the vicinity of a crack approximated to the static distributions about slits in models extended by a fixed displacement at their ends.

However their results do show that the shear stress just ahead of the crack is slightly lower in the dynamic case than in the static case, and also that this lowering of shear stress is caused mainly by an increase in the horizontal stress $\bar{\sigma x}$, although a slight decrease in vertical stress $\bar{\sigma y}$ was seen. Thus the photoelastic stress measurements in columbian resin are at least qualitatively similar to the results obtained from strain gauges on steel plates.

The theoretical results of Akita and Ikeda (1959) (a), and Yoshiki, Kanazawa and Itagaki (1961), are compared with the experimental results of Wells and Post (1958) and Cargill (1963) in figs. 8.5 and 8.6, where $\bar{\sigma y}/\sigma$ is plotted against $(x - a)/a$ for two ranges of crack velocity. These figures show that although all the results indicate a lowering of vertical stress ahead of the crack, the effect is largest for the strain gauge results from steel.

The shear strains obtained from the strain gauge measurements are everywhere in agreement with the isochromatic patterns obtained in this research.

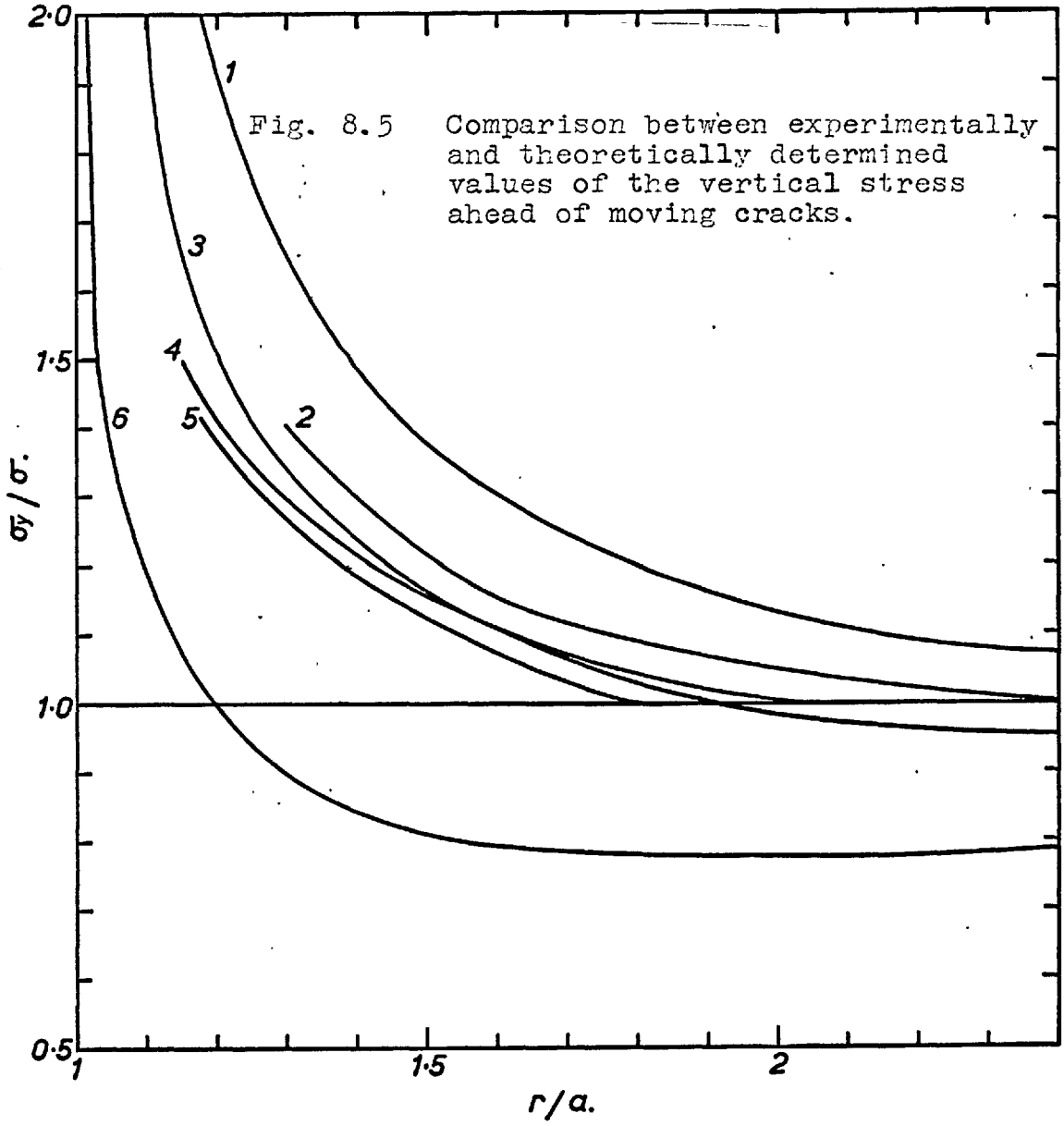

Fig. 8.5 Comparison between experimentally and theoretically determined values of the vertical stress ahead of moving cracks.

Curve Number	Crack velocity / Velocity of sound	Source	Method
1	0	Westergaard (1939)	Theory
2	0.1	Yoshiki et al (1961)	Theory
3	0.2	Akita et al (1959)(a)	Theory
4	0.2	Wells and Post (1958)	Birefringent resin
5	0.2	Yoshiki et al (1961)	Theory
6	0.14	Cargill (1963)	Strain gauges on steel plates

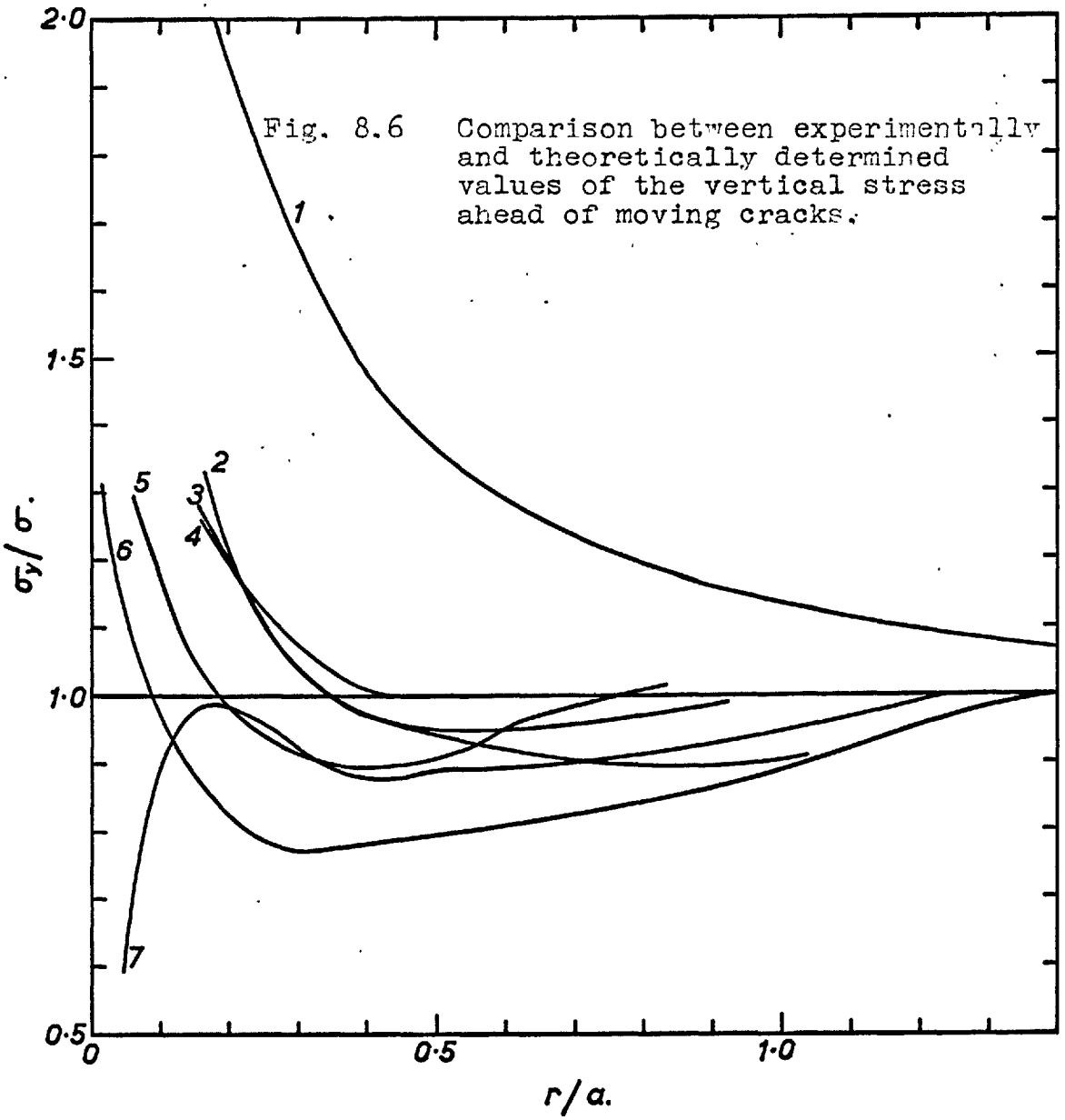

Fig. 8.6 Comparison between experimentally and theoretically determined values of the vertical stress ahead of moving cracks.

Curve Number	Crack velocity / Velocity of sound	Source	Method
1	0	Westergaard (1939)	Theory
2	0.3	Akita et al (1959)(a)	Theory
3	0.3	Yoshiki et al (1961)	Theory
4	0.35	Wells and Post (1958)	Birefringent resin
5	0.35	Yoshiki et al (1961)	Theory
6	0.35	Cargill (1963)	Strain gauges on steel plates
7	0.4	Akita et al (1959)(a)	Theory

From the strain gauge results the stress state within the region of low or zero shear strain can be inferred. About 4 inches ahead of the fracture the reduction in shear stress is caused by an increase in the horizontal stress, to give a region of biaxial tension. Closer to the crack both the vertical and horizontal stresses increase to give a region of large biaxial tension. This region of high biaxial tension on the plate surface is probably indicative of a hydrostatic tension within the body of the plate, which will be of importance in the nucleation and growth of microcracks near the crack tip.

No direct measurements of crack speed were taken, but a reasonable estimate may be made by noting the distance that the crack had travelled beyond the brittle wire before the flash operated. In the second wide plate test reported the crack speed over the relevant area was measured on the rear of the plate as 2,000 feet per second, and from this it is estimated that the crack speeds in the 300 ton rig were all of the order of 3,500 to 4,500 feet per second.

In the second wide plate test the biaxial zone was smaller than that observed in the other results; this zone size-crack velocity dependence is in agreement with the observations of Videon, Barton and Hall (1963), and the theoretical predictions of Yoffé (1951), Akita and Ikeda (1959), etc.

8.2d The Elastic Stress Field

Irwin (1957) used Westergaard's (1939) results to obtain an analytical expression for the stress field about a stationary crack in an elastic material. He predicted that the shape of an isochromatic fringe would be given by:-

$$(2\tau)^2 = \left[\frac{K}{2r} \sin\theta + \sigma_{ox} \sin\frac{3\theta}{2}\right]^2 + \left[\sigma_{ox} \cos\frac{3\theta}{2}\right]^2 \quad \ldots (18)$$

where K and σ_{ox} are constants characterizing the stress field about a crack. Irwin assumed, to simplify the mathematics, that r, the distance from the crack tip to

the isochromatic fringe, is small compared to the crack length. Then, using the fact that along a line of constant τ, $\frac{\delta\tau}{\delta\theta}$ is zero, when r is a maximum, Irwin (1958) eliminated σ_{ox} from equation (18) to obtain:-

$$K = \frac{2\tau\sqrt{2r_m}}{\sin\theta_m}\left[1 + \frac{2\tan 3\theta_{m/2}}{3\tan\theta_m}\right]\left[1 + \left(\frac{2}{3\tan\theta_m}\right)^2\right]^{-\frac{1}{2}} \quad \ldots (19)$$

where r_m is used to denote r maximum and is the furthest distance of the particular fringe from the crack tip; θ_m denotes the corresponding value of θ. Assuming that the stress fields about moving and stationary cracks are similar, Irwin (1958) compared equation (19) with the experimental results of Wells and Post (1958), and found good agreement.

From equation (19) a graph of τ versus $\sqrt{\frac{1}{r_m}}$ should be a straight line. Fig. 8.7 shows values taken from two isochromatic patterns, figs. 7.9 and 7.17, plotted in this way. The graphs are linear over much of the strain field, but deviate both close to, and far away

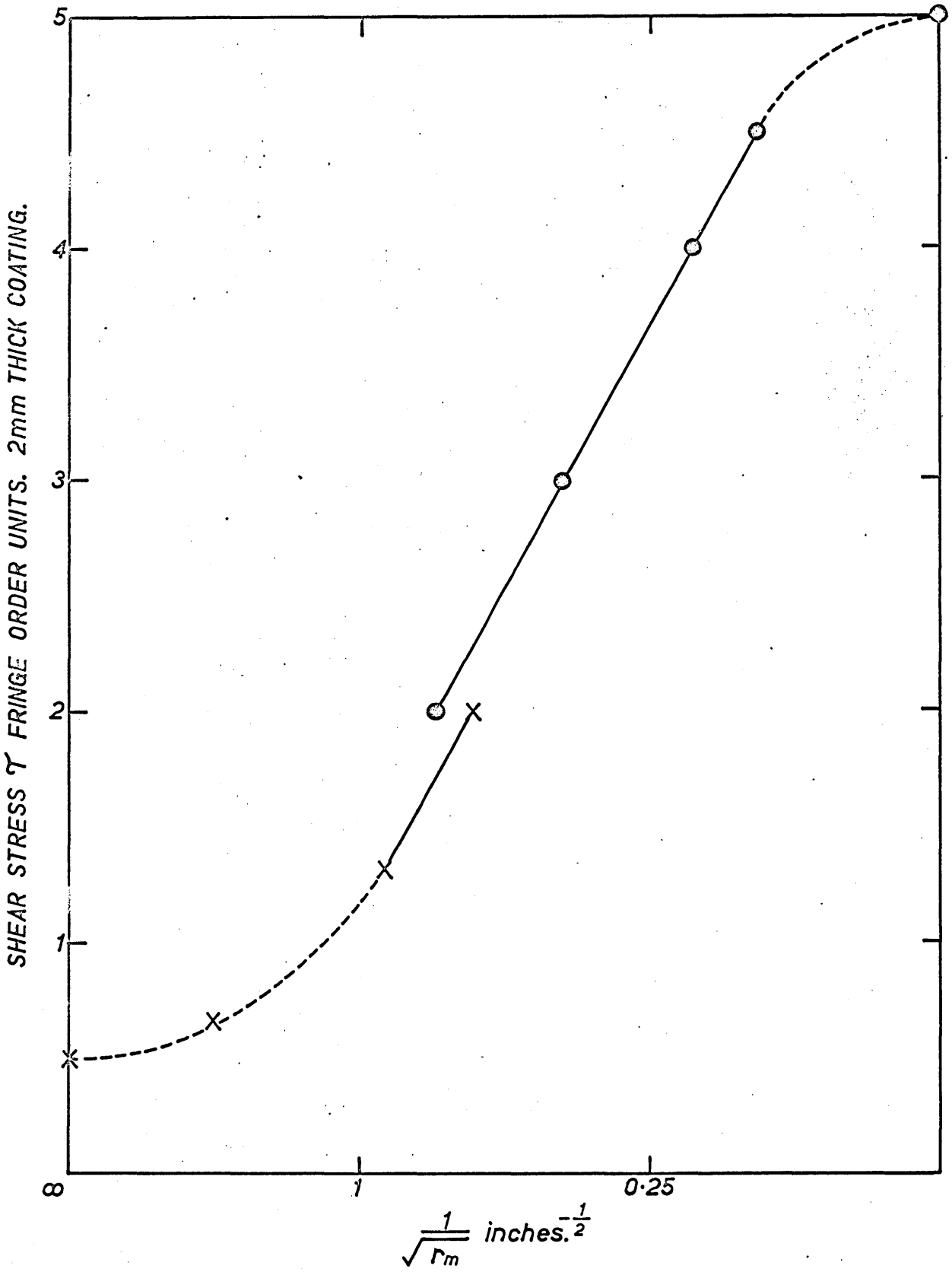

Fig. 8.7 Shear stress versus the reciprocal of the root of the distance from the crack, from two isochromatic stress patterns.

from, the crack. Close to the crack the yielding of the steel must invalidate the solution, and far away from the crack Irwin's assumption that r is small compared to crack length is no longer true. Starting from Westergaard's (1939) results, but without neglecting r when compared to a, equation (17) was derived. The applicability of this equation to the isochromatic stress patterns was tested by comparing the measured and calculated values of shear stress at position r_m. The results, table 1, show that equation (17) gives reasonable values for τ at r_m, except when r_m is small and the effects of yielding at the shear lips will change the isochromatic pattern from the theoretical elastic result, and except for the results from fig. 7.15 which showed large shear lips. Isochromatic fringes predicted by equation (17) are shown superposed on figs. 7.9, 7.17 and 7.20 in figs. 8.8, 8.9 and 8.10, and there is fair agreement between the theoretical and experimental patterns for the fringes shown; these fringes are relatively far from the crack tip, i.e. in the region where the

Table 1

Comparison of Measured and Calculated Shear Strain

Fig. No.	Fringe order 3 mm. coating	Measured shear strain t.s.i.	Crack length inches	r_m inches	Applied stress t.s.i.	Calculated shear strain t.s.i.
7.9	1	6.88	7	3.8	8.0	6.4
	2	13.75		0.60		12.9
7.17	3	20.6	8.1	0.52	11.2	20
	4.5	30.9		0.26		26.4
	6	41.2		0.16		32.2
7.20	3	20.6	6.8	0.35	0.9	19.3
7.15	2	13.75	7.6	0.43	10.8	20.3
	3	20.6		0.28		24.0
	4	27.5		0.21		27.3
	5	34.35		0.15		31.5
	6	41.2		0.09		39.4

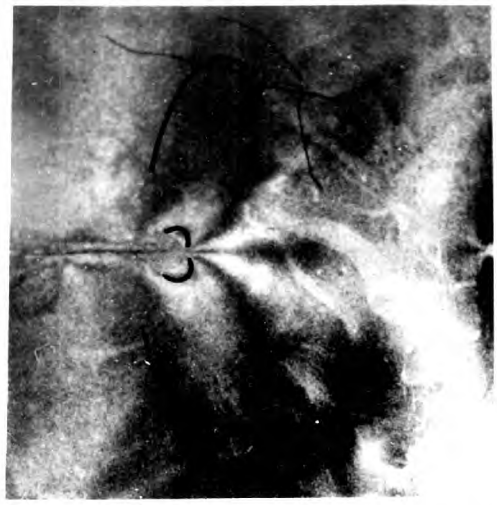

Fig. 8.8. Theoretical isochromatic fringes superposed on Fig. 7.9.

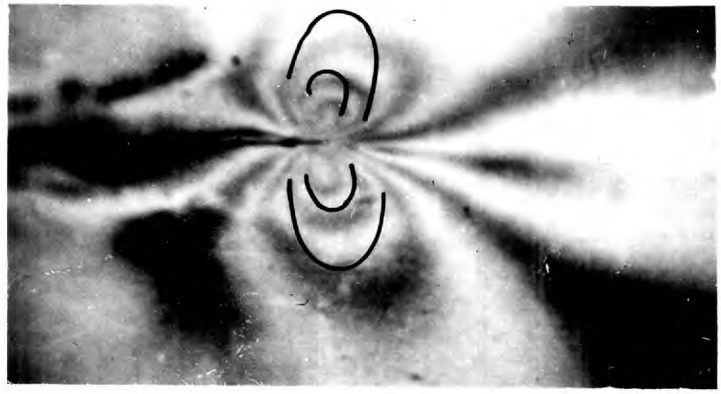

Fig. 8.9. Theoretical isochromatic fringes superposed on Fig. 7.17.

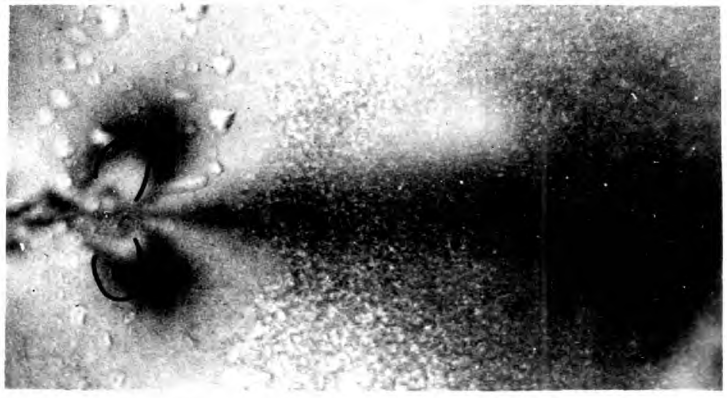

Fig. 8.10. Theoretical isochromatic fringes superposed on Fig. 7.20.

COMPARISON OF THEORETICAL AND EXPERIMENTAL STRAIN DISTRIBUTIONS.

strains are elastic. Theoretical isochromatic fringes superposed upon fig. 7.15 do not lie over the experimental fringes.

Yielding due to shear lip formation causes a relatively large strain contiguous to the crack. This plastic strain in the steel, when transmitted to the photoelastic coating, will cause high birefringence. Thus if the elastic stress-strain relationships are used to determine the stress in the steel, the value of stress so obtained will be too high, so that in table 1 for small values of r_m the calculated shear stress should be smaller than that obtained experimentally. The results taken from figs. 7.17 and 7.15 show this effect. However in the results taken from fig. 7.15 for the larger values of r_m the experimentally measured shear stress is smaller than the calculated shear stress. This effect is contrary to that expected from the above argument. A possible explanation of this effect is that when the shear lips are well defined the crack in the centre of the specimen is ahead of the crack on the specimen surface, and so the measured elastic strain

near the surface crack will be caused by the relatively small load carried by the shear lips. Thus the experimentally measured shear stress should be smaller than the shear stresses calculated from equation (17). The second order fringe in fig. 7.15 branches forward, supporting the above hypothesis, as this effect is probably caused by the stress field associated with the crack tip in the body of the specimen. Thus the isochromatic pattern in fig. 7.15 is probably caused by a small elastic strain produced by the load carried by the shear lips, and a plastic strain produced by the steel yielding to form the shear lips.

8.2e Plastic Flow near the Crack

The isochromatic patterns reported in chapter 7 show that yielding will probably occur near a fracture, from the following reasoning. The sixth order fringe in fig. 7.15 and the fourth order fringe in fig. 7.17 represent contours of shear strain of 0.008. If these were elastic strains the equivalent shear stress would be 41.2 t.s.i. This value of shear stress exceeds the

shear yield stress of the material, even allowing for the increase in yield stress, from the static value, due to the high strain rate at the crack tip.

Now an explanation is offered for the formation of shear lips on the surface of the specimen. From the results and previous work discussed in section 8.2c the stress state near the crack tip in the plane of the plate surface is made up of two large tensile principal stresses $\overline{\sigma_p}$ and $\overline{\sigma_q}$; the third principal stress $\overline{\sigma_r}$ normal to the plate surface is zero. This stress state is represented by Mohr's circles, fig. 8.11, and it can be seen that the shear stress τ_{pr} is greater than the shear stress, measured by the birefringent coating, τ_{pq}. Values typical of those obtained from strain gauge rosettes are also shown in fig. 8.11, $\overline{\sigma_d}$ being the result from the diagonal gauge. In the centre of the specimen where plane strain occurs,

$$\overline{\sigma_r} = \tfrac{1}{3} (\overline{\sigma_p} + \overline{\sigma_q})$$

taking Poisson's ratio as $\frac{1}{3}$. If $\overline{\sigma_p}$ and $\overline{\sigma_q}$ are similar

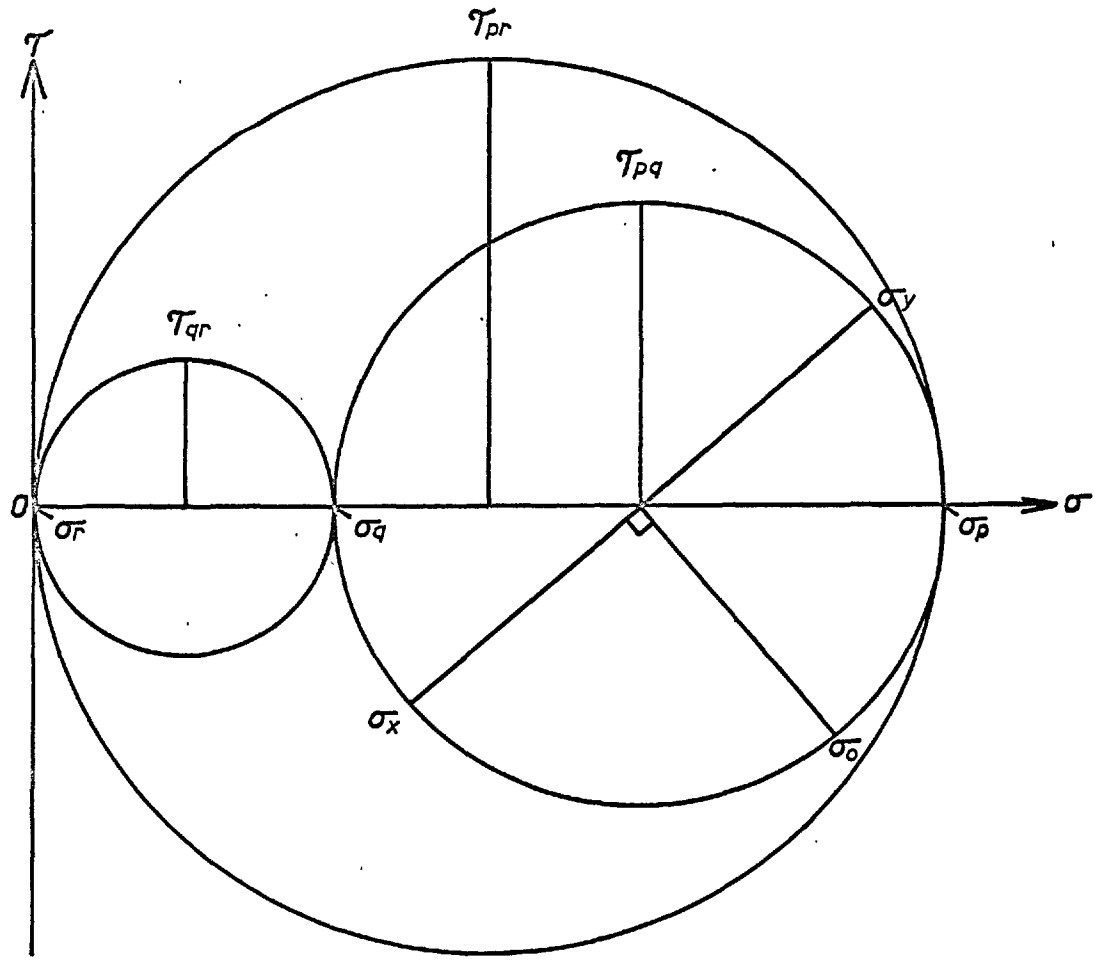

Fig. 8.11 Mohr's circle representation of the stress state on the plate surface (plane stress).

to their surface values, the stress state is as shown in fig. 8.12, and now the largest shear stress is τ_{pq}. Because the maximum shear stress on the plate surface is larger than the maximum shear stress in the centre of the plate, plastic flow is more likely to occur near the plate surface. The above reasoning is similar to that propounded by Liu (1961) to explain the transition from tensile to single or double shear failures in crack propagation in thin sheets. Rooke (1963), using formulae derived from Westergaard's (1939) results for stationary cracks in elastic media, showed that while the von Mises criterion forecasts slightly more yielding in plane stress than in plane strain, the Tresca criterion does not. At high speeds of propagation the stress field near the crack tip will change from the stationary crack stress distribution, so that Rooke's results will only apply to stationary and relatively slowly moving cracks. Near fast cracks the value of the horizontal stress σ_x increases. This will cause an increase in the principal stress σ_q, so that the arguments advanced earlier in this section will be more

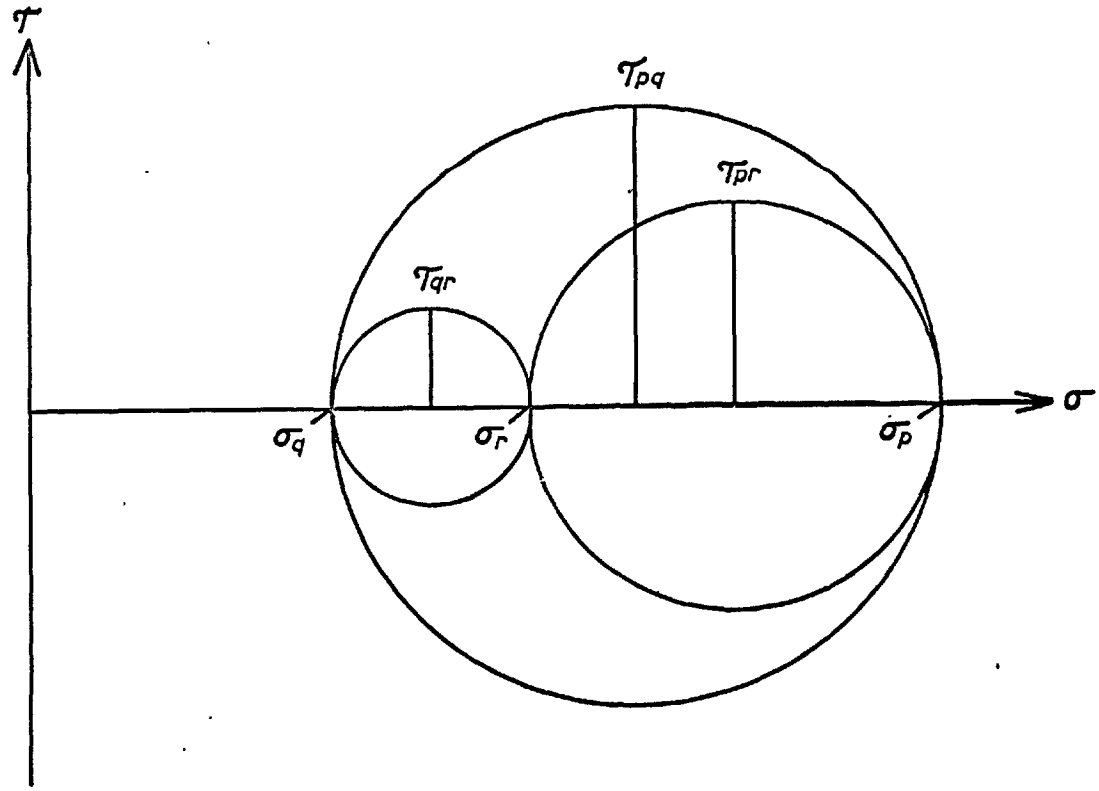

Fig. 8.12 Mohr's circle representation of the stress state in the body of the specimen (plane strain).

effective. Thus faster cracks may be expected to show less yielding in the body of the material, away from the plate surface, than more slowly moving cracks. When a crack arrests thick shear lips occur, but yielding is also visible all around the tip of the arrested fracture, fig. 7.16, in agreement with Rooke's (1963) results.

Attempts are now made to estimate the depth of the plastic zone near a crack tip. Firstly estimates are made from the fractured specimen and the birefringent coating, and then compared with various theoretical predictions for plastic zone size. The specimen from which the isochromatic pattern, fig. 7.17, was obtained is used to illustrate the problem. This specimen showed very small shear lips, less than 0.005 inch thick, fig. 7.18. The effects of these shear lips are neglected in the following.

It is difficult to take measurements from the fracture surface because of its roughness, but the height of the largest chevron marking, close to the position of the crack tip when fig. 7.17 was obtained,

is approximately 0.1 inch. Tipper (1957) showed that chevron formation during crack propagation is caused by isolated regions of cleavage fracture, ahead of the main crack, joining up with each other and the main crack by plastic flow. Cottrell (1963) has shown that various types of fracture all depend in some way or other on plastic yielding. Thus in this case yielding must have occurred at least 0.1 inch away from the crack, in order to initiate the fracture of the regions of cleavage in Tipper's theory.

There are two propagation mechanisms which can satisfy Tipper's theory; either the main fracture initiates a region of cleavage fracture while it is moving, and all the cracks grow until the main fracture arrests as the load is removed from it by the new fracture; or the main fracture arrests, followed by the initiation of a region of cleavage fracture. In the former case a reasonably uniform plastic zone would be expected near the crack, but in the latter case there would be far more yielding near the arrest points, due to the build up of the stress field or the

increased time available for yielding. This would give a reasonably uniform depth of plasticity only if the arrest points were closely spaced. By making the assumption that the rate of release of strain energy tends to a constant value, and that the chevrons are perpendicular to the crack front, Boyd (1957) showed that the chevron shape predicted using the former mechanism agrees with experimental observations. A similar analysis using the latter case would predict a reversed chevron pattern. Van Elst (1964) (a) used the latter mechanism to explain his observations of the emission of shock waves from a moving fracture. Evidence exists for the latter mechanism operating at a slower rate; a brittle fracture may arrest and then after a relatively long period repropagate spontaneously, Cargill (1963) and Videon, Barton and Hall (1963), presumably due to the build up of stress field at the crack tip. There is more plastic flow at the arrest point than at a typical fracture region. Using a dislocation etch technique on iron 3% silicon single crystals containing cracks, Tetelman and Robertson (1962)

observed regions of plastic flow around successive positions of the crack tip with relatively little evidence of flow between these positions. The reinitiations of the fracture were caused by the increasing gas pressure inside the cracks causing a build up of stress at the crack tip. It is not certain which, if either, of the above propagation mechanisms occurs, but provided the fracture arrests and reinitiates often, the plastic zone depth should be reasonably constant.

The depth of the plastic zone was determined by means of a technique similar to that used by Orowan (1946). Successive layers of steel were removed from the fracture surface by etching, and back reflection X-ray photographs were taken of the surface between each etch. The etchant used was 50% nital for 15 minutes to remove a layer of material 0.015 inches thick. The depth of material removed was measured by means of a point ended micrometer. Fig. 8.13 shows the resulting X-ray photographs, the effect of plastic flow being a blurring of the spots on the X-ray film. This technique

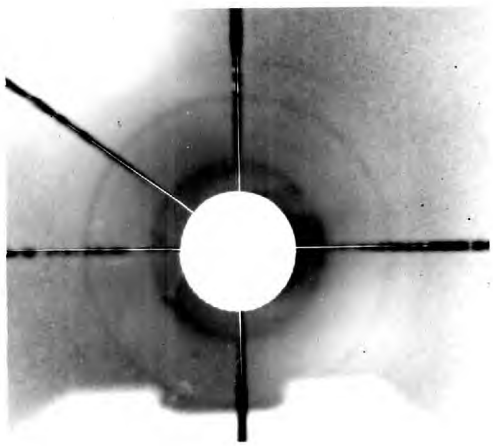

Fracture surface

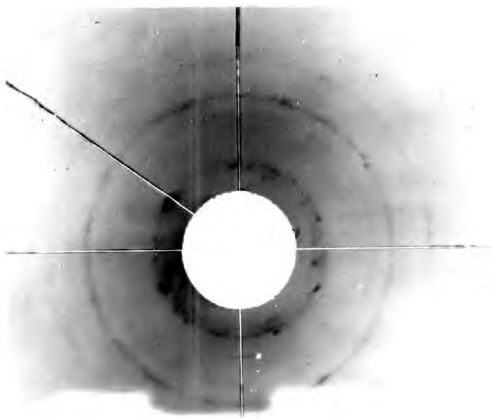

0.03 inches removed

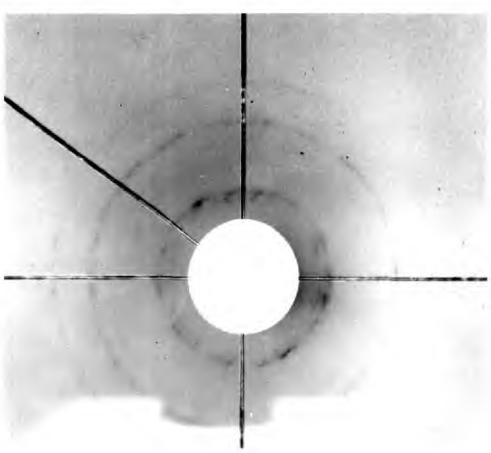

0.06 inches removed

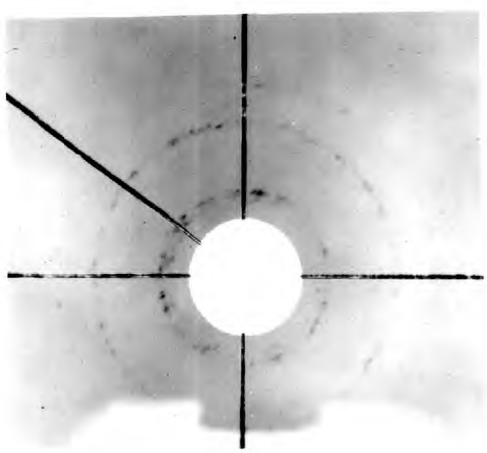

0.075 inches removed

Fig. 8.13 Back reflection X-ray photographs of the fracture surface and sections beneath it.

puts a lower limit on the depth of plastic flow as 0.075 inches. Plastic flow may have occurred at a greater depth than this but the technique is too insensitive to detect very small amounts of plastic flow. In microstructural observations reported later twins were observed in grains 0.02 inches away from the fracture surface.

The major part of the graph, fig. 8.7, showing the variation of shear stress, as calculated in section 7.1, with the reciprocal root of the distance from the fracture, was plotted from fig. 7.17; and this graph is linear up to values of 0.16 inches from the crack, and the non-linearity is then probably caused by plastic flow.

After fracture the birefringent coating still adhered to the plate surface, and the effects of residual plastic strain were observed up to 0.25 inches from the fracture surface. This estimate will be inaccurate, because of surface effects, because the misfit of the plastic zone will cause elastic stresses in the adjacent material, and because very small

strains (below approximately 50 microinches per inch) will not be shown by this technique.

All the above estimates are at the best only rough approximations. Considering these estimates it is reasonable to suggest that the plastic zone near a running crack in steel may in places extend at least 0.1 inches from the crack. The depth of the plastic zone as predicted by several theories will now be calculated.

For the specimen from which fig. 7.17 was obtained

crack length a = 8 inches

applied stress σ = 11.2 t.s.i.

static yield stress σ_{ys} = 15.3 t.s.i.

dynamic yield stress σ_{yd} = 60 t.s.i.

This value for dynamic yield stress is taken as typical of the yield stress for mild steel subjected to the strain rates which occur close to a brittle crack, and was estimated as follows. Taking the plastic zone depth as 0.1 inches, the crack length as 8 inches, and the crack velocity as 5×10^4 inches per second, and using the method described in section 2.8,

the delay time may be calculated as 2.4×10^{-6} seconds, whence, from Krafft and Sullivan's (1962) results, the dynamic yield stress is 60 t.s.i.

A simple estimate for plastic zone depth may be made by assuming that the steel will yield wherever the shear stress upon it, as predicted by equation (17), is greater than the dynamic yield stress. This method gives a value for plastic zone depth as 0.19 inches. Irwin (1960), using an approximate elastic stress distribution, defined a plastic zone correction factor, based upon the distance, from the crack tip along its axis where the maximum principal stress equalled the tensile yield stress. The distance ahead of the crack where this condition is fulfilled is, in this case, 0.14 inches. If this yield criterion is applied all around the crack, the plastic zone depth perpendicular to the axis of the crack would be 0.21 inches. Rooke's (1963) results, fig. 2.5, illustrate the shape of these "elastic yield" zones.

Dixon's (1962) approach predicts a kidney shaped plastic zone at the crack tip, yielding occurring 0.12 inches ahead of the crack tip, and the depth of the plastic zone being 0.20 inches. Dugdale's (1960) analysis forecasts yielding 0.48 inches ahead of the crack tip, the yielded zone being thin and tapering to a fine point. Goodier and Field (1962) combined the dynamic analysis by Craggs (1960) with Dugdale's (1960) crack model, and neglecting non-singular terms in the stress analysis, found that the length of plastic zone ahead of the crack was unaffected by crack velocity. In order to use this analysis to predict the plastic zone size near a brittle crack, the pressurized segment opening the crack is assumed to act upon the whole crack length, so that the shear stress field near the crack is equivalent to that of a crack under biaxial tension. Applying this analysis to the specimen shown in fig. 7.17, the plastic zone extends 0.2 inches ahead of the crack tip.

The crack model set up by Hahn, Gilbert and Reid (1963) predicts a circular plastic zone at the crack tip with radius 0.8 inches. The prediction by the dislocation models of Hahn et alia agree with the delay time measurements of Krafft and Sullivan (1962), and so, as expected, the value of maximum elastic stress near the crack is 60 t.s.i., which corresponds to the value taken for the dynamic yield stress. The crack model proposed in section 2.8 predicts a plastic yield zone depth of 0.28 inches, which is probably a better estimate than that obtained from Hahn, Gilbert and Reid's model.

All the above theoretical predictions probably overestimate the extent of yielding near a crack, because none of them make allowance for the differences in stress fields near moving and stationary cracks. Considerations of the effects discussed in section 8.2c will show that in general shear stresses near moving cracks are smaller than the equivalent shear stresses near stationary cracks.

The energy associated with crack propagation may be estimated as follows

$$\gamma = \sigma_y U_f,$$

where γ is the energy per unit area for crack propagation and U_f is the fracture displacement. Now if the average strain in the yielded region ϵ_p is 1.5%, the strain corresponding to the end of the lower yield plateau in a simple tensile test, and the depth of the yielded region d is 0.1 inch, then:-

$$U_f = \epsilon_p \times d = \frac{0.1 \times 1.5}{100}$$

$$= 0.0015 \text{ inches}$$

Thence

$$\gamma = \sigma_y \, U_f$$

$$= 60 \times 0.0015 \text{ ton wt. inches per square inch}$$

$$= \frac{60 \times 2240 \times 454 \times 981}{2.54 \times 2.54} \times 0.0015 \times 2.54$$

$$= 4 \times 10^7 \text{ erg. cm}^{-2}$$

This is the observed order of magnitude of the work of fracture.

8.2f Steady State Crack Propagation

Rolfe and Hall (1961) found in their studies of cracks in 6 foot wide plates that the magnitude and extent of the strain field near a crack increased with the crack length, for cracks up to approximately 2 feet long; for cracks over 2 feet long, the strain field remained constant and the major portion of the strain field was within 8-10 inches of the crack tip.

Robertson (1957) noted that the depth of yielding near the fracture surface of a broken 6 foot wide plate increased for the first 3 feet of the crack length and thereafter remained constant for the rest of the crack length. These results indicate that the stress field at the crack tip is independent of crack length, provided the crack is over a certain length. The results of Wells and Post (1958) for cracks up to 5 inches long in Columbia resin, and the results obtained in this research for cracks approximately 8 inches long in mild steel, did not show this effect. However in both the wide plate tests the major portions of the strain patterns were within 8 inches of the crack tip, agreeing with the results of Rolfe and Hall (1961). The extent of the birefringence in the photoelastic coating after fracture, due to plastic strain, was only slightly larger for a 31 inch crack than for a 10 inch crack, agreeing with Robertson's (1957) observations. Hahn, Gilbert and Reid (1963) suggested that this steady state propagation is caused by the deterioration of the stress field as the crack speed

increases, figs. 8.5 and 8.6. This effect causes a reduction in the shear stress near the crack, and so as the crack approaches its terminal velocity, the plastic zone near the crack is smaller than would be expected.

8.3 Comparison of the Stress Fields about Moving and Stationary Cracks

A comparison between the stress fields near moving and stationary cracks can yield useful information. There are three main mechanisms which can cause the stress state near a crack in mild steel to vary with crack velocity: by inertia effects as the crack speed approaches relativistic values, by the stress-strain relationships of the medium changing with strain rate, and effects caused by non-uniform fracture propagation. The first mechanism has been studied theoretically by Yoffé (1951), etc. These theories predict that the change in the stress field due to the crack moving increases, as the crack velocity increases. Wells and Post (1958) noted that the change predicted by Yoffé was negligible for crack speeds up to one third the

speed of longitudinal waves, and their experimental results agreed with this assumption. Compared to mild steel, the columbian resin used by Wells and Post shows negligible plasticity, and although its modulus of elasticity changes with strain rate, the strain rate sensitivity of its physical properties is small compared to mild steel. Nevertheless the results obtained in this research also show that the dynamic stress distributions near running cracks are qualitatively similar to the static stress distributions under equivalent conditions. It is of interest to examine such similarities and differences as exist in the results presented in chapter 7. Perhaps the most striking similarity is the shape of the isochromatic fringes in the elastic portion of the plates, and this shape is predicted by equation (17). The effects of the three mechanisms which can cause differences in the stress field have all been observed. The inertia effects cause the lowering of shear stress ahead of the crack. This effect is discussed in section 8.2c. The strain rate sensitivity of steel

causes a smaller plastic zone to be formed around a moving crack than around a stationary one. The effects of shear lips near a moving fracture, and a rough fracture surface may be seen in figs. 7.15 and 7.28 respectively.

9 Microstructure Adjacent to the Brittle Fracture

9.1 Previous Work

The characteristic chevron pattern present to some degree on a brittle fracture surface has been studied by Tipper (1957). She postulated that these surface markings were caused by the arrest and reinitiation of the fracture, and showed that separate regions of cleavage fracture joined together by shearing in the intervening material. Thus if a new region of cleavage is initiated off the crack axis then when this new fracture joins the main crack, by shearing the linking material, a step will be formed on the surface. It is shown in section 8.2c that there is less likelihood of yield occurring in line ahead of a brittle crack, than off the crack axis. Cottrell (1963) has collated the evidence for the initiation of fracture being dependent upon yielding.

9.2 Experimental Technique

To obtain more information about the state of strain ahead of a running crack, sections were taken through arrested cracks. Obviously, cracks which had arrested with large subsequent yielding were unsuitable for this purpose, however secondary cracks, fig. 9.1, showed a number of interesting features. In this instance the crack had forked, and one of the forks, the secondary crack, had stopped after a short way. As the main crack advances ahead of the secondary crack the load would have been rapidly removed from the secondary crack, causing it to arrest without excessive deformation.

To gain a picture of the microstructural damage in three dimensions, a successive polishing technique was used. A very thin layer, approximately 0.0002 inches, was removed by mechanical polish between each metallographic examination. If too much material was removed it was difficult to rediscover the required field, and if too little material was removed the microcracks became excessively wide when etched.

Fig. 9.1. Arrested secondary crack (x20).

9.3 Results and Discussion

The observations of sectioned chevrons agreed with Tipper's (1957) results. Figs. 9.2 and 9.3 show tearing on the chevron step edge between regions which have failed by cleavage. In the arrested secondary cracks, figs. 9.1 and 9.4, regions of separate cracking are visible, but the intervening material has not yet failed. Also in agreement with Tipper's results most secondary cracks appeared to be branches from the main fracture, fig. 9.1, and not new cracks growing into the main fracture. The series of micrographs, fig. 9.5, were obtained by successively polishing the same area. They show several small cracks (a) which appear to be separate in one section, but in three dimensions are connected to the main crack. However fig. 9.5 does show one microcrack (b) which appears to be completely unconnected to the main fracture. At the edges of this microcrack are intersecting twins, an inclusion, pearlite, and grain boundaries.

Fig. 9.2. Small chevron step edge.(x160).

Fig. 9.3. Small chevron step edge, a region of ductile failure between two regions of cleavage fracture. (x400).

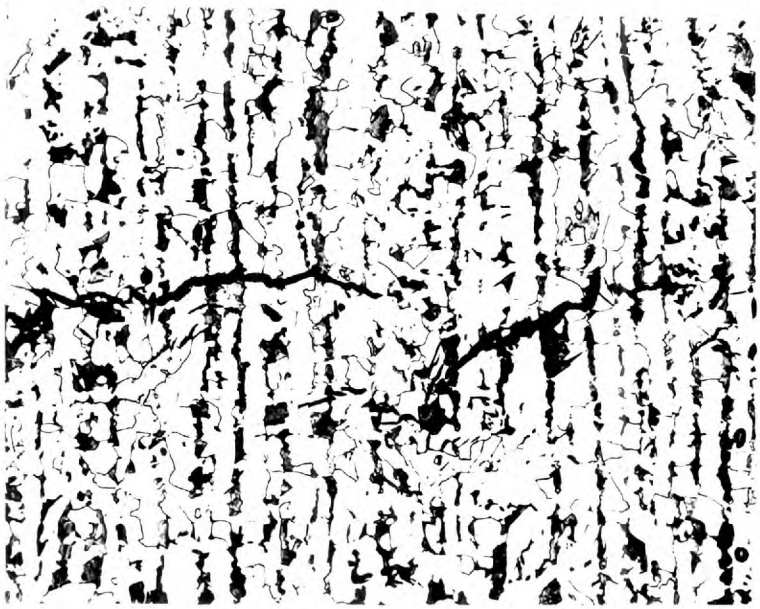

Fig. 9.4. Arrested secondary crack showing two separate regions of cleavage fracture. (x 110).

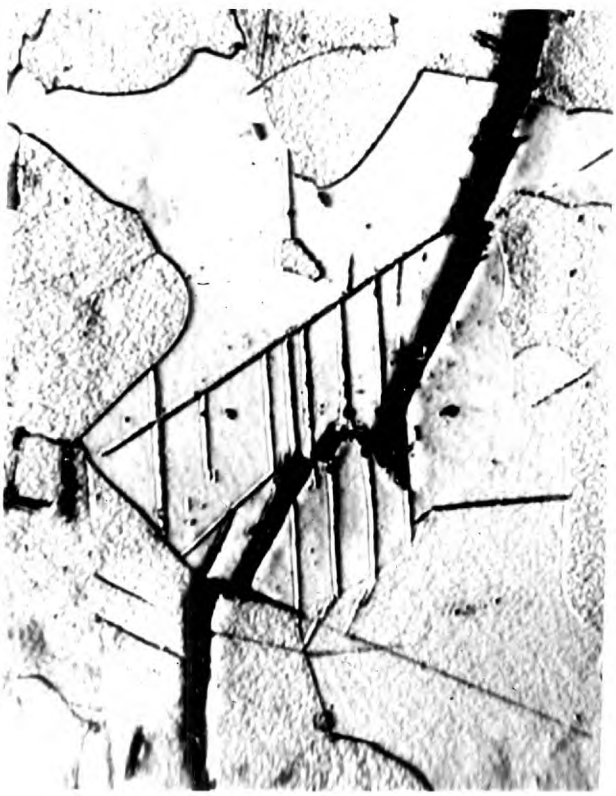

Fig. 9.6. Twins crossed by a microcrack. (x 800).

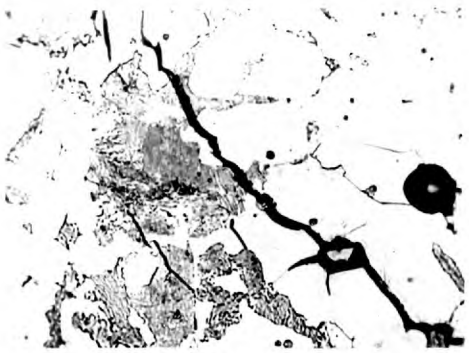

1

2

5

6

9

10

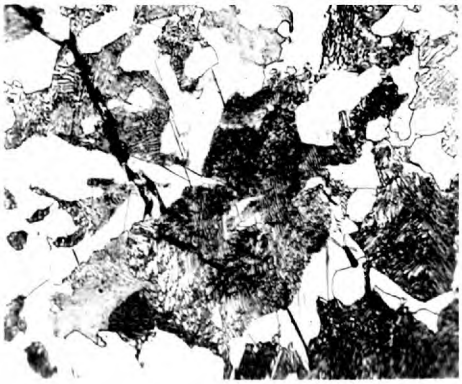

13

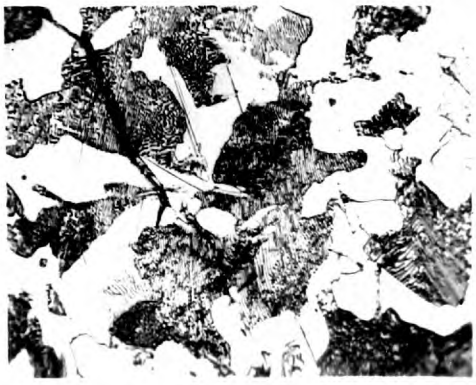

14

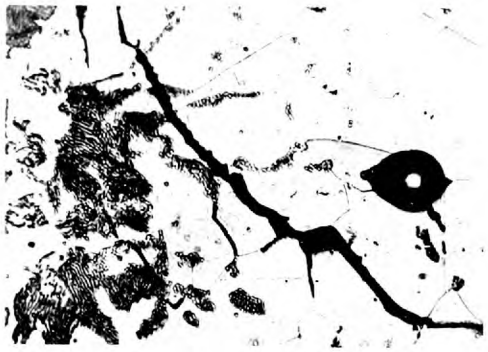

3

4

7

8

11

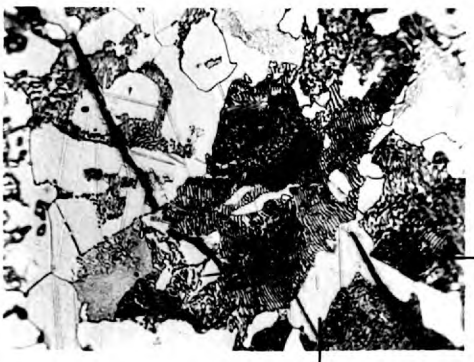

12

Fig.9.5. The variation of microcrack configuration with depth revealed by successive polishing. (x400)

Lubahn (1955) reported the opening up of several parallel sub-cracks in one grain with subsequent bending and tearing to join them into a continuous fracture path. This mechanism has also been described by Low (1955). The successive polishing technique has revealed how these parallel sub-cracks are formed. The mid points of these sub-cracks correspond approximately to points on a single cleavage crack in an adjacent grain. It is suggested that the single cleavage occurred first, then because the cleavage planes in the next grain were not parallel to those in the first grain, the strain was accommodated by several parallel cracks opening in the second grain and tearing at the grain boundary.

Microcracks, which will grow to form the regions of cleavage in Tipper's theory, appear to be associated with either twins or the pearlite phase of the steel. Evidence was found for the occurrence of twins ahead of moving cracks. Fig. 9.6 shows twins crossing a microcrack, as the twins on either side of the microcrack correspond, it is reasonable to assume that

this grain twinned before it cracked. Twins were found ahead of arrested secondary cracks. Several examples, fig. 9.5 crack (b), and fig. 9.7, were found of intersecting twins associated with microcracks, in accordance with the observations of Full (1960). It is not clear whether these twins cause the initiation of microcracks, or whether they accommodate the strain when the microcrack arrests. However Biggs (1955), working upon alpha iron single crystals, has shown by observation of the cleavage surface that microcracks may be nucleated at a twin intersection. Many microcracks were found associated with the pearlite phase of the steel, fig. 9.8. In this typical case the cracks have arrested in the pearlite; in other cases, fig. 9.9, microcracks have spread from the pearlite into the surrounding ferrite. These cracks do not appear to be caused by weakness in the ferrite-cementite interface as the cracks do not run along these interfaces.

Fig.9.7.
Intersecting twins associated with a microcrack.(x850).

Fig.9.8.
Crack arrested in pearlite.(x2000).

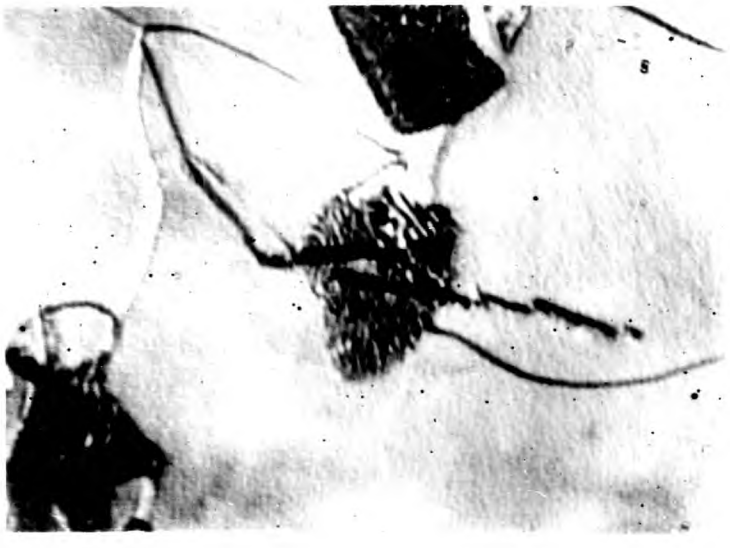

Fig.9.9.
Crack arrested in ferrite.(x1700).

In a specimen fractured at a very low temperature, approximately 100°C below the arrest temperature, there was still evidence of shear in some of the grains in the fracture surface. In contrast to the specimen broken at higher temperatures, no twins or well developed secondary cracks were seen away from the fracture surface. No examples of intersecting twins were found, but pearlite microcracks were still visible.

The above evidence seems to confirm Tipper's (1957) theory for the mechanism of brittle crack propagation in steel. The new evidence of an isolated microcrack shows that separate initiations may occur. Only one example of this was found, due to the practical difficulties of the technique, and possibly because the search was made on too small a scale. The lack of twins and cracks away from the fracture surface at low temperatures agrees with the arguments advanced in section 8.2e, for as the temperature decreases, the yield stress will increase.

10 Conclusions and Suggestions for Further Work

10.1 Summary of Results

A theoretical model, which takes account of the strain rate dependence of the yield stress and delay time in mild steel, has been formulated to predict the extent of yielding near a brittle crack. The isochromatic strain patterns near moving brittle cracks in mild steel have been measured experimentally and compared with theoretical solutions. Evidence obtained from microstructural observations near a fracture surface supports Tipper's (1957) proposed propagation mechanism.

10.2 Theoretical Model

Hahn et alia (1963) formulated the yielding of steel in terms of dislocation dynamics to predict the onset of yielding for any arbitrary loading sequence. Then, adopting a crack model with circular yield zones which support no load, and assuming that yielding ahead of the crack is equivalent to yielding in uniaxial tension, they were able to forecast the extent of

yielding at the crack tip for various crack velocities and applied loads. A more realistic crack model has been proposed in section 2.8. The variation of the shear stress acting upon elements of material near a moving crack, as the crack passes them, was calculated by assuming that the stress fields near moving and stationary cracks are similar. These stress pulses were then compared with the delay time-supported stress results of Krafft and Sullivan (1962) to predict the depth of the plastic yield zone near a moving crack.

The above model could be improved by repeating the analysis for plane stress and plane strain conditions and so allowing for the variation of stress in three dimensions. A further improvement could be achieved by using a dynamic form of the stress field near a crack instead of the static form derived from Westergaard's (1939) results. In brittle fractures of mild steel the crack does not propagate uniformly and fractures may occur on several planes due to forking of the crack and the nucleation of new cracks ahead of the fracture tip; thus even a crack model taking the above factors into account will not be completely applicable.

10.3 Experimentally Determined Stress Field near a Moving Crack

The importance of determining the stress field near a moving brittle fracture was shown in chapter 1. Although, by making simplifying approximations, attempts have been made to predict this stress field theoretically, an exact theoretical evaluation would be exceedingly difficult because of the strain rate dependence of the mechanical properties of mild steel, inertia effects at high crack velocities, etc. Attempts have therefore been made to measure this stress field experimentally and to test the validity of the simplifying theoretical approximations.

The isochromatic strain patterns upon the surface of mild steel plates containing propagating brittle fractures have been obtained by using strain birefringent coating and high speed photographic techniques. The major part of these isochromatic patterns may be described by a formula (derived from Westergaard's (1939) results) for the isochromatic stress field near a stationary crack in an elastic

material. There are however at least three ways in which the measured isochromatic field differs from the field predicted by elastic theory:-

1) Shock waves ahead of the crack

Typical results obtained by van Elst (1963) show isochromatic patterns similar to those obtained in the current work but with complex stress patterns behind the crack, shock waves ahead of the crack, and isochromatic fringes which are not smooth curves. In the research reported in this thesis these shock waves appear to have been caused by the bolt gun used to initiate the brittle fracture.

Future work to determine the effects which cause the formation of shock waves in crack running experiments would be of value. The effect of the method of initiation upon the isochromatic pattern could be determined by performing a series of experiments, upon the same steel under similar stress and temperature conditions, in which the fracture is initiated by impacting the specimen end as in van Elst's work, by firing a bullet transversely to the specimen

as in the present work, and by initiating a crack by static loading as in the double tension test described by Yoshiki and Kanazawa (1960). An attempt to correlate the formation of shock waves with the rupture of the shear lips could yield useful information. The point from which a shock wave is emitted could be found by using high speed cine techniques.

2) Plastic flow near the crack

As a brittle fracture crosses a steel plate bands of plastic flow occur near the fractured surface. In this research estimates of the plastic zone depth have been made from the fracture surface and isochromatic patterns obtained from a typical test. In addition by using an appropriate value for the yield stress which allows for the high strain rate at the crack tip, several theoretical estimates of the plastic zone depth have been made from models for the yielding near stationary cracks. The plastic zone depths forecast by the model proposed by Hahn et alia (1963) and the model propounded in section 2.8 have also been calculated. The above estimates are listed in table 2.

Table 2

Comparison of Experimentally Determined and Theoretically Calculated Plastic Zone Depths about a Running Brittle Fracture

Method of Estimation	Over or under Estimate	Plastic zone depth inches	Length inches
Height of chevron steps	Under	0.1	
Distance of twins from fracture surface	Under	0.02	
X ray results	Under	0.075	
Breakdown of elastic analysis	Over	0.16	
Residual birefringence in coating	Over	0.25	
Theoretical predictions			
Simple shear model		0.19	0.12
Irwin's model		0.21	0.14
Dixon's model		0.20	0.12
Dugdale's model) slim tapering			0.48
Goodier and Field's model) yield zone			0.20
Hahn et al model		0.8	0.8
Model proposed in section 2.8		0.28	

All of the theoretical models forecast too large a value for the plastic zone depth, probably because none of them make any allowance for the degeneration of the stress field at high crack velocities. The model which gives the most reasonable result is that which assumes that yielding occurs wherever the shear stress exceeds the dynamic shear yield stress. Of the more refined models those of Dugdale (1960) and Hahn et alia (1963) overestimate the plastic zone size, and the model described in section 2.8 gives a more reasonable value.

Future work could be done to determine the depth of the plastic zone more accurately. Microhardness and back reflection X-ray techniques have been used by Felix and Geiger (1956) to detect the presence of strain near fracture surfaces. However these techniques are probably not sensitive enough to measure the very small strains near the elastic-plastic boundary. A dislocation etch pit technique on silicon-iron specimens, or a Fry's etch on a high nitrogen steel could be used to reveal the depth of the plastic zone near fractures in these materials.

3) Biaxial tensile stress region

Just ahead of a running brittle fracture there is a region of shear stress lower than that predicted by stationary crack theory but most moving crack stress analyses predict this zone. Its presence is indicated by strain gauge measurements provided that the gauges are positioned sufficiently close to the fracture. From these strain gauge measurements it may be inferred that this low value of shear stress is caused mainly by an increase in the horizontal tensile stress. This effect probably causes the theoretical models in 2) to predict too high a value for plastic zone depth. Because of this biaxial stress region it would be difficult to design a test to simulate the stress conditions near the tip of a moving fracture.

10.3 Microstructural Observations

The evidence obtained from micrographs of the damaged structure near a fracture surface supports Tipper's (1957) theory for the mechanism of brittle crack propagation in steel. The new observation of an isolated microcrack shows that they may be initiated separately. It would be of value to complete an exhaustive three dimensional study of an arrested secondary crack, by using a successive polishing technique. In this way an overall picture of the microstructural features of fracture propagation could be built up.

Notation

The following notation has been used in this thesis:-

x, y	Rectangular coordinates, y vertical.
r, θ	Polar coordinates, origin at the crack tip.
r, θ_1, r_2 θ_2	Polar coordinates as defined in fig. 2.8.
a	Half crack length, crack lies in x direction.
z	$= x + iy = a + r_e^{i\theta}$.
Z	Function of z.
$\overline{Z}$, $\bar{\bar{Z}}$, Z'	First and second integral and derivative of Z with respect to z.
F	Airy's stress function.
σ	Stress applied to propagate fracture.
σ_x, σ_y, τ_{xy}	Normal stresses and shearing stress in the xy plane.
τ	Maximum shear stress in the xy plane.
ϵ_x, ϵ_y, ϵ_z	Strains in the x, y and z directions.
σ_p, σ_q, σ_r	Principal stress at a point.
τ_{pq}, τ_{qr}, τ_{rp}	Principal shear stresses at a point.
ν	Poisson's ratio.
v	Crack velocity.
s	Plastic zone length.
b	Half plate width.

References

Akita, Y. and Ikeda, K. 1959 (a) Transportation Tech. Res. Inst., Tokyo, Japan, Report No. 37.

Akita, Y. and Ikeda, K. 1959 (b) Transportation Tech. Res. Inst., Tokyo, Japan, Report No. 40.

Allen, D. N. de G. and Southwell, R. V. 1949 Phil. Trans. Roy. Soc., A 242, 379.

Bateman, D. A., Bradshaw, F. T. and Rooke, D. P. 1964 Min. of Aviation, Tech. Note C.P.M. 63.

Belsheim, R. O. 1957 Trans. A.S.M.E., 79, 7, 1619.

Bevitt, E., Cowan, A. and Stott, A. L. 1964 J. Brit. Nucl. Ex. Soc., Jan., 16.

Biggs, W. O. 1955, Thesis, University of Birmingham.

Bilby, B. A. and Bullough, R. 1954 Phil. Mag., 7, 45, 631.

Bilby, B. A., Cottrell, A. H. and Swinden, K. H. 1963 Proc. Roy. Soc., A 272, 304.

Boyd, G. M. 1957 Trans. Inst. Naval Arch., 99, 349.

Cargill, J. M. 1963 J. Mech. Eng. Sci., 5, 1, 28.

Christopher, P. R. 1959 A.A.C.S. Proc. Cambridge Conf., Report P. 3, 125.

Christopher, P. R. and Cargill, J. M. 1964 Private communication.

Clark, A. B. J. 1956 Proc. Soc. Expt. Stress Analysis, XIV, 1, 195.

Coker, E. G. and Filon, L. N. G. 1931 A Treatise on Photoelasticity. Camb. Univ. Press.

Cole, C. A., Quinlan, J. F. and Zandman, F. (1960) 5th Int. Con. High Speed Photography, Washington.

Cotterell, B. 1964 Trans. A.S.M.E., J. App. Mech., 12.

Cottrell, A. H. 1961 Crack Propagation Symposium, Cranfield.

Cottrell, A. H. 1963 Bakerian Lecture, Proc. Roy. Soc., 276, A, 1.

Craggs, J. W. 1960 J. Mech. Phys. Solids, 8, 66.

Dixon, J. R. 1960 J. Roy. Aero. Soc., 64, 141.

Dixon, J. R. 1961 N.E.L. Report No. 12.

Dixon, J. R. 1962 N.E.L. Report No. 71.

Dixon, J. R. and Strannigan, J. S. 1963 N.E.L. Report No. 115.

Dixon, J. R. and Visser, W. 1961 N.E.I. Report No. 15.

Dugdale, D. S. 1960 J. Mech. Phys. Solids, 8, 100.

Durelli, A. J., Kobayashi, A. and Hofer, K. 1961 Proc. Soc. Expt. Stress Analysis, XVIII, 2, 91.

Felix, W. and Geiger, T. 1956 Sulzer Technical Review, 1, 14.

Fessler, H. and Mansell, D. O.
1962 J. Mech. Eng. Sci., 4, 3, 213.

Gaus, M. P. 1961 Ship Struct. Com., S.S.C.-129,
5th Report No. SR-137.

Goldsmith, W. and Dabaghian, L. 1961 Proc. Soc. Expt.
Stress Analysis XVIII, 2, 121.

Goodier, J. N. and Field, F. A. 1962 Fracture of Solids,
Proc. Conf. A.I.M.M.P.E., 103.

Guernsey, R. and Gilman, J. 1961 Proc. Soc. Expt.
Stress Analysis, XVIII, 2, 50.

Hahn, G. T., Gilbert, A. and Reid, C. N.
1963 Battelle Research Report, N9-18.

Hall, W. J. and Barton, F. W. 1963 Ship Struct. Com.,
Project SR-155.

Holister, G. S. 1961 J. Roy. Aero. Soc., 65, 610, 661.

Hull, D. 1960 Acta Met., 8, 11.

Hult, J. A. H. and McClintock, F. A.
1957, 9th Int. Congr. Appl. Mech., 8, 51.

Inglis, C. E. 1913 Trans. Inst. Naval Arch., 55, 1. 219.

(3) Irwin, G. R. 1957 Amer. Soc. Mech. Eng., App. Mech. Div. Berkeley Conf.

Irwin, G. R. 1958 Discussion of paper by Wells and Post 1958.

Irwin, G. R. 1960 U.S. Naval Res. Lab. Washington N.R.I. Report 5486.

Jacobs, J. A. 1950 Phil. Mag., 41, 349.

Knott, J. F. and Cottrell, A. H. 1963 J.I.S.I., 201, 249.

Krafft, J. M. and Sullivan, A. M. 1962 Trans. A.S.M.E., 55, 101.

Lazar, J. and Hall, W. J. 1959 Ship Struct. Com., Project SR-137, Report No. 3SC-112.

Liu, J. W. 1961 Discussion, Cranfield Crack Prop. Symp., 514.

Low, J. R. 1955 Int. Union Theor. App. Mech., Madrid, 60.

Lubahn, J. D. 1955 Welding Journal, Res. Sup., XX, 518-s.

McClintock, F. A. and Sukhatme, S. P. 1960 J. Mech. Phys. Solids, 8, 187.

Muskhelishvili, N. I. 1953 Theory of Elasticity, Noordhoff.

Nadai, A. 1950 Theory of Flow and Fracture of Solids, McGraw-Hill, 291.

Neuber, H. 1958 Theory of Notch Stresses, 2nd Ed. Springer.

North, R. J. 1959 National Phys. Lab., Report NPL/Aero/379.

Orowan, E. 1946 Trans. Inst. Eng. and Shipbuilders in Scotland, 89, 165.

Redshaw, S. C. and Rushton, K. R. 1960 J. Mech. Phys. Solids, 8, 173.

Robertson, T. S. 1953 J.I.S.I., 176, 361.

Robertson, T. S. 1955 Admiralty Report No. N.C.R.R./R. 324A.

Robertson, T. S. 1957 Inst. Mech. Eng., Conf. High Rates of Strain, 2, 2.

Robertson, T. S. and Christopher, P. R. Admiralty Report No. N.C.R.E./R. 345.

Rolfe, S. T. and Hall, W. J. 1961. Proc. Soc. Expt. Stress Analysis, XVIII, 2, 113.

Rooke, D. P. 1963 Royal Aircraft Establishment, Tech. Note CPM.29.

Rothman, M. and Ross, D. S. 1955 Engineering, 179, 175.

Rushton, K. R. 1963 J. Mech. Phys. Solids, 11, 269.

Sneddon, I. N. 1946 Proc. Roy. Soc., 187, 9, 229.

Stimpson, L. D. and Eaton, D. M. 1961 U.S. Air Force, Report A.R.L. 24.

Tetelman, A. S. and Robertson, W. D. 1962 Trans. A.I.M.E., 224, 775.

Tipper, C. F. 1957 J.I.S.I., 185, 4.

Van Elst, H. C. 1963 Euratom Report No. M 63-1209-26150.

Van Elst, H. C. 1964 (a) Trans. Met. Soc., A.I.M.E., 230, 3, 460.

Van Elst, J. C. 1964 (b) Private communication.

Videon, F. F., Barton, F. W. and Hall, W. J. 1963 Ship Struct. Com., Project SR-155, Report No. SSC-;48.

Walsh, J. B. and Mackenzie, A. C. 1959 J. Mech. Phys. Solids, 7, 247.

Wells, A. A. and Post, D. 1958 Proc. Soc. Expt. Stress Analysis, XVI, 1, 69.

Westergaard, H. M. 1939 Trans. A.S.M.E. 61, A49.

Williams, M. L. 1957 J. Appl. Mech., 24, 109.

Wilshaw, T. R. 1965 Thesis, London University.

Yoffé, E. H. 1951 Phil. Mag. 42, 739.

Yoshiki, M. and Kanazawa, T. 1960 University of Tokio, Report SR-t004.

Yoshiki, M, Kanazawa, T. and Itagaki, H. 1961 University of Tokio, Report SR-6104.